



Thermo-kinetic multi-zone modelling of low temperature combustion engines

Aneesh Vasudev^{a,*}, Maciej Mikulski^{a,b,*}, Praveen Ramanujam Balakrishnan^c, Xiaoguo Storm^a, Jacek Hunicz^d

^a School of Technology and Innovation, Energy Technology, University of Vaasa, Wolffintie 34, FI-65200 Vaasa, Finland

^b Vaasa Energy Business and Innovation Centre (VEBIC), Yliopistonranta 3, FI-65200 Vaasa, Finland

^c Department of Mechanical Engineering, Eindhoven University of Technology, 5600 MB Eindhoven, the Netherlands

^d Faculty of Mechanical Engineering, Lublin University of Technology, Nadbystrzycka 36, 20-618, Lublin, Poland

ARTICLE INFO

Keywords:

multi-zone models
chemical kinetics
low-temperature combustion
RCCI
control-oriented models

ABSTRACT

Many researchers believe multi-zone (MZ), chemical kinetics-based models are proven, essential toolchains for development of low-temperature combustion (LTC) engines. However, such models are specific to the research groups that developed them and are not widely available on a commercial nor open-source basis. Consequently, their governing assumptions vary, resulting in differences in autonomy, accuracy and simulation speed, all of which affect their applicability. Knowledge of the models' individual characteristics is scattered over the research groups' publications, making it extremely difficult to see the bigger picture. This combination of disparities and dispersed information hinders the engine research community that wants to harness the capability of multi-zone modelling.

This work aims to overcome these hurdles. It is a comprehensive review of over 120 works directly related to MZ modelling of LTC extended with an insight to primary sources covering individual submodels. It covers 16 distinctive modelling approaches, three different combustion concepts and over 60 different fuel/kinetic mechanism combination. Over 38 identified applications ranging from fundamental-level studies to control development. The work aims to provide sufficient detail of individual model design choices to facilitate creation of improved, more open multi-zone toolchains and inspire new applications. It also provides a high-level vision of how multi-zone models can evolve.

The review identifies a state-of-the-art multi-zone model as an onion-skin model with 10–15 zones; phenomenological heat and mass transfer submodels with predictive in-cylinder turbulence; and semi-detailed reaction kinetics encapsulating 53–199 species. Together with submodels for heat loss, fuel injection and gas exchange, this modelling approach predicts in-cylinder pressure within cycle-to-cycle variation for a handful of combustion concepts, from homogeneous/premixed charge to reactivity-controlled compression ignition (HCCI, PCCI, RCCI). Single-core simulation time is around 30 minutes for implementations focused on accuracy: there are direct time-reduction strategies for control applications. Major tasks include a fast and predictive means to determine in-cylinder fuel stratification, and extending applicability and predictivity by coupling with commercial one-dimensional engine-modelling toolchains. There is also significant room for simulation speed-up by incorporating techniques such as tabulated chemistry and employing new solving algorithms that reduce cost of jacobian construction.

1. Introduction

1.1. Principles of LTC

Low temperature combustion (LTC) offers new hope for the internal

combustion engine (ICE). Two conditions must be met to fulfil LTC: (i) premixed fuel and air, and (ii) fuel-lean in-cylinder charge [1]. These LTC conditions facilitate low nitrogen oxides (NO_x), which are suppressed by low local combustion temperatures. Emissions of particulate matter (PM) are also low thanks to a large local oxygen surplus. PM creation also requires a certain temperature threshold for the reactions

* Corresponding authors

E-mail addresses: aneesh.vasudev@uwasa.fi (A. Vasudev), maciej.mikulski@uwasa.fi (M. Mikulski).

<https://doi.org/10.1016/j.pecs.2022.100998>

Received 28 August 2021; Received in revised form 14 January 2022; Accepted 4 March 2022

Available online 21 March 2022

0360-1285/© 2022 The Author(s). Published by Elsevier Ltd. This is an open access article under the CC BY license (<http://creativecommons.org/licenses/by/4.0/>).

Nomenclature and abbreviations

BL	boundary layer	cr	compression ratio
BR	blend ratio	ρ	density
CI	compression ignition	V_D	displacement volume
CAI	controlled auto-ignition	μ	dynamic viscosity
CDC	conventional diesel combustion	N_{eng}	engine speed
CFD	computational fluid dynamics	h	enthalpy
COM	control-oriented models	η	efficiency specified by subscript
CR	compression ratio	F	flow across zone boundary
DAE	differential algebraic equations	φ	fuel-air equivalence ratio
CDF	conventional dual fuel	Q	heat energy
DOE	design of experiments	h	height
EGR	exhaust gas recirculation	h	heat transfer coefficient
GDCI	gasoline direct-injection compression ignition	iEGR	internal EGR
GRI	Gas Research Institute	E	internal energy
HCCI	homogeneous charge compression ignition	\mathcal{D}	mass diffusion coefficient
HL	heat loss	Y_i	mass fraction of species i
HPDI	high-pressure, direct injection	m	mass
HRR	heat release rate	\bar{S}_P	mean piston speed
ICE	internal combustion engine	W	molar mass
IVC	inlet valve closing	ω_i	molar production rate of species
ISFC	indicated specific fuel consumption	Pr	Prandtl number
LES	large eddy simulation	P	pressure
LTC	low temperature combustion	P_{EQ}	pressure equalisation
MVEM	mean-value engine models	r	radius
MZM	multi-zone model	Sc	Schmidt number
NG	natural gas	T	temperature
NTC	negative temperature coefficient	Λ	thermal conductivity
ODE	ordinary differential equations	Δw	zone thickness
ON	octane number	Δr	zone thickness in radial direction
OP	operating point	Δt	time step size
RCCI	start of injection	nR	total number of reactions
NO	nitric oxide	nS	total number of species
NO _x	oxides of nitrogen	nZ	total number of zones
NVO	negative valve overlap	ζ	tuning parameter specified by subscript
PCCI	premixed charge compression ignition	ε	turbulence dissipation
PCI	premixed compression ignition	k	turbulent kinetic energy
PDF	probability density function	R_u	universal gas constant
PPCI	premixed compression ignition	u	velocity
PPC	partially premixed combustion	V	volume
PM	particulate matter	<i>Subscripts</i>	
PRF	primary reference fuel	<i>avg</i>	average
PRR	pressure rise rate	<i>axl</i>	axial
RCCI	reactivity-controlled compression ignition	<i>cool</i>	coolant
RG	reformer gas	<i>cyl</i>	cylinder
SOC	start of combustion	<i>comb</i>	combustion
SOI	start of injection	<i>z</i>	index for zones
SZ	single zone	<i>i</i>	index of species
TDC	top dead centre	<i>iman</i>	intake manifold
UHC	unburnt hydrocarbons	<i>lam</i>	laminar
VVA	Variable Valve Actuation	<i>linr</i>	liner
<i>Symbols</i>		<i>zz</i>	neighbours of zone z
λ	air-fuel equivalence ratio	<i>n</i>	normal direction
A_{Fr}	air-fuel ratio	<i>pist</i>	piston
A	area	<i>rd</i>	radial
B	bore	<i>rad</i>	radiation
δ_{BL}	boundary layer thickness	<i>th</i>	thermal
S_{min}	clearance height	<i>tur</i>	turbulent

to proceed [2]. Combustion in conventional spark ignition (SI) or compression ignition (CI) engines is far from these conditions. Although SI engines are characterised by premixed air-fuel charge, flame propagation limits prevent the fuel being extensively diluted. CI engines can run on very lean global excess air ratios, but locally, in the zones where combustion starts, the mixture is fuel-rich. Practical realisation of a lean premixed charge and its compression ignition in reciprocating engines poses certain challenges [1,3,4]:

- Volumetric, kinetically controlled combustion is very rapid, producing excessive pressure rise rates (PRR), especially at high engine-loads, challenging mechanical durability limits.
- Start of combustion (SOC) lacks a direct control mechanism. There is no direct ignition trigger, like spark discharge in an SI engine or fuel injection into hot gas in a CI engine. Instead, SOC timing is determined by the compression temperature histories and auto-ignition properties of the in-cylinder mixture.
- Although laboratory experiments demonstrate excellent results in steady states, efficient engine operation under transient conditions is extremely challenging due to the control issues mentioned above.
- LTC's benefit in terms of low NO_x and PM, are accompanied by high emissions of CO and unburnt hydrocarbons (UHC), which straightforwardly reduce combustion efficiency.
- The benefits of LTC cannot be fully exploited using typical SI or CI combustion systems. SI engines fuelled with gasoline or other high octane-number (ON) fuels must have low compression ratios. CI engines have in-piston combustion chambers that are designed for late fuel injection: with early fuel injection this design's squish effects pose challenges in terms of emissions.
- When higher boiling-range fuels typically used for CI engines are injected early, at low in-cylinder pressure, they are prone to wet cylinder liners and pistons, resulting in fuel films, pool fires and oil dilution.

Several advanced combustion systems have been proposed, each aiming to increase the feasibility of LTC combustion by addressing the above-mentioned issues. They are presented and evaluated in abundant worldwide research. Notably, the studies cover a wide range of fuels,

from conventional diesel and gasoline, through alcohols, natural gas and biodiesels to advanced renewable fuels with a minimal carbon footprint.

Homogeneous charge compression ignition (HCCI) realises the LTC principle to the greatest extent. It involves completely evaporated and well-premixed fuel before combustion starts. Combustion is also generally homogeneous (volumetric). However, temperature gradients caused by heat transfer through cylinder elements can create local auto-ignition sources in close time-proximity. Fig. 1 illustrates the fundamental differences between conventional combustion modes and HCCI. Specifically, HCCI (Fig. 1c) combustion initiates at multiple sites in the cylinder [5] and progresses rapidly towards completion. There is no flame propagation as in SI (Fig. 1a) because HCCI combustion is driven by chemical kinetics. This is central to the difference between HCCI and conventional combustion modes.

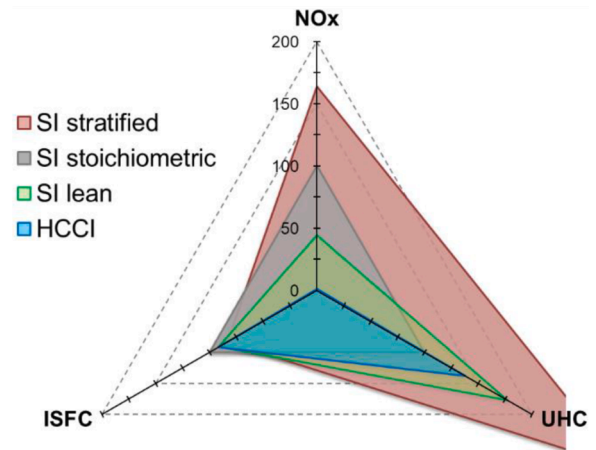


Fig. 2. Relative change in emissions and fuel consumption for stoichiometric HCCI using NVO and different SI technologies, with stoichiometric SI as a baseline (100 %). Data adopted from Osborne et al. [17]. Experiments performed on a car engine with compression ratio 11.7:1 at 2000 rev/min and 2.7 bar IMEP

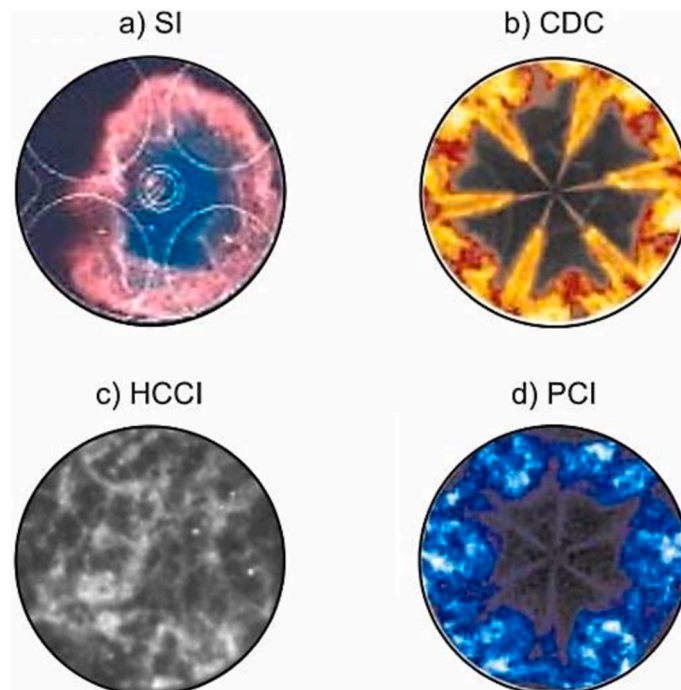


Fig. 1. Combustion image of conventional (a and b) and LTC (c and d) concepts. Adopted from Mueller & Upatnieks [16] with permission from authors.

Fig. 2 compares HCCI and different spark ignition technologies in terms of NO_x and UHC emissions, and indicated specific fuel consumption (ISFC). HCCI's outstanding attribute is reduction of NO_x emissions by 99 % in comparison to stoichiometric SI, penalised by only a 38 % increase of UHC emissions. HCCI also offers 8 % reduction of fuel consumption, which is comparable to lean homogeneous SI concept but 10 % higher than stratified SI.

The two main challenges for HCCI engines are controlling the start of combustion, especially at transient conditions and in changing ambient conditions, and high PRR at high loads. Many research projects have addressed these twin issues, yielding different HCCI combustion control concepts. Their strategies include: (i) fast thermal management on the intake side [6]; (ii) variable valve actuation enabling internal exhaust gas recirculation (EGR) or exhaust rebreathing [7]; (iii) variable compression ratio; (iv) tailoring fuel reactivity by mixing two fuels [8, 9]; (v) modification of fuel reactivity by in-cylinder reforming [10]; (vi) thermal stratification by late direct fuel injection [11] or water injection [12]; (vii) spark assistance [13]; and (viii) HCCI/SI mode switching [7]. HCCI, adopting one or more of those control systems, is also referred to as controlled auto-ignition (CAI), particularly when so-called negative valve overlap is used to trap exhaust gas [14]. Work by Duan et al. provides a good review of different means to realise HCCI [15]. Notably, any single control approach is insufficient to gain combustion control. Therefore, HCCI combustion requires a complex approach that embraces fuel, the gas exchange system and engine mechanical design, thus making this technology extremely demanding.

Looking at examples of applied HCCI, stationary two-stroke engines employing this combustion concept were demonstrated in the late 1970s for electricity generation. The first automotive application of an HCCI engine was recorded in 1995 when a two-stroke activated radical combustion system was employed in a 205 cm^3 engine powering a Honda prototype motorcycle. HCCI combustion in four-stroke gasoline car engines was demonstrated by major engine and car makers in the first decade of the twenty-first century [18]. Recently, Mazda marketed gasoline spark-assisted HCCI technology [19]. Nevertheless, pure HCCI engines are not commercially available even today, despite huge research efforts. It should be noted that emissions and efficiency benefits of HCCI in real automotive applications proved less spectacular than demonstrated by laboratory experiments [20].

Another LTC strategy is premixed compression ignition (PCI). The concept is less homogeneous than HCCI (compare Fig. 1's photographs b and d) and is a step in the progression from conventional diesel combustion (CDC) towards LTC. PCI is also known by other names, such as partially premixed combustion (PPC) [21] or partially premixed compression ignition (PPCI) [22]. PCI achieves LTC by application of

high EGR rates, often exceeding 50 %. This increases fuel dilution and thus reduces combustion temperature, at a given air excess. In CDC, such high EGR rates cut NO_x production but causes soot formation. Therefore, PCI combustion uses a much larger fraction of premixed, kinetic combustion than in CDC, aiming at simultaneous smokeless combustion. A larger premixed fraction is achieved by the elongated mixing time provided by a lower compression ratio (CR) with near top dead centre (TDC) injection. PCI combustion in diesel engines is supported by extended intake and EGR thermal management [21].

The first demonstration of PCI combustion mode in a diesel engine was in the late 1990s by Nissan [23], which dubbed the combustion system Modulated Kinetics. It incorporated a low compression ratio and a high swirl combustion chamber design. The concept enabled divergence from the usual NO_x -PM trade-off. Fig. 3 shows the scale of improvement: at a PM emission level typical for non-EGR CDC, NO_x emissions are reduced by 98 %.

Premixed charge compression ignition (PCCI) is similar to PCI but utilises earlier injection timings to create a premixed fuel fraction [24]. Consequently, start of combustion becomes decoupled from the injection event [25]. PCCI requires tailored spatial fuel distributions in the cylinder, provided by sophisticated multiple injection strategies [2]. This also necessitates modifying injector nozzles to avoid piston and cylinder-liner impingement by early injected fuel [24].

It should be noted that the borderline between PCI, PCCI and CDC is fuzzy. Contemporary diesel engines utilise EGR in combination with a higher premixed fraction to reduce NO_x and PM simultaneously.

Although PCI and PCCI are feasible for diesel engines, this concept favours gasoline-like fuels because they allow operation with higher compression ratios and better air-fuel mixing due to longer ignition delay and faster evaporation [4]. When using gasoline, this concept is called gasoline direct-injection compression ignition (GDCI) [26]. GDCI is currently in development by Aramco, among others [27].

Using two fuels of different reactivity to achieve HCCI-like combustion was first postulated in 2006 by Inagaki et al. [28]. So-called reactivity controlled compression ignition (RCCI) was further developed by Kokjohn et al. [29], who used gasoline injected into the intake manifold and diesel fuel injected directly into the cylinder. The diesel was injected early enough to form a premixed charge before auto-ignition, providing reactivity stratification along the cylinder centreline. RCCI's heat release rate is driven by chemical kinetics and controlled predominantly by fuel reactivity stratification, which is enhanced by different auto-ignition properties of the fuels. Contrary to HCCI, thermal stratification plays a secondary role. Fig. 4 shows how typical RCCI spray patterns translate into spatial mixture stratification in the engine cylinder. n-Heptane and iso-octane were used as high- and

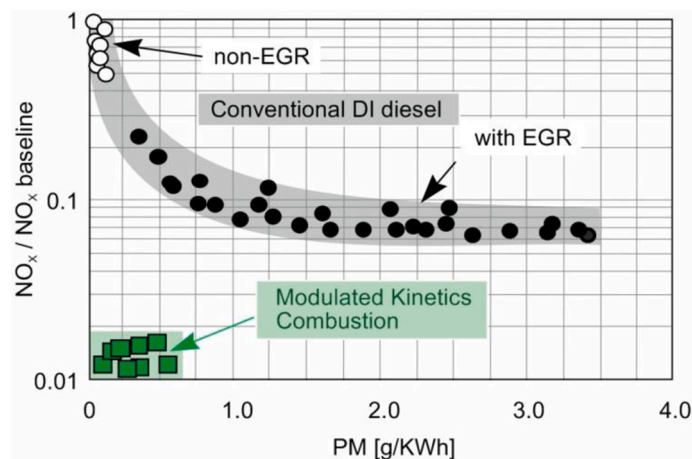


Fig. 3. NO_x -PM trade-off for CDC and PCI combustion at variable injection strategies and EGR. Experiments performed on an automotive diesel engine at 2000 rev/min and 6 bar BMEP. Data adopted from Kimura et al. [23]

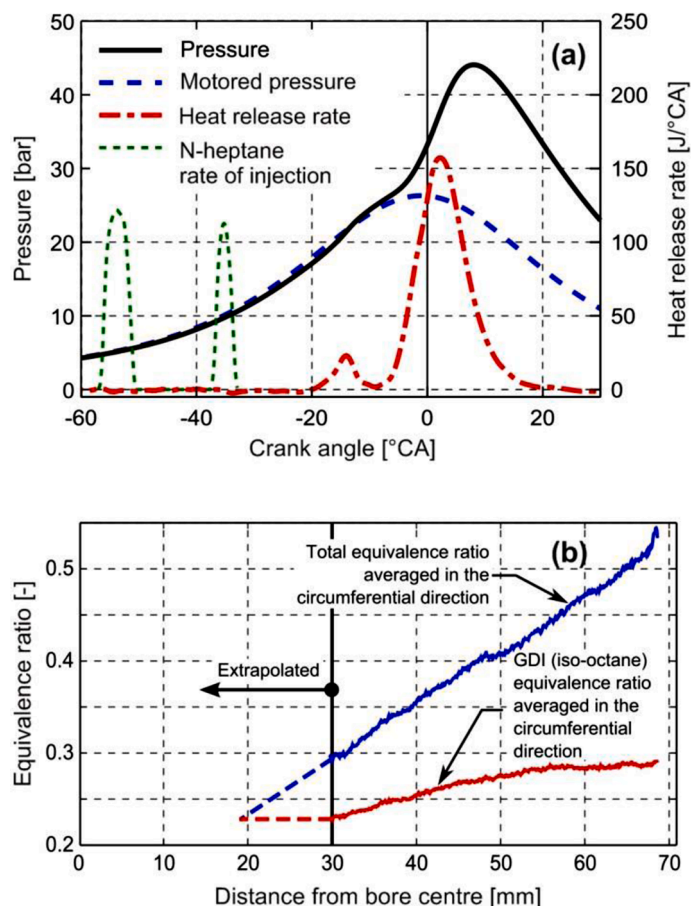


Fig. 4. Low-reactivity (iso-octane) and high-reactivity (n-heptane) fuels stratification in early injection RCCI [30]. n-Heptane injected with two pulses at -60 CA and -40 CA (a). Equivalence ratios (b) at -10°CA are from the fuel tracer PLIF measurements. (Reproduced from Combustion and Flame with permission from Elsevier)

low-reactivity fuels respectively.

Note that single-fuel RCCI was proposed to make the technology more feasible for the automotive sector. Variable reactivity was achieved by making the first injection of diesel fuel directly to the cylinder,

while its second stream passed through an exhaust-gas steam reformer, which produced low-reactivity syngas [31].

One should note that all the acronyms are quite often used interchangeably in the literature – there is no strict classification. However,

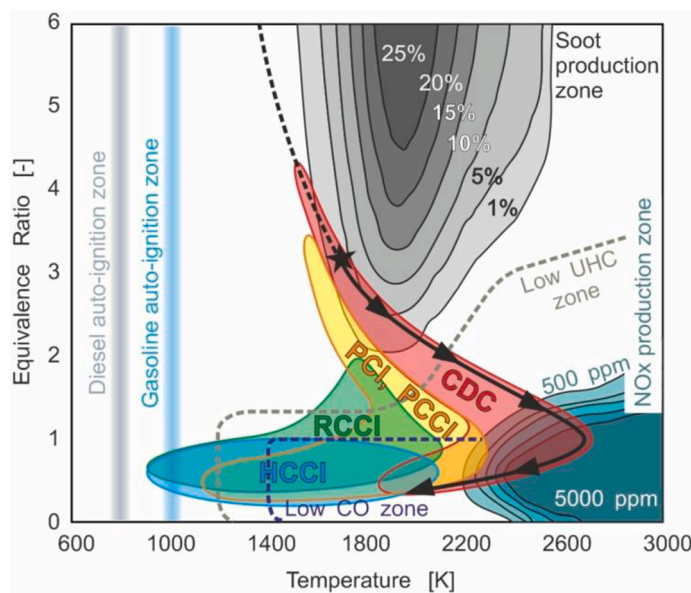


Fig. 5. Temperature-equivalence ratio map of soot and NO_x yields from h-heptane combustion, adopted from Kimura et al. [23], Kim et al. [22], Paykani et al. [32] and Dec [25]. Low UHC and low CO zones are designated in such a way that combustion efficiency drop inside is lower than 2%. The black line is a typical non-EGR CDC combustion path, with asterisk denoting point where high temperature reactions start.

the classification ambiguity relates only to the control approach. For example, different approaches use one or two fuels, or some other agents, e.g. water, while naming the combustion systems HCCI, PCCI, PPCI or RCCI. Nevertheless, the difference between combustion modes lies within their characteristic combustion paths, as clearly shown in Fig. 5. Typically, CDC runs along the black line when EGR is not considered. High temperature combustion starts at high fuel excess, moving the combustion regime towards the soot production zone. Combustion, progressing in time, but also moving outside the fuel stream core, becomes nearly stoichiometric and runs in the high temperature zone, increasing NO_x formation. PCI and PCCI combustion progress qualitatively in a similar way. High EGR rates, characteristic for both concepts, reduce mixture temperature; longer mixing time increases air excess at the start of combustion. Therefore, the combustion pathway bypasses the zones where both soot and NO_x are intensively created. RCCI is based on a much more premixed charge, characterised by a narrower equivalence ratio span, so combustion starts at excess air, which produces hardly any soot. HCCI combustion is assumed to entail equal fuel vapor distribution across the combustion chamber. Combustion theoretically runs along the horizontal line (dashed blue) in Fig. 5, hence is completely smokeless. This high fuel dilution limits combustion temperature. Fig. 5 also illustrates why LTC combustion can be incomplete. Namely, when mixing time is increased and combustion is delayed to reduce PRR, the combustion pathway is broken by lowering temperature due to progressing cylinder expansion. Work by Dec [25] provides a detailed analysis of different LTC combustion pathways.

Thanks to its uncompromised emission mitigation benefits and its ability to accommodate carbon-neutral fuels, LTC development is currently high on the agenda of the global engine research community. Progress so far is summarised in numerous reviews and books. For

example, Stanglmaier & Roberts documented the state of the art in HCCI as it was in 1999 [1]. This work pointed out HCCI's drawbacks and control issues, indicating general control approaches which remain unchanged till today. In 2007 Zhao edited a [33] book collating the work of other leading researchers describing the history and progress in HCCI research. The later review of Yao et al. [3] focused on combustion control, indicating that multi-mode combustion is necessary for HCCI in practical engines. They also highlighted the need to develop control-oriented models. Remedies for specific key issues of HCCI combustion, such as tailored HCCI fuel design [8], high-load extension [34] or cycle-to-cycle variability [35] have been reviewed in recent years. For example, Duan et al. [15] comprehensively reviewed and evaluated HCCI control approaches, providing systematised reference. Fig. 6 sets out the range of governing methods when striving for controllable HCCI combustion. Notably, the control methods summarised by Duan et al. cover the requirements of all LTC concepts.

Reitz & Duraisamy [36] published a review of the progress in RCCI research. The paper provided deep insight into engine design, control approaches, emissions, efficiency and the operating range of RCCI engines. It focused primarily on the achievements of the University of Wisconsin-Madison research group. Importantly, the study determined the PRR-constrained maximum engine load in RCCI mode for different fuels, providing a favourable pathway for high ON fuels like natural gas and alcohols. Ultimately, the study showed a clear route towards 50 % brake thermal efficiency for heavy-duty engines working in RCCI mode. The recent review by Paykani et al. [37] focused on RCCI control techniques to enable engine operation in transient conditions, including multi-mode combustion. The study put forward arguments for commercial feasibility of RCCI engines, also addressing life cycle analysis and cradle-to-grave CO₂ emissions. Notably, the study underlined the

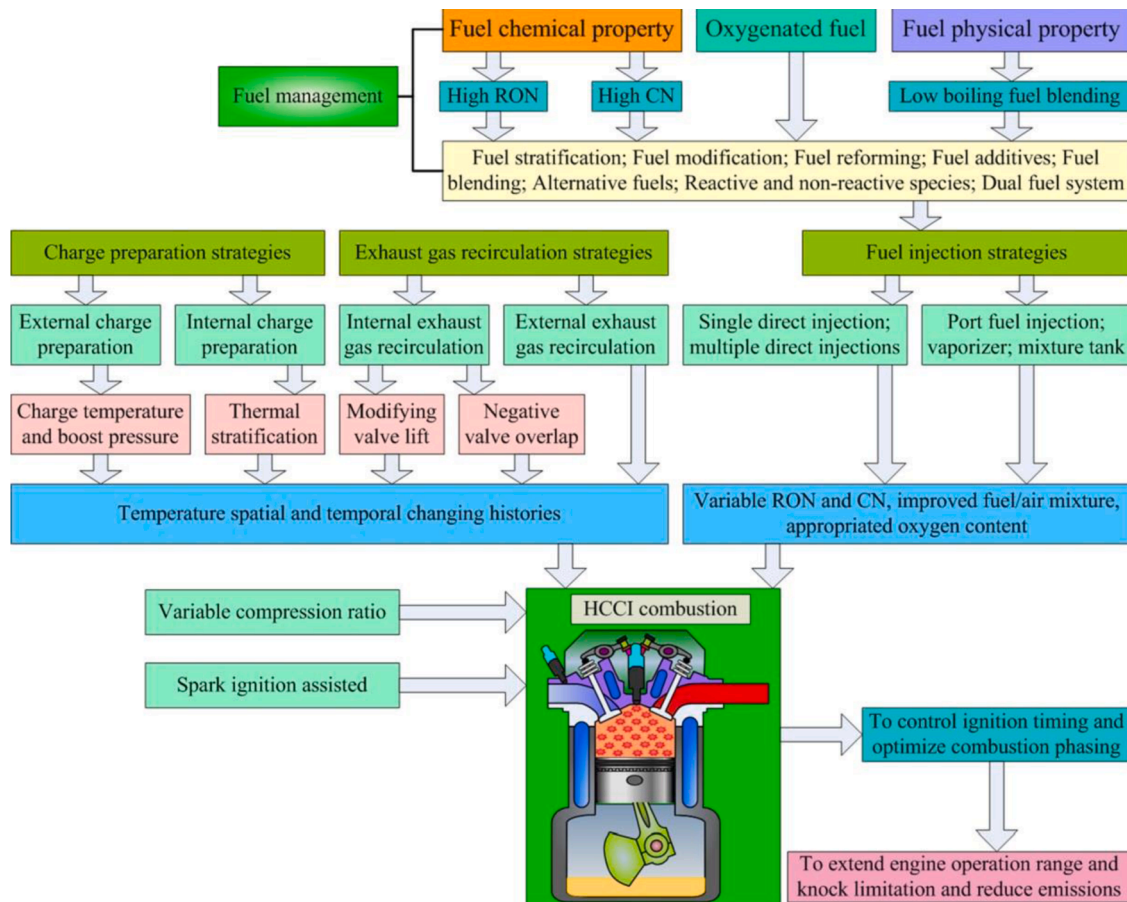


Fig. 6. Strategies for controlling the ignition timing and combustion phase of the HCCI engine [15] (Reproduced from Fuel with permission from Elsevier)

need to develop physics-based control-oriented models (COM) as enablers. This conclusion underpins and mandates our study.

1.2. Overview of LTC modelling approaches

The challenges discussed in the previous subsection make combustion modelling instrumental for further development of technologies like RCCI, HCCI or PCCI. The phenomenological complexity of the process and challenging control make it particularly difficult to rely solely on engine experiments. Models can be used either to support the fundamental understanding of the governing phenomena or help move the concept to towards industrial application. To this end, different LTC modelling approaches exist and their common categorisation is presented in Fig. 7, along with the application range and complementary experimental techniques.

In terms of physical models, rapid developments in Computational Fluid Dynamics (CFD) propel research on fundamental aspects of LTC, complementing experimental-driven studies on mixture formation and in-cylinder stratification. The availability of commercial CFD packages containing direct engine templates encourages many researchers to engage in the hot topic of LTC research. This review has identified that many such studies published in the last couple of years are of doubtful quality: their sheer number makes it increasingly difficult to separate the wheat from the chaff. For example, many of the available literature sources aim to analyse LTC phenomena using only simulation results, without approaching detail model validation. In this case, widely used yet relatively coarse Reynolds-averaged Navier–Stokes (RANS) approaches for modelling turbulence, combined with other simplifying assumptions on spray modelling and reaction kinetics (crucial for LTC phenomena), can lead to biased conclusions. This is particularly true if the authors lack a proper engine background. In contrast, a good overview of CFD approaches for HCCI and RCCI combustion can be found in [38,39].

In-cylinder turbulence and spray formation play a vital role in more complex LTC strategies involving mixture stratification. Thus, contemporary CFD studies, gradually move from RANS to more accurate large eddy simulation (LES) combustion. In a recent study, Tekgül et al. [40] investigated the influence of diesel injection timing on NG-diesel-fuelled RCCI combustion. They used a CFD set-up similar to an Engine Combustion Network (ECN) spray chamber, and emulated the influence of piston motion on in-cylinder thermodynamic state by additional source term [41] in the conservation equations. This was done mainly to reduce computational load, but also simplified the physics by eliminating

spray-wall interactions. Thus, LES enabled detailed visualisation of the combustng spray characteristics under engine-relevant conditions. In another recent work, Zhong et al. [42] broadened the horizon of novel single-fuel RCCI [31] by studying n-heptane sprays in a reform gas environment composed of partially oxidised intermediate species of the fuel. The large eddy simulation-probability density function (LES-PDF) combustion model was able to resolve the double-layered flame structure exhibited around the spray tip and periphery.

However, detailed combustion modelling with LES requires hours of simulation time, even using supercomputer clusters, greatly limiting the applicability of this approach. Direct numerical simulation (DNS), is nowadays technically feasible but far too computationally expensive for reactive flow. Thus, its application in LTC is limited to mixture formation studies or kinetic ignition studies in constant volume reactors [40, 43–46].

On the opposite end of LTC modelling applications (right-hand side of Fig. 7) are the empirical (black-box) combustion models. They are mostly data-driven correlations of selected combustion parameters of the engine. As such, they are not predictive (invalid outside the calibration space) and not transferable to different engine platforms. They are essentially a set of algebraic relations or look-up tables, so this simplicity means they can be computed in real time within a single engine-cycle and thus are very suitable for on-board applications such as virtual sensors or as parts of engine control. An overview of HCCI and RCCI control models is provided in reviews by Fathi et al. [47] and Hall et al. [48].

Empirical models require a large amount of data for building a proper surrogate of the phenomena. This implies use of large-scale tests of the combustor/engine prototype, driven by design of experiments (DOE). Alternatively, one can use a predictive nature of detail physical models to build a calibration map. In the latter case, the detailed model is calibrated using a very limited spectrum of experimental (optical engine research, for instance) cases and transposition to real engine operation is made by simulation. Both the experimental and model-based approaches were found suitable for calibrating legacy engine concepts. However, for LTC, the core issue is the number of independent control variables required for efficient realisation of combustion. Thus, the conventional DOE approach fails to provide a global multi-parameter optimum in reasonable time. Fig. 8 illustrates this issue.

Quasi-dimensional models form an application bridge between the detailed CFD and the black-box models. This approach, instead of imposing explicit spatial discretisation of Navier–Stokes equations (as in CFD) relies on a zero-dimensional (0D) routine which solves only the

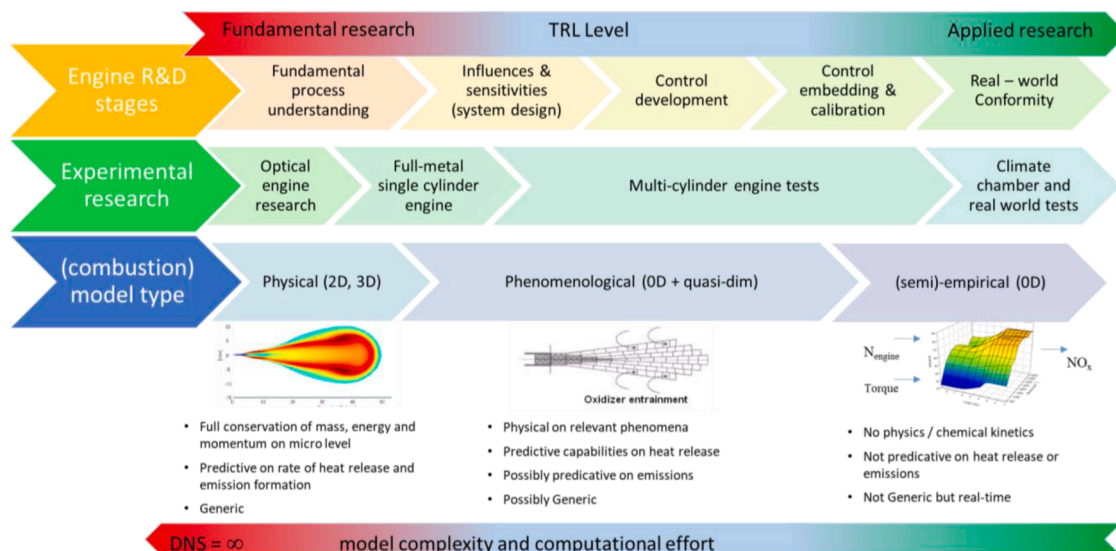


Fig. 7. Combustion model type and its applicability

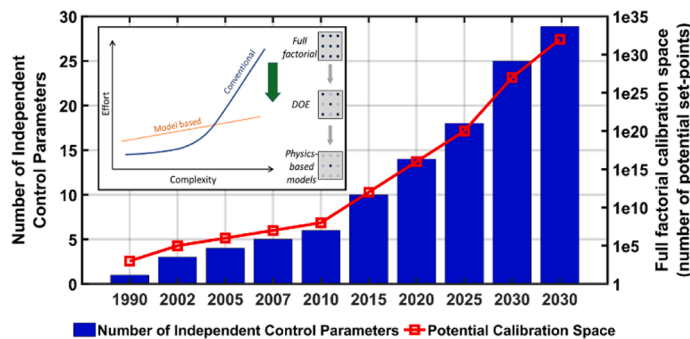


Fig. 8. Engine calibration space showing the exponential increase in the calibration burden as the number of independent control parameters increase. Data from Atkinson [49]

time-dependent energy equation. (See Section 2 for governing equations). Spatial inhomogeneity in temperature and composition, important from the perspective of H/P/RCCI concepts, is captured in a simplified way by dividing the cylinder volume into several zones (in principle separate OD reactors). The way in which zone-to-zone and zone-to-environment interactions are defined can shift the predictivity/computational time trade-off either towards more data-driven approaches or towards the more phenomenological approach.

By far the biggest impact on this trade-off is the way the combustion term is solved. In the simplest case, experimental data are used to define the burn rate, either via a directly imposed look-up table or by a shape function. This makes the model potentially real-time capable but impinges on its predictive nature. The main advantage of this approach compared to straight black-box modelling lies in its more direct correlation of combustion to in-cylinder parameters, creating more flexibility in dealing with complex non-linearity in combustion behaviour. This is particularly relevant for LTC. One of the most common engineering methods in this so-called grey-box approach is to use experimentally correlated Wiebe shape function to represent the burn rate. This technique was widely used in the early-days HCCI control developments. Work by Ghojel [50] includes a comprehensive review of applications of the Wiebe function, including LTC engines.

The predictivity of quasi-dimensional modelling can be improved by phenomenological modelling of combustion. Many combustion models have been proposed to match the framework quasi-dimensional modelling. According to GT-Suite [51], in the context of conventional

SI, there may be turbulent flame model; and the diesel multi-pulse or diesel jet model may be used for conventional DI diesel combustion. For a further collection of quasi-dimensional models, the reader is directed to the work of Verhelst and Sheppard [52] for SI multi-zone models (MZM) and to Kumar et al. [53] for a review of CI engine models.

For fast, yet fully predictive, LTC modelling, the quasi-dimensional approach is commonly coupled with reaction kinetics. In principle, this follows an assumption that HCCI, PCCI and RCCI are predominantly controlled by this mechanism. Since mixture formation and ignition are majorly decoupled in premixed LTC combustion, mixing phenomenon is either omitted (HCCI) or dealt with in a simplified manner – by zonal interaction. Such defined combustion models form the core of the present review. The following subsection explores the background of physics-based multi-zone models and their relevance to LTC development.

1.3. Quasi-dimensional thermo-kinetic models for LTC simulation

The quasi-dimensional chemical kinetics-based models, further referred to as MZM (multi-zone models), offer computational performance an order of magnitude better than CFD. Fig. 9 is an adaptation of an image by C. Allen [54] that captures the ideological difference between the two approaches and underlines MZM’s computational efficiency benefits.

The single-core simulation times typically vary from a couple of seconds to a couple of hours for a single engine cycle, depending on the

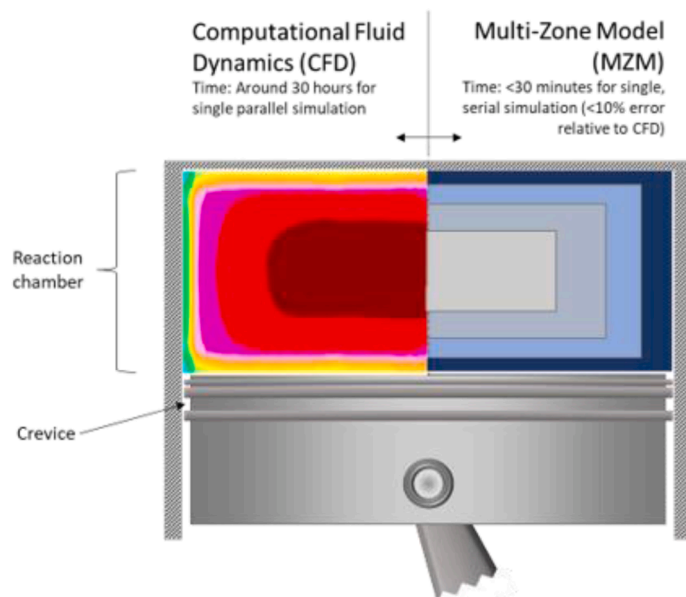


Fig. 9. Comparison of CFD and MZ models (Based on [54])

zonal resolution, size of the mechanism and submodels involved. The physical nature of an MZM in general aims to provide trend predictivity (outside the calibration space) in terms of combustion parameters and emission indicators. However, some authors set absolute-level accuracy targets. Wilson and Allen for instance assumed 10 % maximum error in emissions for their MZM vs. detail CFD calculation [55]. Mikulski et al. aimed at in-cylinder pressure to be within the experimental cycle-to-cycle variations [56].

Predictivity/accuracy combined with fast simulations times enables MZM's wide scope of applications, ranging from fundamental-level studies through to control development endeavours (Fig. 7). Importantly, their speed and accuracy make them suitable for co-simulation with typical 1D [57–59] or mean-value engine models [60,61] for a complete system-level analysis. This fills the mentioned applicability gap between CFD and black-box models, in the context of a complete model-based engine development framework. This methodology, postulated amongst others by Indrajana et al. [62] for RCCI and depicted in Fig. 10, allows the system complexity issues to be overcome. The removal of this bottleneck helps to take LTC concepts towards real-world applications.

In principle, either validated CFD or engine tests are used to build a narrow design space of several operating points (for instance, 14 independent control parameters and four point-sweeps without parameter combination). A physics-based MZM captures the non-linearity between the coarse nodes of the calibration space and can extrapolate beyond it. MZM combined with an engine model allows development of full multi-cylinder engine LTC pre-calibration, including global multi-parameter optimisation routines [57] and development of controls [62]. Further development stages usually involve embedding the control and final testing. It is relatively easy to make MZM real-time capable, for instance, by creating a data-driven metamodel for heat release and emissions [63]. Experimental validation is recommended at each development stage, gradually moving from model- and software-in-the-loop (MIL/SIL) to hardware-in-the-loop (HIL) testing [64,65]. According to Fig. 10, building an MZM and employing it in engine development end-to-end, by far surpasses conventional incremental (experimental) approach when the objective is multi-cylinder RCCI or advanced H/PCCI.

MZM are thus extremely important for moving LTC technology towards the market. Note, however, that the complete model-based development framework with MZM so far has not been demonstrated: individual studies have focused on individual elements of the framework. A recent RCCI review by Paykani et al. [37], aiming to map out the “pathways towards commercial viability,” highlighted the development of a proper control-oriented model (COM) as one of the key enablers. The authors examined two physics-based multizone models incorporating chemical kinetics. They concluded that current RCCI COM have

limitations and need improvement. Many similar MZM have been proposed for HCCI development. A control-oriented review by Fathi et al. [47] mentions over 15 works committed to quasi-dimensional modelling of HCCI. Due to a broad scope, however, the authors committed only a paragraph or so to this issue. On the other hand, Komninos & Rakopoulos [66] dedicated their whole review to heat-loss modelling in HCCI MZM, without particular attention to other aspects. The work is extremely valuable to researchers looking at detailed information on quasi-dimensional modelling and demonstrates the issues complexity. However, it lacks the critical perspective to accommodate different approaches, and its highly focused nature does not allow the reader to grasp the essence of application-tailored MZM modelling. Note that the authors underlined the value of their review when observing that current literature does not cover MZM comprehensively.

1.4. Motivation and scope of the present paper

Our introduction advocates LTC as a technology for next-generation combustion engines. Further subsections have focused on the major hurdle to be overcome, namely system complexity, and proposed MZM as a tool to deal with it. We also have indicated that those tools need constant evolution because LTC technology is evolving to include more actuators and more complex phenomena. At the same time, there is no single recipe for an ultimate MZM toolchain: it needs to be tailored to fit the desired application. This means balancing the trade-off between accuracy and calculation time with a proper selection of submodels, which often need specific assumptions in terms of zonal configuration and an adequate numerical solver. Consequently, there is no mature commercial solution for a physics-based LTC MZM framework. For instance, the industrial standard 1D engine simulation toolchain GT Suite accommodates application of reaction kinetics in only a single-zone framework, sufficient only for a very coarse estimation of fully homogenous combustion [51]. Neither is the subject comprehensively described in any books related to combustion engine simulations, so establishing the model is a challenging task.

As discussed in the introduction, although LTC development has been already extensively reviewed, MZM so far has not been given sufficient attention, except in the mentioned work by Komninos & Rakopoulos [66] with its shortcomings. The topic becomes even more relevant as advanced multi-fuel LTC concepts move from fundamental level studies towards applied research. The present work aims to fill this knowledge gap with a comprehensive and critical view on the current state of the art in physics-based MZM suitable for control-oriented LTC simulation. The aim is to provide sufficient details on governing physics and mathematics to enable approach reproduction, while assessing individual submodels for fitness for purpose, accuracy and impact on

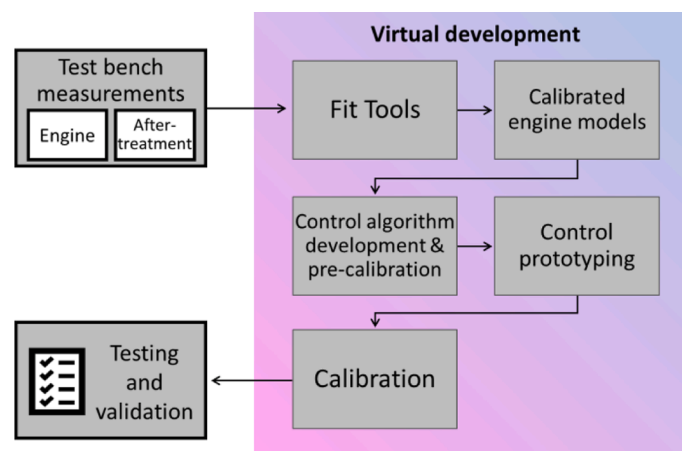


Fig. 10. Pathway for model-based engine development with the use of MZM (adopted from [62])

computational efficiency.

This aim can be distilled to four research questions:

- Q1 How do MZ models evolve and what is the current state of the art in terms of model configuration and submodels?
- Q2 What is the accuracy/calculation-speed trade-off issue for MZ models, and how can it be addressed and improved?
- Q3 What is the application area for MZM in terms of combustion concepts and associated fundamental-level phenomena?
- Q4 How do MZ models support applied-level research?

Section 2 introduces the governing assumptions for all MZ models, aiming to provide a complete picture. It also contributes input towards Q1, which ultimately is answered by sections 3 and 4, examining zonal configurations and available submodels respectively. Section 5 addresses the simulation procedure, directing the discussion towards computational efficiency and thus contributing to answering Q2's trade-off issue. The accuracy side of Q2's trade-off is addressed in subsection 6.1's detailed review of MZM validation results. The crucial, forward-looking issue of MZM application is raised in Q3 and Q4 and answered in subsection 6.2. This reviews the whole range of MZM applications foreseen by Fig. 7, from fundamental-level studies to control embedding. Finally, section 7's discussion and outlook, pulls together all the individual strands to provide a concise roadmap of MZM evolution.

2. Multi-zone modelling framework

The purpose of this chapter is to provide an introduction to the theoretical framework of multi-zone modelling. This begins with listing the governing equations and describing the assumptions common to all multi-zone models. Importantly, it explains the terms and concepts commonly used in literature.

2.1. Governing equations and common assumptions

Construction of an MZ framework is based on a network of homogeneous reactors. Thus, the combustion chamber's volume is segmented into zones, each with its own thermodynamic state. Although this is analogous to domain discretisation in CFD, the division is much coarser, typically not exceeding 40 zones. As such, the zones represent lumped regions of the in-cylinder space like crevice, boundary layer or core region.

Each zone is assigned any number of boundaries, separating it from neighbouring zones or from the environment (combustion chamber surfaces). The boundaries can prescribe shape to the zones and serve as interfaces for exchanging heat, mass and/or work. Fig. 11 illustrates a zone within the MZ framework, along with its boundaries and interactions. The solid red arrows represent interzonal heat exchange; the solid blue arrows represent interzonal mass exchange and the black arrows represent interzonal work exchange. The dashed arrows represent the zone's interaction with the combustion chamber surfaces.

The primary assumption of MZM is that pressure remains uniform across all zones at each time step. This follows the premise that pressure between zones equalises rapidly [67], at a rate equal to the speed of sound. This is connected to the presupposition of MZM not resolving the in-cylinder flow field, by disregarding the surface forces of pressure and viscous effects. As a result of pressure equalisation, momentum conservation is deemed satisfied, and so is not explicitly modelled.

Analogous to homogeneous reactors, the governing equations of MZM constitute a coupled set. Each zone in general requires equations for balance of mass Eq. (1), energy Eq. (2), species Eq. (3) and a coupling between pressure and temperature via equation of state, specifically ideal gas equation Eq. (4). The equations below are listed in their generic form, where subscript z is the index for zones and nZ is the total number of zones. In the energy equation Eq. (2), heat transfer to cylinder walls is explicitly captured by dQ_z/dt . In the species conservation Eq. (3), $\dot{\omega}_{i,z}$

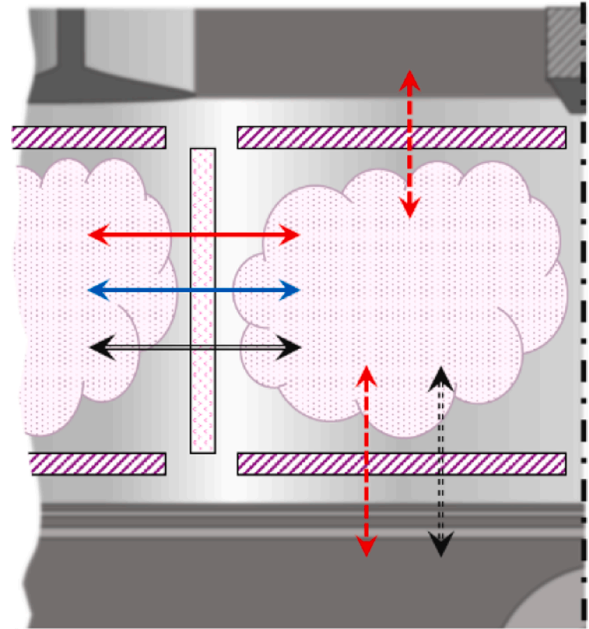


Fig. 11. Generalised MZ framework; red arrow – heat flow, blue arrow – mass flow, black arrow – work

represents the molar production rate of species i , and W_i is its associated molar mass. R_u in Eq. (4) is the universal gas constant of a zone and \bar{W}_z is the mean molar mass of z .

$$\frac{dm_z}{dt} = \sum_{zz}^{(m)} F_{zz \rightarrow z} \quad (1)$$

$$\frac{dE_z}{dt} = \frac{dQ_z}{dt} - P_{cyl} \frac{dV_z}{dt} + \sum_{zz}^{(E)} F_{zz \rightarrow z} \quad (2)$$

$$\frac{dY_{i,z}}{dt} = \frac{\dot{\omega}_{i,z} W_{i,z}}{\rho_z} + \sum_{zz}^{(Y)} F_{i,zz \rightarrow z} \quad (3)$$

$$P_{cyl} V_z = m_z \frac{R_u}{\bar{W}_z} T_z \quad (4)$$

$$\sum_z^{nZ} V_z = V_{cyl} \quad (5)$$

In each equation, the term F with superscript m , E and y represent interzonal transport of mass, energy and species respectively. Summation ensures contribution from all neighbours (zz) to a particular zone (z). Moreover, $^{(E)}F_{zz \rightarrow z}$ can include contributions from both interzonal heat transfer and mass transport (enthalpy). The F terms are expressed within the context of the associated submodels, as will be described in section 4. Equations (5) and (4) enforce the condition of uniform pressure (P_{cyl}) across the zones.

2.2. Zonal configuration

Charge stratification is the rationale behind the division of the in-cylinder volume into zones. In the context of MZ models, the main focus is on stratification in the bulk portion of the combustion chamber gases [68–70]. With uniform zonal pressure in the MZ framework, stratification across the zones pertains to temperature and composition. It is the manner in which the zones are arranged that enables the model to capture the influence of in-cylinder inhomogeneity on combustion, in a computationally efficient manner.

Thus, zonal configuration refers to the arrangement of the zones in a

multi-zone model. A rudimentary sense of the arrangement is established by the numbering of zones. Furthermore, zonal configuration determines the number of neighbours to a particular zone. Evidently (Fig. 11), the number of boundaries of a zone corresponds to the number of neighbouring zones, in addition to the bounding combustion chamber surfaces. Following convention, this paper's indexing of the zones starts with the outermost zone or the zone associated to the liner.

The properties of a zone and its associated boundaries will be referred to in the present review as zonal attributes. Taking the example of crevice zone, as in [71], which was prescribed as a constant volume implying that it remained isochoric throughout the simulation. Thus, references to zone boundaries in literature may include a range of properties: adiabatic, fixed zone mass (implying no interzonal mass flow) and geometry or shape. Apart from fixed volume, zones may be fixed temperature or even have chemical kinetics disabled. All in all, zone attributes in a MZ model can be dissimilarly specified in order to reinforce the notion of charge stratification in the zonal configuration.

2.3. Mechanism of pressure equalisation

In practice, pressure equalisation across the zones is achieved as a result of readjusting either volume or mass of the zones. This is illustrated in Eq. (6), obtained by combining Eqs. (4) and (5). In the latter it is assumed that the volume distribution of zones remains fixed throughout the simulation. In other words, the proportion of the zonal volumes with reference to the in-cylinder volume does not change after being set at the initialisation stage. Instead, mass among the zones is readjusted, manifesting as interzonal mass transfer. The mechanism of this mass transfer is not based on processes of convection, nor diffusion, but rather is driven by thermodynamics Eq. (6). This means of bulk mass transfer will be referred to as P_{EQ} based interzonal mass transfer in this review paper. Further discussions on this mechanism will resume in the context of the associated submodel (section 4.3).

On the other hand, when pressure equalisation is achieved by readjusting zonal volumes, it is presumed that the mass of each zone remains fixed, or if interzonal mass transfer occurs, it may be based on the diffusion mechanism (section 4.3). Thus, volume of the zones is readjusted at every time step to maintain equal pressure among all zones. In other words, zonal volume distribution prescribed at initialisation will have changed with the progress of the simulation. This process manifests itself as interzonal work transfer. In such a case, volume change of a zone is due to both piston motion and interzonal work transfer.

$$P_{cyl} = \frac{1}{V_{cyl}} \sum_z^{nz} m_z \frac{R_u}{W_z} T_z \quad (6)$$

3. Classification of multi-zone models

Development of thermo-kinetic MZ modelling has progressed in parallel with improvements in LTC engines. Initially used for HCCI simulations [72], the models have become more sophisticated in terms of submodels and numerical schemes, able to predict performance of advanced strategies such as RCCI on VVA hardware [56]. There are numerous realisations of MZ models in literature and they generally fall into one of two major groups: balloon and onion-skin models. There are also two minor groups: stochastic MZ models and spray MZ models. Balloon models can be further sub-divided into two types: one-way coupled CFD-balloon and two-way coupled CFD-balloon MZ models. As the names suggest, this grouping is based on how MZ models are coupled with CFD models. Onion-skin models also can be sub-divided into two types, based on commonality of their zonal configuration: annular and enclosed type models.

Fig. 12 illustrates this classification and depicts the relative proportions of the groups within the reviewed literature. Broadly speaking, zonal configuration is a common theme for the models' classification, so the current section elaborates on each class from the perspective of zonal

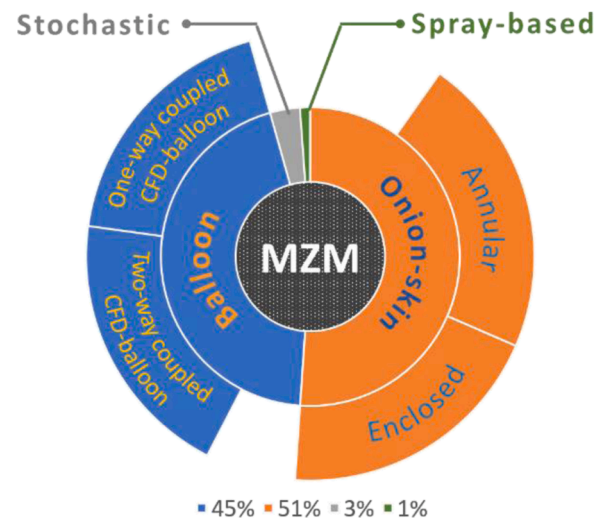


Fig. 12. Classification of multi-zone models. Size of the sectors corresponds to the volume of literature of a certain model type in proportion to the total body of reviewed works.

configuration. It focuses on aspects such as interzonal interaction, zonal attributes, geometric constraints and possible reasons behind a particular zonal arrangement. Since stratification plays a key role on the phenomenology of LTC, we assess the ability of a zonal configuration to reflect the same. There is also an overview of how zonal configuration influences model predictivity, simulation time and choice of submodels.

3.1. Balloon configuration

Being the simplest of zonal configurations, the balloon type was popularly employed during early developments in MZ simulation of LTC engines. The distinguishing characteristic is that the zones lack shape. Furthermore, the zonal configuration has a non-existent to weak physical connection to the topology of the combustion chamber. Consequently, the zones have no real sense of surface area. Still, each zone is prescribed a volume, which can change as the simulation progresses. The arrangement can be conceptualised as a collection of balloons containing reacting gases, constrained within the in-cylinder volume.

In most of the early balloon models all zones had the same attributes and interzonal heat and mass flows were excluded [73,74]. This modelling simplicity meant that charge inhomogeneity was primarily captured at the initialisation phase. In other words, MZ predictivity hinged on proper estimation of initial inhomogeneity of properties, i.e., temperature, volume, mass and fuel concentration. Since this initial inhomogeneity could not be straightforwardly determined from experimental data, CFD results were used. As in the works of Aceves et al. [75, 76], the balloon model was coupled with a CFD model, where the initial phase until combustion initiation, was handled by the CFD simulation. The CFD results were then processed to provide initial conditions of the MZ model, by generating a temperature-mass (T-m) or temperature-equivalence ratio (T- ϕ) distribution. T-m mapping provided information about zonal mass and temperature distribution, while composition was assumed uniform across the zones. This was acceptable for HCCI simulations. T- ϕ mapping also provided information regarding mixture strength distribution among the zones, relevant in simulations of PCCI [77,78] or VVA strategies [79]. Section 5.2 has further discussion of model initialisation methods.

Briefly, the approach of mapping from CFD to balloon involves identifying representative regions [80] within the in-cylinder space. The CFD grid is arranged into a number of regions, equal to the number of zones. The approach for division is to lump together cells with similar properties. This is then mapped to the corresponding zones of the

balloon model, via T-m or T- ϕ distributions. For instance, for HCCI, regions of similar T are brought together. In the initial work of Aceves et al. [73] from a total of 10 regions, three regions (amounting to 3 % of in-cylinder mass) represented the crevice; four regions (amounting to 10 % mass) represented boundary layer; and the remaining three regions (amounting to 87 % mass) represented the central or core region. Similarly, for PCCI, representative regions were formed based on temperature and mixture strength, as in [77], where five from a total of 40 regions (amounting to 4.5 % of in-cylinder mass) represented the combustion chamber's coldest and leanest space. Section 5.3 elaborates on calibration of zone size. The essence of the approach is that zonal division was carried out in T-m / T- ϕ space, as opposed to physical space. Fig. 13 provides a brief overview of this. The corollary is that without intrinsic coupling with CFD, stand-alone balloon models were used in the context of parametric studies (see section 6.2 on application for further details).

Charge inhomogeneity in the zonal configuration is further emphasised by non-uniformly setting up attributes among the zones. This can be done by application of (well-known) wall heat loss correlations to MZM. This raises the question regarding distribution of the resulting cylinder-averaged heat flux among the zones, which is relevant since it links to thermal stratification. Distribution of cylinder-averaged wall heat loss may be based on zonal mass distribution [81] or volume distribution [74]. In addition, Kodavasal et al. [81] proposed an elaborate approach for establishing thermal stratification using heat loss modelling, as they aimed for a stand-alone MZM. CFD results only aided model calibration, and were not used to generate initial conditions. In their MZ approach, distribution of overall heat loss among zones was modulated by 'heat-loss multiplier'. The idea was based on fact that the central portion of the combustion chamber remained warmer than regions close to the walls. Thus, zones representing the BL and crevice experienced more heat loss than the zones representing the core region. Section 4.1 has more details on wall heat transfer modelling in MZM.

Due to the simplicity of balloon models, interzonal transport of heat and mass are usually not modelled. Work exchange remains the only interzonal interaction, in accordance with the pressure equalisation condition (Eq.(6)). However, the study of Hergart et al. [78], considered the flow of heat and mass among the zones. Due to the lack of spatial topology of balloon configuration, a pseudo flow area was conceived, shown in Eq. (7). This is the surface area of a sphere formed by summing volumes of adjacent zones. Furthermore, the interzonal flow was based on wall heat loss correlation, where interzonal mass transfer was assumed proportional to the heat loss coefficient. Interzonal heat transfer was then based on the enthalpy of the exchanged mass. Further details of these submodels are presented in Section 4.3.

$$A_z = \pi \left(\frac{3}{4\pi} (V_z + V_{z+1}) \right)^{2/3} \quad (7)$$

Balloon models' simplicity [74] means their computational expense is lower (disregarding CFD initialisation) than other MZ approaches.

Although a larger number of zones can be simulated (as many as 100 [80]), this does not necessarily translate into improved model predictivity. Balloon models are generally poor in emission predictions, crucially of CO, NO_x and UHC, as recognised by Flowers et al. [82], due to the lack of interzonal heat and mass flow. Section 5.3 includes further discussions on Flowers et al.'s findings, together with an assessment of model calibration and validity.

From an application perspective, balloon configuration is largely popular for HCCI simulations [76,79,81,83]. The suitability is due to the volumetric nature of combustion, where the chemistry timescale is much too short compared to the flow timescale. Aceves et al. [84] used this explanation to justify the exclusion of interzonal flows. They performed a sensitivity analysis by artificially introducing interzonal mixing, based on diffusion. The effect of turbulence was emulated by scaling molecular diffusivities by 100-fold. The authors reported a small sensitivity of CO and HC emissions, with around 1 % difference between runs with and without interzonal flow. It is worth noting that they conducted this study on a flat piston geometry.

3.2. Onion-skin configuration

An onion-skin model differs from other classes of MZM because its zones have a defined shape. Following the explanation in section 2.2, the geometric properties specified to zonal boundaries also fall under the attributes of the associated zone. The arrangement of such zones into a zonal configuration establishes a strong sense of spatial association to the topology of the combustion chamber. Furthermore, geometric constraints are required to govern the shape of the zonal configuration in response to the changing combustion chamber volume. This makes onion-skin zonal configurations more sophisticated than the balloon types.

Shape and arrangement of the zones are defined in a way that capture in-cylinder charge inhomogeneity. Since the topology between the stratification in temperature and fuel may be dissimilar, in addition to their relative importance for a given LTC concept, there are a variety of realisations of onion-skin models. However, all the zonal configurations are built from one of three simple elementary zone shapes: (a) cylinder or disc (b) annulus or ring (c) enclosed, as shown in Fig. 14. These are logical derivatives of a cylinder and are popularly employed in literature, despite complexities in combustion chamber geometry, such as piston bowl shapes, as in seen in implementations [85,86].

Table 1 summarises different realisations of onion-skin zonal configuration, based on select examples. The following general observations can be made. First, the central or core zone is typically large due to lower temperature gradients at the combustion chamber centre. Second, intermediate zones that surround the core are either annular, as in the work of Neshat & Saray [87], or of enclosed shape as in Komninos [88]. Finally, the outermost zone corresponds to the boundary layer (BL) region and is modelled as a thin zone. Approaches such as Kongserpearp & Checkel [89] and Kozarac et al. [90] further split the BL zone

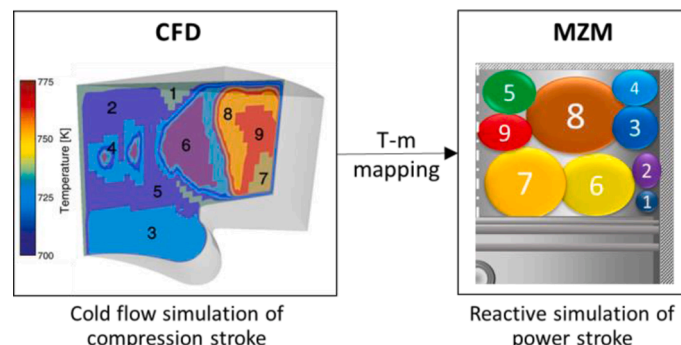


Fig. 13. Illustration of the one-way coupled CFD-balloon MZM via temperature-mass (T-m) mapping. Adopted from Hergart et al. [78].

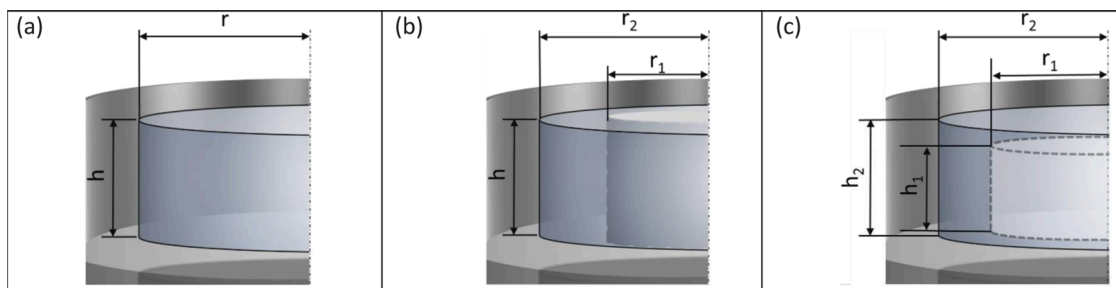


Fig. 14. Typical zone geometries under the onion-skin MZM; (a) cylinder, (b) annular, (c) enclosed

according to individual combustion chamber surface – head, liner and piston. Notably, in an effort to better capture the BL phenomenon, Fiveland et al. [91] apportioned the liner region axially, with ring-shaped zones stacked on top of each other. Geared towards improved emissions predictivity, their model captured UHC emissions with around 10-20 % error and CO emissions within 50 % error, tested over a range of turbocharged conditions.

Onion-skin models account for interzonal heat and mass transport with their zone geometry enabling physics-based approaches. As will be elaborated in sections 4.2 and 4.3, this pertains to computations of gradients of properties and the flow area. Therefore, geometric properties of a zone influence the direction and magnitude of heat and mass flow. For instance, in an annular zonal configuration [92], interzonal flow occurs only in a radial direction. It is worth noting that outer zones, or zones closer to the combustion chamber surfaces, have larger surface areas than inside zones, influencing heat and mass flow.

In the work of Kongsreeparp & Checkel [89] a zone had up to four neighbours and the interzonal heat transfer occurred both in radial and axial direction, as can be seen in Tab. 1. In the model of Neshat & Saray [87] for instance, the BL zone solely had a different geometry. It was of the enclosed type, encapsulating all the remaining (annular) zones. Thus, its outer side was in contact with the combustion chamber surfaces (liner, head and piston), and the inner side contacted the annular zones – specifically, their axial (top and bottom) surfaces. This arrangement allowed it to exchange heat and mass with all the other zones. In other words, each annular zone exchanged heat and mass with its radial neighbours (inner and outer) as well as the BL zone (axial).

As mentioned earlier, the notion of thermal stratification was further emphasised across the zones by dissimilarly defining the zonal attributes. Since the central portion of the combustion chamber is the warmest, the core zone is often modelled as adiabatic [93]. Easley et al. [94] additionally considered disabling mass transfer across the core zone boundaries. In a similar vein, a dedicated crevice zone was included to improve emissions results. This zone was assigned a small volume, 1-3 % of clearance volume as in [95,96]. Furthermore, the zone was set up as isothermal [97,98] by imposing the cylinder liner temperature

Owing to the fact that onion-skin models take account of physical effects of in-cylinder flows, this alleviates the requirement for high-fidelity initial conditions. In contrast, the T-m map generation from CFD simulation is case-dependent for sequential CFD-balloon models. Thus, simulation predictivity of the model as a standalone entity is substantially improved in onion-skin approaches. Taking the example of the HCCI model by [87], a spatially averaged value of temperature at initialisation was sufficient to provide results within the required accuracy limits. It is worth bearing in mind that despite the sufficiency of spatially averaged thermodynamic state, it must be estimated reasonably well due to the sensitivity of kinetics-driven auto-ignition. To this end, lower-fidelity valve flow or air-path models are employed, as will be discussed in section 5.2.

3.2.1. Annular type

In an annular configuration, division of the combustion chamber volume into zones begins from a central cylindrical zone and subsequent zones encase each other only in the radial direction, analogous to annular rings. In other words, the MZ model mainly is composed of annular-shaped zones, all sharing the same height. However, each zone has a unique radius (Fig. 14b). This can be observed in the model of Neshat & Saray [99] in Tab. 1, or in [92]. From this topology, it is apparent that the outermost zone corresponds to gases close to the liner, and vice versa for the innermost zone. The configuration can be conceptualised as radial discretisation of the in-cylinder space. In terms of charge stratification, the zonal configuration is able to reflect the profile only in a radial direction.

Geometry of the zones changes in congruence with the evolving combustion chamber volume and possibly interzonal work transfer. Therefore, constraints are applied on the zone dimensions, namely its radii (r_z). According to the approach of Egüz et al. [100], a zone's radius was the distance between the common axis and its outer interface. Thus, the radius was recalculated at each time step, based on volume of the zone. The approach is a manifestation of constraint Eq. (5). In other words, Eq. (8) implies that zonal radii have one degree of freedom but are constrained by Eq. (5). Indexing in the below equation below starts from the outer zone.

$$r_z = \sqrt{\frac{1}{\pi h_{cyl}} \left(V_{cyl} - \sum_{j=1}^{z-1} V_j \right)} \quad (8)$$

On the other hand, Neshat & Saray [87] dimensioned their zonal configuration based on Δr_z , referred to as thickness of zone. This was the distance between the radial interfaces of a zone. Importantly, Δr_z of each zone was considered fixed throughout the cycle. This meant that the volume of the zones remained in proportion to the in-cylinder volume at each time step.

Following the explanation for pressure equalisation (section 2.3), it is apparent in the approach of Egüz et al. included interzonal work transport. In contrast, in Neshat & Saray's model, P_{EQ} -based interzonal mass transfer occurred, whereby pressure equalisation among the zones occurred as a result of readjusting zonal mass. It is worth noting that the model of Egüz et al. nevertheless enabled interzonal mass transfer, but governed by the diffusion mechanism, where the gradient in species concentration was the driving force.

These geometry constraints connect the zonal configuration to the interzonal transport submodel. In the case of interzonal heat and mass transport, the flow area is the curved surface area ($_{(radial)}A_z$), which can be simply computed from the radii (Eq. 8). The approach of Mikulski et al. [101] took advantage of the zonal configuration to couple wall heat loss to thermal stratification. This is because, the heat loss area of a zone was based on its axial area ($_{(axial)}A_z$), which contacted the head and piston surfaces. As such, the prescribed zone size distribution affects $_{(axial)}A_z$, which in-turn can influence thermal stratification.

Table 1
Various implementations of onion-skin zonal configuration, using selected examples.

Reference	Illustration	Description
Kongsereeparp & Checkel [89]		Single cylindrical core zone Annular zones of increasing height in radial direction Disc zones of increasing radius in axial direction
Kozarac et al. [90]		Single cylindrical core zone Single enclosed-type intermediate zone Annular-shaped liner BL zone Disc-shaped piston and head BL zone Fixed-volume crevice zone
Fiveland & Assanis [91]		Cylindrical adiabatic core zone Multiple, stacked annular zones for liner BL Single disc zone for both head and piston BL
Neshat & Saray [87]		Cylindrical core zones Annular outer zones Enclosed BL zone Fixed-volume crevice zone
Komninos [88]		Enclosed zones surrounding core zone Fixed-volume crevice zone

3.2.2. Enclosed type

This configuration is essentially an arrangement of zones enclosed one inside the other, akin to nesting (matryoshka) dolls. Thus, each zone possesses the geometric properties of height and radius (see Fig. 14c). This gives a zonal topology whereby the outermost zone contacts all combustion chamber surfaces (liner, head and piston).

In response to the changing combustion chamber volume, the shape and volume of each zone is governed by applying constraints to its

radius and height. The common approach is to couple both into a single parameter, and to this end, various implementations exist. The approach of Bissoli et al. [96] maintains the proportion of each zone (Eq.(9)) in accordance with the combustion chamber geometry at each time step (Eq.(10)). The other approach employs a single parameter, zone thickness (Δw_z), referring to the distance between the walls or interfaces. Here, the presumption is that the thicknesses in both radial and axial directions are equal (Eq.(11)). Importantly, thickness of a zone is considered fixed throughout the cycle. This approach was applied in works such as Komninos et al. [71], Tzanetakis et al. [67] and Voshtani et al. [102].

Following the previously utilised route for analysis, it is apparent from the former approach that zonal pressure equalisation was achieved by interzonal work transfer. According to Eq.(10), the radius of a zone is updated, based on the readjusted volume of the zones. As such, to implemented interzonal mass transfer, Bissoli et al. [96] relied on diffusion approach. On the other hand, Δw_z maintains the thickness of each zone during the progress of heat release. Here, P_{EQ} based interzonal mass transfer is used to achieve equal pressure across the zones.

$$\frac{r_z}{h_z} = \Theta \equiv \frac{B/2}{h_{cyl}} \quad (9)$$

$$r_z = \sqrt[3]{\frac{\Theta}{\pi} \left(V_{cyl} - \sum_{j=1}^{z-1} V_j \right)} \quad (10)$$

$$\Delta w_z \equiv \Delta r_z = \Delta h_z \quad (11)$$

In influencing interzonal heat and mass transport modelling, the flow area is the overall surface area of the zone ($(radial)A_z + 2(axial)A_z$). Similarly, heat loss area is the total surface area of the combustion chamber, in the case that it is imposed only on the outer zone. Furthermore, with the outermost zone contacting all combustion chamber surfaces (liner, head and piston), a surface-averaged wall temperature is commonly prescribed.

This zonal configuration enables capture of the in-cylinder charge stratification profile in both radial and axial directions [103]. This is especially suitable for reflecting thermal stratification, evident from its shape. As such, the outermost zone stays cooler and temperature increases approaching the core zone. Taking advantage of this fact, some works aim to accurately model heat loss phenomenon by finer discretisation of the near-wall regions [104] and incorporating more sophisticated heat transfer submodels [96].

3.3. Spray-based multi-zone models

These models traditionally find their application in conventional diesel combustion (CDC) concepts where the phenomenology of diffusion-spray combustion must be captured accurately. As noted by Kook et al. [105], in the context of LTC, these models simulate concepts that maintain the coupling between combustion and injection event, such as PPC/PPCI/PCCI [106–109] and to some extent RCCI [58]. The focus of the current discussion is the singular work by Eichmeier et al. [58], where chemical kinetics was employed to simulate RCCI combustion. In contrast, the other approaches mentioned above use empirical correlations to model combustion end emissions, and so are considered out of scope of the present paper. However, the reader is directed to the work of Kumar et al. [53] for a comprehensive review on phenomenological spray combustion models.

These models' zonal configuration may be conceptualised as tracking the evolution of fuel spray in space and time, analogous to a Lagrangian description. Eichmeier et al. [58] adopted the popular packet approach originally proposed by Hiroyasu et al. [110]. The zonal configuration was a 2D discretised the spray space along axial and radial directions. The zones were identified by an ordered pair of indices, and a zone had up to four neighbours. Although the zones individually lacked shape, the zonal configuration on the whole was bounded by physical

characteristics of the spray. For the axial direction, the correlation for spray-tip penetration was used, as proposed in [110]. The configuration was set up with 15 zones in the radial direction and two zones in the axial direction, giving 30 zones in total. This choice was based on sensitivity analysis in which the model showed more ϕ_{diesel} stratification along the radial zones.

The working methodology is illustrated in Fig. 15, reflecting Eichmeier et al.'s use of the model for gasoline-diesel RCCI simulation. The premixed gasoline-air charge was represented by a single zone until the injection event. Starting at SOI, new zones were created in the axial direction at every time step. The packets were initialised with liquid droplets of diesel (SMD [111]) and thus included models for the evaporation process. Air entrainment into the packets was based on simple momentum balance in the axial direction, and on mass diffusion in the radial direction. Thus, the packet evolves to contain liquid diesel, diesel vapours, air, gasoline and burnt gas. The authors did not consider interzonal heat transfer, with thermal stratification due to heat loss (correlation) model and fuel evaporation. Therefore, diesel stratification was primarily captured across the zones.

Thus, it can be said that the model has the potential to capture complex multi-injection RCCI concepts. Equally, it should, in principle, be capable of reflecting transitional behaviour between RCCI and CDF combustion modes – an important advantage over onion-skin models. On the other hand, despite the rhetoric used in the paper, in our view the validity of the assumptions was not confirmed by the presented results. The heat-release shape showed clear double peak behaviour, suggesting separate combustion of diesel and gasoline fraction – a phenomenon not observed in RCCI. Furthermore, the limited application (singular) of these models in the context of chemical kinetics-based LTC studies makes it difficult to assess the capabilities of this approach. Accordingly, the following sections devote limited attention to this model.

3.4. Other related modelling approaches

3.4.1. Two-way coupled CFD – balloon models

While many MZ approaches employ CFD models as part of their initialisation or calibration routine (section 5), there are methodologies which fully couple the two models. These can be found under different names in literature: the most common are two-way coupled [112], fully coupled [80] and interactively coupled [113] CFD-MZ models. The approach was adopted in response to the poor emissions predictivity [83] of early MZ models. Its principle is to primarily run a CFD simulation but solve for chemistry at every time step within a MZ framework. By alleviating chemical kinetics calculation, this methodology can be identified as an accelerating technique for CFD, as noted by Wei et al. [114], where it resides among other techniques such as tabulated chemistry. Since two-way coupled CFD-MZ models are mainly CFD-oriented, they are not discussed explicitly in this review. The following text justifies this decision and highlights some differences with stand-alone MZ models.

To explain the approach briefly, there are two information streams connecting the CFD and MZ model. Analogous to the time-splitting approach, at every time step, the CFD solver advances without

computing chemistry, and passes information regarding the in-cylinder flow field to the MZ model. Using this, the MZ model then advances the chemistry solver to the same time step. The heat release information is fed back (remapped) to the CFD model, and the solution algorithm loop repeats. Fig. 16 is a schematic of the approach. The MZ model employed is usually of the simple balloon type [83]. Later works accounted for interzonal heat and mass transport, but it was done in an artificial manner, based on the heat-loss correlation [112] or drew from the CFD information [113]. Heat loss to walls was captured only in the CFD model. For forward mapping, parallels can be drawn to the sequential CFD-balloon approach (section 3.1), such as T- ϕ mapping. The real challenge, however, lies with backward mapping, which would introduce an error pertaining to artificial mixing/diffusion [80,114].

A comparison can be made with sequential CFD-balloon, since it is closest to the present approach. Results of the simple two-way coupled CFD-MZ model by Flowers et al. [83] showed that the error in UHC prediction reduced by a factor of 4.5 and CO prediction error reduced by factor of more than two. Interestingly, error in combustion duration increased by a factor of two. This can be attributed to errors introduced during the mapping procedures, as previously explained. Later approaches [115] were more sophisticated and achieved results closer to full CFD simulations. Regarding simulation speed, it can be expected that this approach is computationally heavier than stand-alone MZ approaches. In the analysis by Felsch et al. [113] the two-way coupled model was nearly two orders of magnitude slower than a sequential CFD-balloon approach. Nevertheless, as a CFD-accelerating technique, it can be about an order of magnitude [116] faster than full CFD runs. Thus apparent, these approaches are not similar to standalone MZ run over the closed cycle, and far from rapid, low-fidelity means for control-oriented modelling.

3.4.2. PDF-based multi-zone models

The authors acknowledge that there is a noteworthy body of literature based on so-called stochastic reactors (SR), which fall within chemical kinetics-based predictive, low-fidelity modelling for low temperature combustion. Each zone is a stochastic reactor and thermodynamic quantities of temperature and composition are modelled as probability density functions (PDF). They are popularly found in the form of single-zone (SZ) models used for concepts like HCCI [117], DI-HCCI [118] and PCI [119]. To the authors' knowledge, multizone stochastic reactor (MZ-SR) models are rare and some examples include the works by Montorsi et al. [120], Cao et al. [121] and Lundgren et al. [122].

Similar to the previously discussed multi-zone homogeneous reactor (MZ-HR) models, PDF-based MZ-SR models make a simplifying assumption on the in-cylinder flow field. Fundamentally, SR models differ from HR models in making the assumption of statistical homogeneity of the physical quantities within each zone. This is different from the spatial homogeneity in a zone for HR models. In practice, interpretation of the results obtained from SR models also differs. Taking the example of the in-cylinder pressure trace, each simulation run differs from the other [123] for the same set of initial conditions. This is analogous to the physical cycle-to-cycle variation.

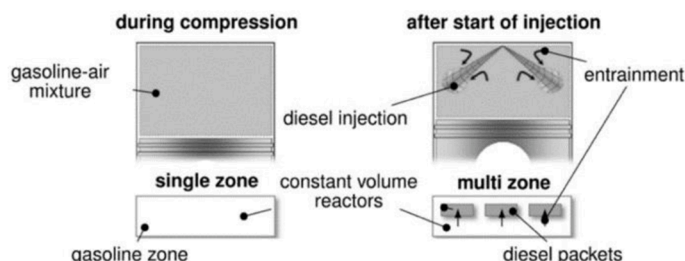


Fig. 15. Schematic of zoning approach in spray-based MZM for RCCI simulation [58]. (Reproduced with permission from SAE International)

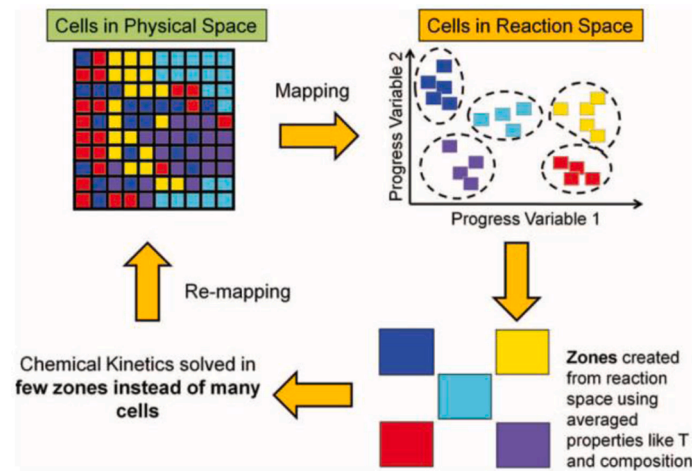


Fig. 16. Illustration of the two-way coupling between CFD and balloon MZM by Kodavasal et al. [115] (Reproduced with permission from Combustion Theory and Modelling, Taylor & Francis)

The governing equations of SR-MZ models track the temporal evolution of the probability distribution associated to each quantity of the zone. Statistical distribution is implemented via stochastic particles [124], each comprising its own temperature and chemical composition. The mass density function (MDF) transport equation [124] governs the nature of stochastic particles in a zone. The particles exchange heat and mass between each other and also experience wall heat loss. The submodels describing heat loss and interzonal mixing are also based on stochastic processes.

As such, a stochastic particle is analogous to a zone in MZ-HR models. Compared with MZ-HR models, SR models require large number of particles - usually around 50 - for reliable results [123]. On the other hand, Cao et al. [121] postulated the necessity of 200 particles in three zones to accurately reflect PCCI combustion. The zones were representations of bowl, squish and crevice regions. Error against experiments for CO emissions was 968 ppm and for UHC was 137 ppm, while achieving a simulation time of two hours. Montorsi et al. [120] divided the combustion chamber into two representative zones, core and BL. The BL zone consisted of 50 stochastic particles while the core was only one. Although the simulation lasted around three hours, they managed to obtain good trend predictions on emissions and combustion phasing quantifiers. In particular, the error in UHC predictions was 5 g/kWh and that for NO_x was 47 mg/kWh. Lundgren et al. [122] used two zones for their PPC simulation: a rich zone consisting of particles introduced due to fuel injection, and a lean zone consisting of the fresh charge. Interzonal heat and mass transfer captured the evolution of zonal stratification.

However, SR models depart from the modelling approaches discussed in the present review work. As the name suggests, they model in-cylinder inhomogeneity and mixing as a stochastic process. The governing equations, submodels and interpretation of results are substantially different, demanding extensive discussion on their own [97]. Thus, SR models will not be further covered in the current work.

4. Relevant submodels

The in-cylinder physics may be broken up into individual phenomena to efficiently manage model implementation. Each submodel encompasses distinct processes such as turbulence, wall heat transfer, interzonal heat and mass flows, etc. Specifically, this pertains to the terms on the right-hand side of the governing equations (Section 2.1). Therefore, submodels play an elemental role in the construction of an MZM. As with choice of zonal configuration and number of zones, selection of appropriate submodels to suit the application (LTC concept and type of study) influences the trade-off between model accuracy and

calculation time. It is worth reiterating that the submodels are phenomenological in nature, following the approach of thermochemical models. This section provides a detailed description of the submodels available in literature.

4.1. Wall heat transfer

These submodels aim to capture the process of heat transfer between the gas and combustion chamber walls. Historically, they have formed an integral part of combustion engine modelling studies intent on achieving tangible results. In terms of phenomenology, convection forms the dominant means of wall heat transfer in the context of most LTC concepts. Although a few studies [99,125] included the contribution of radiation, it is of minor importance owing to the lean, premixed nature of combustion resulting in low soot [126]. Thus, wall heat transfer is mainly restricted to the near-wall regions where temperatures are lower than that of the bulk gas. The temperature gradient is steep moving towards the wall, with a thin thermal boundary layer, in the order of a few millimetres [69]. Therefore, with slower reactions and delayed combustion, they are potential sites for formation of CO and UHC emissions.

These submodels are required for LTC modelling in order to reliably reproduce the heat release rate profile and emissions. They serve as a building block in MZ models for establishing the thermal stratification across the zones, thus influencing model predictivity for combustion phasing and peak pressure. The following text does not provide a detailed treatment of the phenomenology and historical development of heat transfer modelling. For this, the reader is directed to the excellent work by Komninos & Rakopoulos [66]. However, the goal here is to provide a comprehensive review of the modelling choices in MZ literature by classifying the approaches based on phenomenological sophistication, starting from simple, correlation-based approaches, and moving towards more fundamental treatment of the physics.

4.1.1. Correlation-based modelling

Models in this category capture the phenomenon of heat loss from the combustion chamber by employing empirical relations. They aim to provide a spatially averaged yet instantaneous value for wall heat flux by basing on bulk thermodynamic properties and scaling arguments on in-cylinder geometry. Using the temperature difference between bulk gas and combustion chamber walls, Newton's law of cooling (Eq. (12)) furnishes a lumped approach for capturing convection heat transfer. Since the quantity of interest is heat transfer coefficient (h) from gas to wall, the various approaches in literature were formulated towards its estimation.

$$\dot{Q}_{loss} = hA(T - T_{wall}) \tag{12}$$

Although originally intended for conventional CI and SI engines, the traditional approaches of Annand [127], Hohenberg [128] and especially Woschni [129], were popularly used in MZ models. Evidently, this leads to overpredictions in the context of LTC engines, as acknowledged by many works from experimental analysis [126], CFD results [58], single-zone [130] and MZ [131] models. In particular, radiation heat transfer is implicitly accounted for in correlations of Hohenberg and Woschni [66], thus amounting to 20-35 % of net heat loss [132], of which soot is a well-known contributor. Furthermore, some works [102, 133,134] explicitly appended a term for radiation (Eq. (13)), similar to the approach of Annand. They justified its inclusion in order to accurately model heat loss, with the main contributors being CO, CO2 and H2O. In (Eq. (13)) ζ_{rad} is a tuning factor and σ is the Stephan Boltzman's constant.

$$\dot{Q}_{loss,rad} = \zeta_{rad}A\sigma(T^4 - T_{wall}^4) \tag{13}$$

Nevertheless, the popular Woschni model was modified for use in the context of LTC MZ simulations, mainly pertaining to the estimation of characteristic velocity. This can be observed in the work of Ogink et al. [93] for gasoline HCCI combustion. Mehl et al. [135] coupled a 0D turbulence (K-k) model to the characteristic velocity relation to enhance the prediction of the heat loss (HL) correlation. Orlandini et al. [74] used separate HL correlations for simulating HCCI with different fuels; the

Woschni relation for diesel and Bargende [136] for gasoline. The landmark work by Chang et al. [126] set out to establish a universal HL model like the above, but applicable to HCCI-type heat release concepts. They conducted an extensive study on the suitability of the traditional HL correlations for HCCI engines, based on heat flux measurements from multiple locations. Basing on the Woschni approach, they proposed modifications including changes to the relation on characteristic velocity. Since its conception, the correlation by Chang et al. has been extensively used in literature.

The discussion thus far has focused on issues relating to the correlation itself. However, application in MZ models is not straightforward since the correlations were developed in the context of zero-dimensional or single-zone (SZ) models. The variety of implementations in literature offer a range of modelling choices. As discerned by Komninos & Rakopoulos [66], these can be split into two categories. One uses zonal averaged properties; the other is based on the local thermodynamic state of a zone. Thus, observing the canonical form of the heat loss correlation (Eq. (12)) each of the quantities in the relation can be treated in the above manner. Table 2 summarises the details.

The column 'zones applied' shows which of the zones in the MZM experienced wall heat loss. This is either 'all' or specific zones, in which case the number is presented in brackets. In the latter case they were typically described as boundary layer (BL) zones. This is typically a group of zones or a single zone representing the lumped region of boundary layer on combustion chamber surfaces. Then is the question of

Table 2
Tabulation of the modelling options of correlation-based wall heat loss models in MZM

Reference	Model	Concept	h calc.	Flow area	T	Zones applied	Distribution	Radiation term
Aceves et al. [75,76]	Woschni	HCCI	—	—	Zonal	5 or 7 BL zones	Equal weights	—
Aceves et al. [84]	Woschni	HCCI	Global	Global	Zonal	All	Equal weights	—
Aceves et al. [77]	Woschni	PCCI	Global	Global	Zonal	All	V_z/V_{cyl}	—
Noda & Foster [72]	Woschni	HCCI	Global	Global	Global	All	—	—
Babajimopoulos et al. [79]	—	HCCI	Global	Global	Zonal	All	V_z/V_{cyl}	—
Orlandini et al. [74]	Woschni (diesel) Bargende (gasoline)	HCCI/DI- HCCI	Global	Global	Global	All	V_z/V_{cyl}	—
Xu et al. [137]	Woschni	—	—	—	—	—	—	—
Kodavasal et al. [81]	Woschni	HCCI	Global	Global	Global	All	m_z/m_{cyl} *heat-loss multiplier	—
Hergart et al. [78]	Chang	PCCI	Global	Wall surface area fraction	—	All	Wall surface area fraction	—
Mehl et al. [135]	Woschni-Kk	HCCI	BL (based on adiabatic core)	Global	BL zone	BL zone	—	—
Easley et al. [94]	Woschni	HCCI	BL (based on adiabatic core)	Global	Zonal	BL zone + crevice	—	—
Ogink et al. [93]	Woschni	HCCI	Global	Global	Global	all	V_z/V_{cyl}	—
Tzanetakis et al. [67]	Chang	HCCI	Global	Global	—	BL zone	—	—
Visakhamoorthy et al. [138]	Chang	HCCI	Global	Global	—	BL zone	—	—
Guo et al. [134]	Woschni	HCCI	—	Global	—	BL zone	—	CO ₂ , H ₂ O & CO radiation
Voshtani et al. [102]	Chang	HCCI	Global	Global	—	BL zone	—	all zones
Komninos et al. [71, 139]	Annand	HCCI	Global ($f(Re)$ only)	—	BL	BL zone	—	BL zone
Nobakht et al. [140]	Chang	HCCI	—	—	—	—	—	—
Egüz et al. [100]	Chang	PCCI	Zonal	Zonal	Zonal	All	Zonal config	—
Egüz et al. [141]	Hohenberg	RCCI	Zonal	Zonal	Zonal	All	Zonal config	—
Kongsereparp et al. [99]	Woschni	HCCI	—	BL	BL	BL	Zonal config	all zones, $\zeta_{rad} = 0.6$
Kongsereparp et al. [89,133]	Woschni	HCCI	Zonal	Zonal	BL	3 BL zones	Zonal config	Yes, all zones
Kozarac et al. [90]	Woschni	DI-HCCI	Global	Zonal	Zonal	3 BL zones	—	—
Fathi et al. [142]	Chang	DI-HCCI	—	—	—	—	—	—
Nazoktabar et al. [125]	Chang	HCCI	—	Zonal	Zonal	3 BL zones	Zonal config	Yes, $\zeta_{rad} = 0.6$
Eichmeier et al. [58]	Chang (Hohenberg, Hensel)	RCCI	Global	Global	Global	All zones	V_z/V_{cyl}	—

how the cylinder-averaged heat loss may be distributed. This is shown under ‘distribution’, and has been based on fraction of in-cylinder mass [81]; fraction of in-cylinder volume [74]; fraction of total in-cylinder surface area [78]; or evenly distributed [84] (equal weights). The column ‘h calc’ refers to which set of thermodynamic quantities were used in computing the correlation. Here, ‘global’ refers to cylinder-averaged value; ‘zonal’ refers to the associated zones. The same choice arises with bulk temperature ‘T’ and the same notation is used.

Geometry of the zonal configuration becomes relevant when discussing the flow area for heat flux. In the ‘flow area’ column, ‘global’ refers to the overall in-cylinder surface area, while ‘zone’ denotes the surface area of the particular zone contacting the combustion chamber surfaces. It is evident that the latter concerns onion-skin models, thus, topology of the zonal configuration with respect to the combustion chamber geometry. This topic was covered in section 3.2, showing how flow area of zones can be computed.

Kodavasal et al. [81] followed a different approach by intrinsically tying thermal stratification to the correlation approach for heat loss. Their balloon model used Woschni correlation to compute bulk cylinder heat flux and it was distributed among the zones based on weights they called heat-loss multipliers. This is shown as c_z in Eq. (14) and Eq. (15). The former was used for the compression phase; the latter was used once ignition occurred. Eq. (14) relied on CFD results under motoring conditions, where an approach similar to T-m distribution determined $T_{z, TDC, CFD}$ of each zone. $T_{adb, TDC}$ refers to a hypothetical adiabatic temperature of the in-cylinder gases reached, should there be no heat loss. $T_{adb, TDC}$ was obtained assuming that the cylinder mass underwent isentropic compression until TDC, and simple thermodynamic relations were employed to this end. Importantly, Eq. (14) is supposedly evaluated only once, during model calibration for a given engine geometry. Section 5.4 provides further details of this. On the other hand, quantities in Eqs. (15) and (16) were obtained directly from the MZM. T_{avg} is the averaged zonal temperature and ξ is a normalising factor, defined in Eq. (16) and used to maintain consistency between the cumulative heat loss by all zones and the bulk heat loss predicted by the correlation. The effect of the approach can be observed in the left-hand plot of Fig. 17, where temperature of zones decreases with the zone index. Fig. 17’s right-hand plot shows the values of heat-loss multipliers of the corresponding zones. Note that c_z for the innermost zone is zero, in order to maintain it as the warmest zone.

$$c_z = \frac{T_{adb, TDC} - T_{z, TDC, CFD} \cdot m_z}{T_{adb, TDC} - T_{avg, CFD} \cdot m_{cyl}} \quad (14)$$

After ignition

$$c_z = \frac{1}{\xi} \frac{T_z - T_{wall} \cdot m_z}{T_{avg} - T_{wall} \cdot m_{cyl}} \quad (15)$$

$$\xi = \sum_z \frac{T_z - T_{wall} \cdot m_z}{T_{avg} - T_{wall} \cdot m_{cyl}} \quad (16)$$

So much diversity in implementation means it is challenging to make

definitive statements regarding the most appropriate approach. The design choice is coupled with the implementation of zonal configuration and interzonal flows. Dealing with a similar situation for heat loss correlation, Komninos & Rakopoulos [66] note that, at least in the context of HCCI simulations, the question remains open. However, Komninos [88] also mentions that the error in combustion predictions across the HL correlations is usually systematic in nature. Based on this fact, the obtained heat transfer coefficient may simply be scaled by matching, for instance pressure curve or available wall heat flow data, as in the work of Barroso et al. [143] or Eichmeier et al. [58].

From a holistic perspective, the authors opine that the correlation-based approach is most suitable for balloon-type models. Consequently, Aceves et al.’s [73] approach, of computing the cylinder-averaged heat loss coefficient and then apportioning it among the zones based on individual zone temperatures and mass, appears closest to the procedure used in designing the HL correlation itself. From onion-skin MZM onwards, the more rigorous means of zonal discretisation deviates from the lumped nature of capturing physics as used in HL correlations. Furthermore, it is desirable that physics-based modelling of interzonal heat flows in onion-skin MZM matches the modelling approach for wall heat loss, as will be explained in physics-based approaches, below.

A perception of the sensitivity of the modelling choices in balloon MZM can be obtained by comparing the simplest and most sophisticated option. The models of Flowers et al. [82] and of Kodavasal et al. [81] both implemented Woschni correlation in a 40-zone MZM for HCCI simulation by disregarding interzonal heat and mass flows. However, Kodavasal et al.’s approach was sophisticated in its ability to reflect the profile of thermal stratification and in being a stand-alone balloon MZM. Our analysis of their results focuses on emissions predictions. In the best case, Kodavasal et al.’s model predicted CO within 400 ppm; the error in the worst case was over 900 ppm. For HC emissions, best case was within 600 ppm and the worst was over 900 ppm. In the work of Flowers et al., the error in CO predictions was 600 ppm and for HC it was 200 ppm. Evidently, the question regarding suitable modelling choices for balloon MZM is still open. Nevertheless, it can be said that the attempt by Kodavasal et al. to create a stand-alone MZM based entirely on heat loss modelling shows potential against the coupled CFD-balloon model.

4.1.2. Fundamental approach

Broadly, the approaches described in the following text aim to circumvent use of the heat loss correlations. By basing on physics, the fundamental thermal condition of the boundary layer given in Eq. (17), is used. The quantity of concern in Eq. (17) is the temperature gradient, with r_n being a coordinate normal to the wall. Therefore, the approach is most suitable for onion-skin type models where its zonal configuration has a geometric association to the in-cylinder space. Specifically, the condition is applied to the outermost zone or BL zone/s as discussed in section 3.2. In fact, in the review work by Komninos & Rakopoulos [66], the authors reason that the interzonal heat transfer and cylinder-wall heat loss phenomena are coupled. They emphasise that it is imperative

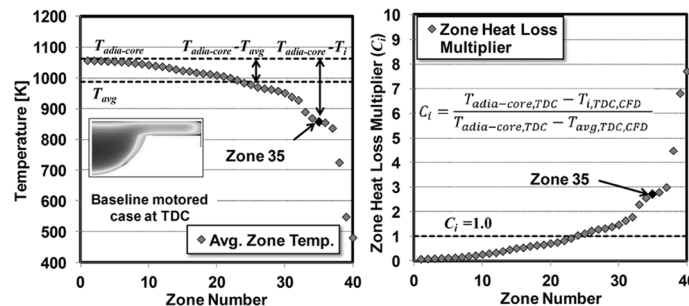


Fig. 17. Approach of leveraging heat loss correlation to set up zonal thermal stratification according to Kodavasal et al. [81]. Temperature distribution across the zones (left) heat-loss multipliers of zones (right). (Reproduced with permission from International Journal of Engine Research, SAGE)

to have a consistent modelling approach across both processes (Ex. diffusion based). On the contrary, among the previously discussed models, for instance in [102], interzonal heat flow was based on the diffusion approach, and heat loss was modelled using correlations. Komninos & Rakopoulos state that this inconsistency might inhibit the MZMs ability to capture combustion performance accurately.

$$\dot{q} = -\Lambda_{gas,r_n=0} \left. \frac{\partial T}{\partial r_n} \right|_{r_n=0} \quad (17)$$

Neshat & Saray [131] used a simple linear approximation (Eq. (18)) of the gradient by assuming a thickness of the BL zone, based on the combustion chamber geometry (see section 3.2.1). The temperature difference involved T_{wall} and that of the BL zone ($T_{z=BL}$). They validated this approach on HCCI using a wide range of operating conditions, including different fuelling – methane and n-heptane. The evaluation methodology was indirect, i.e., based on cylinder pressure and emissions data. Furthermore, they compared the results against the correlation-based approaches of Annand, Hohenberg, Woschni and Chang. Based on a 10-zone model, the results showed that the pressure trace fit of the fundamental approach was better than the correlations implementation. Emissions results of this fundamental approach also agreed much better with the experimental data than the correlations. On the other hand, worth noting that emissions predictions are in part influenced by interzonal mass transfer. Nevertheless, the authors showed the potential of this approach over the correlation models.

$$\left. \frac{\partial T}{\partial r_n} \right|_{r_n=0} \approx \frac{T_{z=BL} - T_{wall}}{\Delta w_{z=BL}/2} \quad (18)$$

In the analysis of Komninos [88], the authors aimed at better capturing the temperature profile in the near-wall region. They assumed the gradient to be of the form Eq. (19), based on a (one-sided) second order approximation of (an assumed) T profile near the wall. This form was used only when $T_{mean} > T_{wall}$ and $T_{wall} < T_{z=BL} < T_{z=BL-1}$. Eq. (18) was used for the other cases. The authors then [104] validated the approach using CFD models of three different engines under motoring operation, using heat flux data and monitoring the T profile at the near-wall region. They used the same enclosed zonal configuration as the previous work, but used more zones - 16. Based on a 'grid dependency' study, the authors showed that although the zone number could be reduced, the zone thickness had to be progressively smaller near the wall, to capture the T profile well. Furthermore, due to switching between the two relations, Eq. (18) and Eq. (19), the expected discontinuity was rather small, given that sufficient zones were present at the boundary region. Ultimately, the authors in another study [88] proved that for HCCI combustion simulations, this approach captured the pressure trace and HRR well, and closely captured the emissions trend.

$$\left. \frac{\partial T}{\partial r_n} \right|_{r_n=0} \approx \left(\frac{T_{z=BL} - T_{wall}}{\frac{\Delta w_{z=BL}}{2}} \right)^2 \left(\frac{T_{z=BL-1} - T_{z=BL}}{\frac{\Delta w_{z=BL} + \Delta w_{z=BL-1}}{2}} \right)^{-1} \quad (19)$$

Bissoli et al. [96] went a step further by incorporating a wall-function formulation for the thermal boundary layer, by Han & Reitz [144]. This is a more sophisticated submodel, based on the solution of the energy equation at the boundary layer. Such submodels are typically applied in the context of CFD, but the authors adapted it for use in their MZM. As in the previous two works, the authors established an enclosed zonal configuration, and the heat loss model was applied to the BL zone. Thickness of the BL zone changes as a result of interzonal work exchange, which in turn was accounted for in Eqs. (22) and (23). It is important to note that although Eq. (20) represents the analytical solution, there are still some empirical aspects to it. Based on trends in experimental data, an assumed function for the variation of (μ_{tur}/Pr_{tur}) with y^+ is used, resulting in Eqs. (22) and (23). Also, the tuning parameter ζ_{wall} in Eq. (21) needs to be adjusted for a given engine geometry. Thus, the authors successfully tuned and validated their

submodel, based on heat flux and wall temperature profile data from different engines (CFD) and across different operating points (motoring). Furthermore, compared with the previous implementation by Komninos & Kosmadakis [104], the error in heat flux trace was similar and the discontinuity mentioned above was avoided.

$$Q_{wall} = A \frac{u_{wall}^*}{T^+} (\rho c_p T)_{z=BL} \ln \left(\frac{T_{z=BL}}{T_{wall}} \right) \quad (20)$$

$$u_{wall}^* = \zeta_{wall} S_P \quad (21)$$

$$T^+ = \begin{cases} 7.42 \tan^{-1}[0.0037(24y^+ + 25)] - 0.69 & , y^+ \leq 40 \\ 8.89 + 2.098 \ln(3.34 \cdot 10^4 y^+ + 10^5) - 29.74 & , y^+ > 40 \end{cases} \quad (22)$$

$$y^+ = \frac{u_{wall}^* \Delta w_{z=BL} \rho_{z=BL}}{\mu_{z=BL}} \quad (23)$$

In a similar vein, Fiveland & Assanis [145,91] focused on modelling the physics of wall heat loss by capturing the entirety of the boundary layer phenomenon, comprising boundary layer growth, trapped mass in boundary layer and near-wall turbulence. Their study [145] employed a two-zone model consisting of a dedicated BL zone and an adiabatic core zone. The wall-heat transfer coefficient was obtained by integrating over the BL thickness (δ_{BL}) according to Eq. (24), where y was a coordinate normal to the cylinder walls. Thickness of BL zone varied with time as prescribed in Eq. (25), which was obtained by applying a one-dimensional compressible energy equation [146]. Variation of density (ρ) with y was assumed to follow a cubic shape according to Eq. (26), which was subjected to boundary conditions of Eq. (27). Similarly, variation of the effective Prandtl number (Pr_{eff}) within the BL zone followed the approach [144]. Finally, mass transfer with the core zone was considered as a result of variation in density and thickness of the BL zone.

$$h = \int \frac{1}{\delta_{BL} \frac{c_p}{\rho c_p} \left(\frac{\mu_{eff}}{Pr_{eff}} \right)} dy \quad (24)$$

$$\frac{d\delta_{BL}}{dt} = \frac{1}{c_p \frac{P}{R_g}} \left[-\delta_{BL} \frac{c_p}{R_g} \frac{dP}{dt} + c_p T_{z=BL} \frac{d}{dt} \int_{\delta_{BL}} (\rho dy) + q_w \right] \quad (25)$$

$$\rho = \rho_{core} \left[a_1 + a_2 \frac{y}{\delta} + a_3 \left(\frac{y}{\delta} \right)^3 \right] \quad (26)$$

$$y = 0 \quad \rho = \rho_{wall}(t) \\ y = \delta \quad \begin{cases} \rho = \rho_{core}(t) \\ \frac{d\rho}{dy} = 0 \end{cases} \quad (27)$$

Fig. 18 depicts the predictions of the two-zone model, which exhibits variation of density, thickness and trapped mass in the BL zone. Results were in qualitative agreement with data from literature [147], although the latter was for conventional SI operation. Nevertheless, their model predicted an increase in thickness during compression from 0.5 mm to 2 mm, and 30-35 % of in-cylinder mass trapped in the BL zone at the time of ignition. In a follow-up study [91], the authors enhanced their model to capture the axial variation of the boundary layer. They proposed to axially discretise the BL region, thus creating or erasing zones in accordance with piston motion (see Tab. 1). Results showed trend-wise predictions in emissions, with UHC overpredicted by 20 % and CO underpredicted by 50 %. Ignition angle was within 1-2 CAD and combustion duration within 7 CAD.

4.1.3. Wall temperature

From the canonical equation (Eq. (12)) for wall heat loss, the final quantity required is that of combustion chamber wall temperature

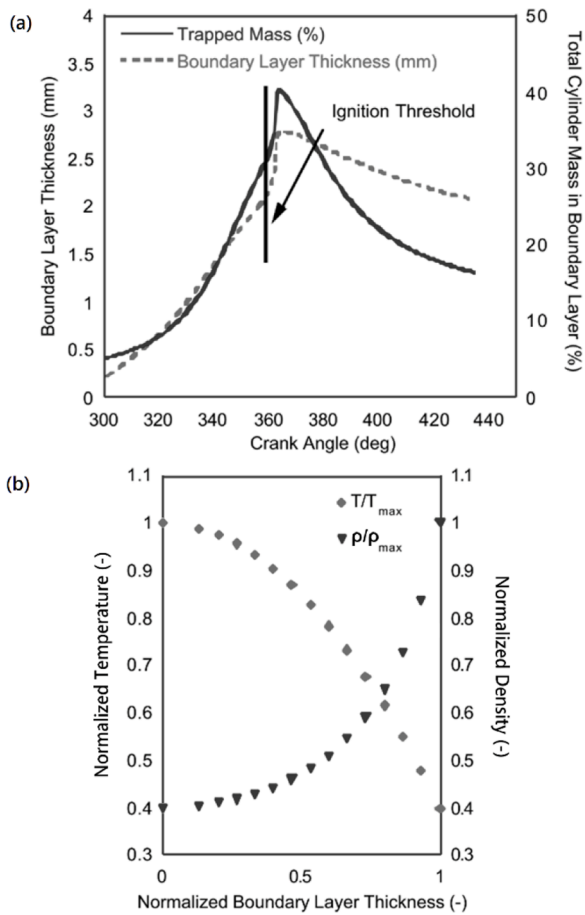


Fig. 18. Evolution of thickness and mass trapped within boundary layer zone (a) and variation of density and temperature with thickness of the BL zone (b), according to the work of Fiveland & Assanis [145]

(T_{wall}). The simplest approach involves imposing a fixed value by making educated guesses, for instance, based on coolant data [58]. As such, T_{wall} was usually considered constant across operating conditions, and furthermore, no distinction made among in-cylinder surfaces.

Nevertheless, with chemical kinetics-driven combustion being so sensitive to the in-cylinder thermal state, some research works included a sensitivity study of T_{wall} on model predictivity. Bissoli et al. [96] varied the surface-averaged T_{wall} from 400K to 500K, noticing a 2 % change in combustion phasing. Easley et al. [94] similarly showed that for HCCI simulations, increase in T_{wall} from 370 to 410K gave IMEP sensitivity of 6 %, 4 % for UHC and 22 % for NO_x .

Thus, to capture physics accurately, the model must encompass heat transfer processes from gas to wall, across the cylinder wall and wall to (liquid) coolant. To this end, there are sophisticated approaches such as finite element-based wall-temperature solvers [51]. Work by Fonseca et al. [148] provides an overview of other available approaches. However, for MZ modelling, the following approaches are considered more sophisticated than the simpler ones already mentioned.

Kongsereeparp & Checkel [149] employed a correlation to obtain surface-averaged wall temperature from measurement data of engine load and coolant temperature, as shown in Eq. (28). They also included a term to account for the effect of knock, correlating it to peak PRR. On the other hand, estimates of component surface temperatures can be obtained by following the approach by Kodavasal et al. [81]. They applied the correlation [150] based on readily available cylinder-head temperature data to provide estimates on liner Eq. (29) and piston Eq. (30) temperatures.

$$T_{wall, avg} = T_{cool} + \frac{rpm}{6} (0.945 - 0.0078 \cdot T_{cool}) + 4.2 \cdot IMEP \quad (28)$$

$$T_{pist} = 2(T_{head} - T_{cool}) + T_{cool} \quad (29)$$

$$T_{linr} = 5/16 \cdot (T_{head} - T_{cool}) + T_{cool} \quad (30)$$

Mikulski et al. [92] formulated an advanced approach to compute time-averaged, in-cylinder surface temperatures \bar{T}_{wall} , and attempted to utilise readily available engine measurement data. Proposed in their earlier work [151], the approach considered the three-way heat transfer between gas side to wall, and eventually from wall to coolant. In Eq. (31), \bar{h} is the bulk gas heat transfer coefficient, U_{wall} is overall heat transfer coefficient of the individual surfaces indexed with wall. The overbar represents the cycle time-averaged quantity, so \bar{T}_{wall} is the weighted average of bulk gas temperature and coolant temperature. In the computation of U_{wall} (Eq. (32)) the material properties of the individual surfaces were considered, namely thermal conductivity (k) and material thickness (δ_{wall}), in addition to heat transfer coefficient of coolant (h_{cool}). Since Eq. (31) relies on time-averaged data of h and T , it was proposed to obtain them from the model itself, by running the MZM in cycle-to-cycle connection. Section 5.4 gives further details of this.

$$\bar{T}_{wall} = \frac{\bar{h}\bar{T} + \bar{U}_{wall}T_{cool}}{\bar{h} + \bar{U}_{wall}} \quad wall \in \{head, pist, linr\} \quad (31)$$

$$\bar{U}_{wall} = \left(\frac{1}{\frac{1}{h_{cool}} - \frac{\delta_{wall}}{k_{wall}}} \right) \frac{1}{t_{cycle}} \int_{t_{cycle}} h dt \quad wall \in \{head, pist, linr\} \quad (32)$$

4.2. Interzonal heat transfer

The purpose of inter-zonal heat transfer is to emulate the effect bulk fluid motion has on the thermal state of the in-cylinder charge. Heat is exchanged between neighbouring zones by virtue of the relative difference in their thermal state. This means of interaction is essential, because, as Komninos & Rakopoulos [66] noted, the absence of external means of ignition signifies a strong coupling between chemical kinetics and heat transfer. Jia et al. [85] studied the sensitivity that heat exchange had on HCCI combustion performance and emissions. Between interzonal work exchange and interzonal heat flow, combustion efficiency showed an increase for the latter case, and so did burn duration. UHC showed particularly high sensitivity, exhibiting a reduction of 120 %.

Note that the term ${}^{(E)}F_z$ in energy conservation Eq. (2) encompasses contributions of two processes (Eq. (33)). The first is due to the temperature difference between zones, analogous to heat conduction. The second comes from the bulk mass transfer between zones, transporting enthalpy. Ideally, both contributions are included but implementations vary across MZM studies. The choice is partially constrained by the zonal configuration. For instance, the diffusion-based heat flow requires information on zonal geometry and topology, thus is found only in onion-skin type models. Furthermore, as discussed in the previous section, there is the elemental coupling between interzonal heat transfer and wall heat loss. Studies that modelled heat loss only on the BL zones require interzonal heat transfer to reinforce thermal stratification across all zones. With this means of zonal interaction playing such a decisive role, the following text elaborates on the mechanisms implemented in MZM.

$${}^{(E)}F_{z \rightarrow z+1} = IZT \dot{Q}_{z \rightarrow z+1} + IZT \dot{m}_{z \rightarrow z+1} \hat{h}_z \quad (33)$$

4.2.1. Based on diffusion

This is a physics-based approach, popularly used in onion-skin models. Heat flux between zones is driven by temperature gradient and is based on the Fourier's conduction law, as in Eq.(34). The

proportionality constant, Λ , is based on thermal conductivity of the gas mixture. Although laminar conductivity has been used [99], it proved insufficient [100] to capture the effects of macroscale mixing on heat flow. The influence of turbulence is reflected by enhancing the diffusion mechanism by multiplying the effect of laminar conductivity. Section 4.4 examines the connection to a turbulence submodel in greater detail.

Choice of zonal configuration plays an important role in determining the total heat flow, which mainly pertains to, interzonal interface area (A) and zone thickness (Δw). These quantities change with crank angle, since dimensions of the zones evolve during the cycle. In addition, zonal configuration provides information on the number of neighbouring zones. Along with thermal conductivity (Λ), these quantities need to be determined at the interface between zones, to which end, the common practices employed in finite volume methods [152] may be used.

$${}^{IZT}\dot{Q}_{z \rightarrow z+1} = \left(\Lambda A \frac{\Delta T}{\Delta w} \right)_{z \rightarrow z+1} \quad (34)$$

Among onion-skin models, heat flow can occur along radial (curved surface) and axial (flat surface) directions of a zone. Furthermore, heat flux can be different across the curved and flat surfaces when different neighbours lie along radial and axial directions [89,125]. For example, the work by Neshat & Saray [87,131] used a single enclosed-type zone representing the BL, which encompassed the remaining annular zones. Heat flow among the annular zones occurred along a radial direction and was modelled according to Eq. (35). Additionally, each annular zone exchanged heat with the BL zone in the axial direction, which was simply calculated according to Eq. (34). In an enclosed MZM, heat flux is uniform for both directions, with Δr referring to zone thickness and A being the overall surface area. In an annular MZM, the flow occurs only in the radial direction, as in the work of Egüz et al. [100,141].

$${}^{IZT}\dot{Q}_{z \rightarrow z+1} = \frac{\pi l (T_{z+1} - T_z)}{\ln \left(\frac{r_{z+1}}{r_z + \frac{\Delta r_z}{2}} \right) + \ln \left(\frac{r_{z+1} + \frac{\Delta r_z}{2}}{r_z} \right)} \quad (35)$$

4.2.2. Based on enthalpy transport

This is the heat exchange associated with interzonal mass flow, by virtue of thermal energy contained by the moving mass. Thus, unlike the diffusion-based mechanism, the heat flow's magnitude and direction are based on the transferred mass. So, if a model captures both interzonal heat and mass flow, both processes make contributions to the heat exchanged, as shown in Eq. (33).

As mentioned, while all studies that enable interzonal mass transfer include this mechanism, some differences in implementation still exist. In the work of Komninos et al. [71,88,139], there was no explicit mention of interzonal enthalpy transport. In stark contrast, enthalpy transport was the sole mechanism to capture interzonal thermal flow in the approach used for works [78,93,94]. Easley et al. [94] and Ogink & Golovitchev [93] allowed interzonal mass flow only among the outer core zone, crevice zone and BL zone, so enthalpy transport occurred among these zones. In the one-way coupled CFD-balloon model of Hergart et al. [78] the mass flow (section 4.3) causing enthalpy transport was interestingly based on wall heat loss correlation. Kozarac et al. [97] followed an empirical approach as in Eq. (36). $\Delta Q_{z \rightarrow z+1}$ was referred to as heat transfer potential, and ζ_{HTP} was actually a tuning parameter. Although their description of heat transfer potential was sparse, it is our understanding that it may have referred to the difference in enthalpy between neighbouring zones ($m_z c_{p,z} T_z - m_{z+1} c_{p,z+1} T_{z+1}$). Although it may be understood that tuning of ζ_{HTP} will be case dependent, Kozarac et al. set it to a constant value of 1e-3 s. Ultimately, in terms of results, they were able to reasonably capture the qualitative trends in CO and HC with λ .

$${}^{IZT}\dot{Q}_{z \rightarrow z+1} = \frac{\Delta Q_{z \rightarrow z+1}}{\zeta_{HTP}} \quad (36)$$

4.2.3. Based on heat-loss correlation

This mechanism for interzonal heat flow is simply based on the heat loss correlation, as discussed earlier (Section 4.1). As such, the heat flow is proportional to the temperature difference between neighbouring zones and flow area. The heat transfer coefficient is computed from the bulk properties of the cylinder gas. This approach was used by Tzanetakakis et al. [67] and Visakhamoorthy et al. [138], both of whom used the Chang correlation [126]. Due to connection with zonal configuration, both authors used the enclosed-type MZM.

The physical basis for this approach exploits the assumption that turbulence stays relatively homogeneous throughout the combustion chamber. This is supported by the fact that both authors used their MZM to simulate HCCI combustion. Specifically, Tzanetakakis et al. [67] stated that their experimental engine was designed to minimise the spatial variation of turbulence. Chang et al. [126] concluded that spatial variation of heat flux was small from different measurement locations within the cylinder. One of the modifications they made in computing the heat transfer coefficient was on the estimation of bulk gas velocity.

It is important to note that both models [67,138] did not enable interzonal mass exchange. As a connecting point, wall heat transfer in both models was prescribed on the outermost (BL) zone, following from zonal configuration. Still, the results of [138] indicate this approach was able to achieve a representative thermal stratification.

4.3. Interzonal mass transfer

Earlier attempts relied on work exchange between zones (coupled to heat exchange) to achieve combustion predictions, but these studies were limited to HCCI. Nevertheless, it became increasingly apparent that interzonal mass transfer was necessary for reliable predictions of engine-out emissions and for application to fuel-stratified LTC concepts. This is because formation of emission is spatially inhomogeneous. CO and UHC occur in the cooler crevice and BL regions [153], due to incomplete combustion, while NO_x forms in the core region, due to high temperatures. Komninos & Hountalas [139] observed the flow of emissions species and noted that CO and HC move to the outer core region during the expansion stroke, where they undergo partial oxidation. Additionally, there is some production of CO during this phase, due to partial oxidation of HC. Thermal mixing of the hot and cold regions as a result of enthalpy transport also influences overall predictions of combustion performance.

To this end, there are a variety of approaches to capture the interzonal mass exchange. For instance, Hergart et al. [78] modelled it as proportional to the wall heat transfer (correlation) coefficient. Perhaps the motivation for their approach was: (i) wall heat transfer coefficient being a cylinder-averaged value; and (ii) isotropic turbulence assumption. Fiveland & Assanis' approach [145] was based on modelling the boundary layer phenomenon, where mass flow across the BL zone was a consequence of the time evolution in its thickness and thermodynamic conditions. Broadly, however, there are two main approaches for capturing interzonal mass flows; one based on the pressure equalisation mechanism, the other on the diffusion mechanism.

4.3.1. Based on pressure equalisation (P_{EQ}) mechanism

This is a phenomenological-based approach for mass transfer widely used among onion-skin MZM, for example in the enclosed model of Komninos et al. [71] and in the annular model of Neshat & Saray [87]. It takes advantage of the governing assumption (section 2.1) that the zones share a common pressure. The mechanism is unlike that of convection or diffusion, and occurs as a result of zonal mass readjustment due to pressure equalisation, as discussed in section 2.3. It was also mentioned that interzonal work exchange is absent in the context of P_{EQ} mass

transfer, since both are governed by the same process.

In implementing this approach, the time-splitting solution algorithm is used, as will be explained in section 5.1. Briefly, the solution of the system of equations at every time step is split into a sequence of chemistry solution and flow solution. The chemistry step occurs by disregarding interzonal exchange, and similarly, chemistry is not considered in the flow step. Of importance for P_{EQ} mass transfer, is the consideration that the zones in the chemistry step are non-interacting constant volume reactors. Consequently, by the end of the time step, the zones would have developed disparate pressures. In the ensuing flow step, this serves as the driving force for interzonal mass transfer.

Thus, the methodology is described in the following steps. First, the equalised zonal pressure (P_{cyl}) is calculated according to Eq. (6). Based on it, the zonal mass is computed, as in Eq. (37). In order to quantify the interzonal mass exchanged, the change in mass of a zone over a time step is calculated by Eq. (38). Thus, mass exchanged (${}^{IZT}m_z$) by zone z with its neighbours $z-1$ and $z+1$ is Eq. (39), which in turn is subject to boundary conditions in Eq. (40). The boundary conditions follow from the zonal configuration, where change in mass of zones located at the periphery, i. e., innermost and outermost zones, is the mass exchanged with their respective neighbours. Furthermore, the associated exchange of species as in the term ${}^{(Y)}F_{i,z}$ of Eq. (3), can be expressed as Eq. (41).

$$m_z = \frac{1}{R_u} \frac{P_{cyl} V_z \bar{M}_z}{T_z} \quad (37)$$

mass change from time step $t-1$ to t

$$\Delta \dot{m}_{z,t} = \frac{m_{z,t} - m_{z,t-1}}{\Delta t} \quad (38)$$

$$\Delta \dot{m}_{z,t} = {}^{IZT} \dot{m}_{z \rightarrow z+1} - {}^{IZT} \dot{m}_{z-1 \rightarrow z} \quad (39)$$

Subject to boundary conditions

$$\begin{aligned} {}^{IZT} \dot{m}_{1 \rightarrow 2} &= \Delta \dot{m}_1 \\ {}^{IZT} \dot{m}_{nZ \rightarrow nZ-1} &= \Delta \dot{m}_{nZ} \end{aligned} \quad (40)$$

Species exchange

$${}^{(Y)}F_{i,z-1 \rightarrow z} = \frac{{}^{IZT} \dot{m}_{z-1 \rightarrow z}}{m_z} (Y_{i,z} - Y_{i,z-1}) \quad (41)$$

An algorithm illustrating the process is shown in Fig. 19, taken from the work of Komninos et al. [71]. Between the chemistry and flow step an error is introduced as a result of the interzonal mixing. As such, the flow step is iterated over a loop until the conservation equations of mass and energy are satisfied.

Finally, it is worth noting that turbulence effect is not explicitly considered in the bulk motion. This reduces modelling complexity. On the other hand, the iteration scheme could be a potential source of computational load, as it introduces stiffness in the system of differential equations. Section 5.1 examines this aspect more closely.

4.3.2. Based on diffusion

In this approach, the diffusion mechanism drives mass flux, which is based on the Fick's law Eq. (42)). Thus, the composition gradient dictates direction and magnitude of the flow, so geometry of the zones and topology of the configuration are central to its computation. This approach is widely used in onion-skin models. Eq. (42) represents the mass flow at the interface between zones $z-1$ and z . Since the mass exchanged consists of a bulk component dm_z/dt and passive scalar $dY_{i,z}/dt$, (associated to ${}^{(m)}F_z$ and ${}^{(Y)}F_{i,z}$ respectively), for ease of implementation, the corresponding Eqs. (1) and (3) may be combined giving species mass balance, as in [100]. As before, with the requirement of the quantities \mathcal{D} , ρ and dr being at the zonal interface, approaches used in finite volume methods [152] may be adapted.

$${}^{IZT} \dot{m}_{i,z \rightarrow z+1} = \left(\mathcal{D} \rho A \frac{\Delta Y_i}{\Delta w} \right)_{z \rightarrow z+1} \quad (42)$$

It is important to note that in the above equation, the diffusion coefficient is presented in a generic form. Owing to the consideration of multiple components (species) in the system, different models [154] are available to capture the phenomenon of molecular diffusion. However, within the scope of the reviewed literature, 'mixture-averaged' and 'unity Lewis number' approximations have been used. The former was incorporated in the work of Bissoli et al. [96], and the diffusion coefficient identifies differently for each species, as shown in Eq. (43), with \mathcal{D}'_{ji} as the binary diffusion coefficient [154]. On the other hand, in unity Lewis number approximation, the diffusion coefficient is independent of the species and given as Eq. (44). It was used in the work of Egüz et al. [100]. Although the mixture-averaged approach is a more accurate model for molecular diffusion, unity Lewis number approximation facilitates modelling by reducing computational load.

$$\mathcal{D}'_i = \frac{1 - Y_i}{\sum_{j \neq i} X_j / \mathcal{D}'_{ji}} \quad (43)$$

$$\mathcal{D} = \frac{k}{c_p \rho} \quad (44)$$

Nevertheless, modelling interzonal mass flux solely based on molecular diffusion proves largely insufficient to reflect the in-cylinder flows. In-fact, the flux influenced by turbulence can effectively be 1000 times higher [100]. To this end, the model presented here needs to be coupled with a turbulence submodel, described later in section 4.4. Regarding computation of the gradient and flow area, which, as mentioned earlier, depends on zonal configuration, Egüz et al. incorporated this submodel on their annular MZM for simulation of PCCI [100] and RCCI [141]. Here the flow area is the curved surface area (in the radial direction). In the work of Bissoli et al [96], the enclosed configuration was used to simulated HCCI. In their case, the flow is symmetrical in the axial and radial directions.

The implementation by Eichmeier et al. [58] followed a different approach, since their basis was a spray combustion MZM. From their model description in section 3.3, interzonal mass transfer referred mainly to the entrainment of charge from the premixed charge zone (z_{air}) to the spray zones (z_{ax} and z_{rd}). As such, the mass flow was one directional. Entrainment before EOI was defined according to Eq. (45)

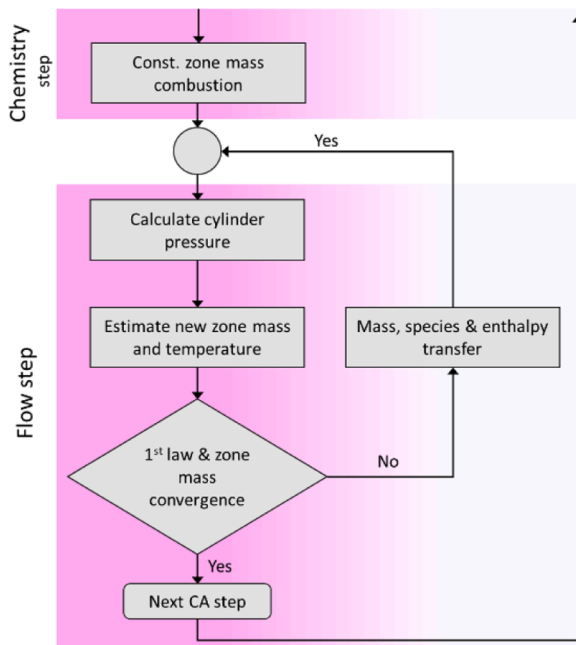


Fig. 19. The algorithm for P_{EQ} -based mass transfer, adopted from the work of Komninos et al. [71]

which used the assumption that momentum of diesel droplets exiting the nozzle equals the rate of entrainment of charge into the spray zones. Here the variation in mass flow was along the axial zones (z_{ax}). After EOI, entrainment was defined according to the diffusion process (Eq. (46)), with flow occurring mainly along the radial zones (z_{rad}). The equation was derived as the analytical solution to a point source diffusion problem. ζ_{mix} is an adjustable constant and \mathfrak{D} and τ refer to turbulence diffusivity and turbulent timescale respectively, which were obtained from a turbulence submodel (explained in section 4.4).

$$ax \dot{m}_{air \rightarrow z} = \frac{m_{diesel} u_{0inj}}{s} Y_{air} \text{ for } t < EOI \quad (45)$$

$$rad \dot{m}_{air \rightarrow z} = \zeta_{mix} \frac{m_{air}}{\tau} \exp\left(\frac{a z_{rad}^2}{\mathfrak{D} t}\right) \text{ for } t > EOI \quad (46)$$

4.4. Turbulence

Since the flow regime in the combustion chamber is fully turbulent, the combustion process is globally influenced by it, from the temperature and fuel stratification to emissions formation. However, the findings of Aceves et al. [84] are noteworthy, as they showed that combustion's sensitivity to turbulence varies during the cycle. Turbulence has a small effect during the main heat release event, due to the high HRR (tested for IMEP 6.5-7.3 bar). In other words, the timescale of chemical kinetics is much too fast for the fluid motion to have an effect. But turbulence certainly impacts the events before and after the heat release, i.e., charge stratification, ignition and emissions formation.

Importantly, turbulence also affects wall heat loss and the boundary layer phenomenon. Works by Aceves et al. [84] and Yu et al. [155] show that higher levels of turbulence cause more heat loss, a thicker boundary layer and lower bulk cylinder temperatures. Accordingly, the contribution of turbulence is implicit in submodels for heat loss. Furthermore, as explained in Section 4.1, works that incorporated the traditional Woschni correlation, made modifications to the estimate of characteristic velocity, with Mehl et al. [135] coupling a zero-dimensional turbulence model.

Inclusion of bulk flow field effects on combustion has been previously discussed in interzonal heat and mass transfer submodels. However, examination of diffusion-based approaches remains incomplete since the means of computing the diffusion coefficients were not discussed. The following text gives a brief account of the popular approaches for turbulence modelling in MZM. For a background on the phenomenology, plus a comprehensive collection of turbulence models in connection to quasi-dimensional models, the reader is referred to work by Vasudev [156].

Egüz et al. [141] incorporated the influence of turbulence by scaling the molecular diffusivities by a tuning constant they called turbulence factor (ζ_t) shown in Eq.(47). Based on the unity Lewis law, ζ_t was applied identically to both diffusion coefficients. Thus, Λ_{eff} and \mathfrak{D}_{eff} refer to the effective diffusion coefficients of heat and mass respectively. Due to its simplicity, this approach was not predictive, and required tuning on a case-by-case basis. Thus, in the follow-up work on RCCI simulations, Mikulski et al. [92] created a map for obtaining ζ_t in accordance to operating conditions, which was characterised by speed, load, EGR %, fuel blending and SOI. Section 5.4 provides further details in the context of calibration.

$$\Lambda_{eff} = \zeta_t \Lambda \text{ and } \mathfrak{D}_{eff} = \zeta_t \mathfrak{D} \quad (47)$$

For a phenomenological treatment, Eichmeier et al. [58] employed a single equation to model turbulent kinetic energy (k). The turbulence length scale (L_t) and turbulence dissipation (ε) were estimated from algebraic relations. The methodology starts with relation for mass diffusion coefficient, \mathfrak{D}_{eff} , since interzonal heat transport was not considered in their MZM. The first term in Eq. (49) was concerned with generation of turbulence. It followed the rapid distortion theory [157],

the basis for many zero-dimensional turbulence models. The third term accounted for the addition of turbulence due to DI, with u_{0inj} representing the velocity at the moment of SOI. The second term represented dissipation of turbulence, given in Eq. (50). Turbulence length scale (L_t) is based on geometrical arguments of the combustion chamber, as shown in Eq. (51). ζ_{tur1} , ζ_{tur2} , ζ_{tur3} and ζ_{tur4} are global tuning constants of this model. The tuning procedure will be discussed in section 5.4.

$$\mathfrak{D}_{eff} = \frac{k^2}{\varepsilon} \quad (48)$$

$$\frac{dk}{dt} = \zeta_{tur1} \frac{2}{3} \frac{k}{\rho_{cyl}} \frac{d\rho_{cyl}}{dt} - C_{tur2} \varepsilon + \zeta_{tur3} \frac{u_{0inj}^2}{m_{cyl}} \frac{dm_{inj}}{dt} \quad (49)$$

$$\varepsilon = \frac{\left(\frac{2}{3} k\right)^{\frac{3}{2}}}{L_t} \quad (50)$$

$$l_t = \zeta_{tur4} \frac{4V_{cyl}}{\pi B} \text{ with } L_t \leq \frac{B}{9} \quad (51)$$

Alternatively, phenomenological approaches based on Yang & Martin [158] have been popularly used in MZM. These approaches account for the spatial variation of Λ_{eff} and \mathfrak{D}_{eff} , thus making it appropriate for onion-skin models. While Yang & Martin intended it as a wall function formulation for CFD (RANS) models, the methodology was adopted for MZM, as in the works of Komninos et al. [71,88,139], Guo et al. [134] and Neshat & Saray [87]. The core idea is employing an algebraic relation between the viscosity ratio, μ_{tur}/μ_{lam} and normal distance from the wall (r_n^+), based on fitting to experimental data. This approach starts with defining an effective diffusion coefficient as the sum of laminar and turbulent contributions. This is shown for heat diffusion coefficient in Eq. (52), but can be straightforwardly obtained for \mathfrak{D}_{eff} based on Eq. (54). Here, the turbulent values of Prandtl and Schmidt numbers may be assumed as unity, as in [69], or following the work of Bissoli et al. [103], Pr_{tur} may be set to 0.85 and Sc_{tur} to 0.7.

$$\Gamma_{eff, z} = \Gamma_{lam, z} + \Gamma_{tur, z} \quad (52)$$

$$\frac{\Gamma_{tur, z}}{\Gamma_{lam, z}} = \frac{Pr_{lam, z} \mu_{tur, z}}{Pr_{tur, z} \mu_{lam, z}} \quad (53)$$

$$\mathfrak{D}_{tur, z} = \frac{\mu_{tur, z}}{Sc_{tur, z} \rho_z} \quad (54)$$

Ratio of turbulent to laminar viscosity was obtained from the functional form expressed in Eq. (55). The constants κ and a were set to 0.41 and 0.06 respectively [158]. In Eq. (56) r_n^+ is the dimensionless distance perpendicular to the cylinder walls, with μ_{wall} being the dynamic viscosity at wall temperature. u^* is the characteristic velocity, and was popularly scaled to the mean piston speed (\bar{S}_p) using the tuning constant ζ_u as given in Eq. (57). By integration, starting from the cylinder walls (r_n), in Eq. (56), the variation of μ_{tur}/μ_{lam} with respect to the dimensionless r_n^+ (Eq. (55)) can be obtained. Fig. 20 shows this variation as in the original work of Yang & Martin. In practice, integration in Eq. (56) is handled discretely, using properties of subsequent zones. The implication is that effective coefficients (Λ_{eff} , \mathfrak{D}_{eff}) have higher values in the inner zones and smaller values in the outer ones.

$$\frac{\mu_{tur}}{\mu_{lam}} = \kappa r_n^+ \left[1 - \exp(-2\kappa a r_n^+) \right] \quad (55)$$

$$r_n^+ = \frac{u^*}{\mu_{wall}} \int_0^{r_n} \rho \, dr \quad (56)$$

$$u^* = \zeta_u \bar{S}_p \quad (57)$$

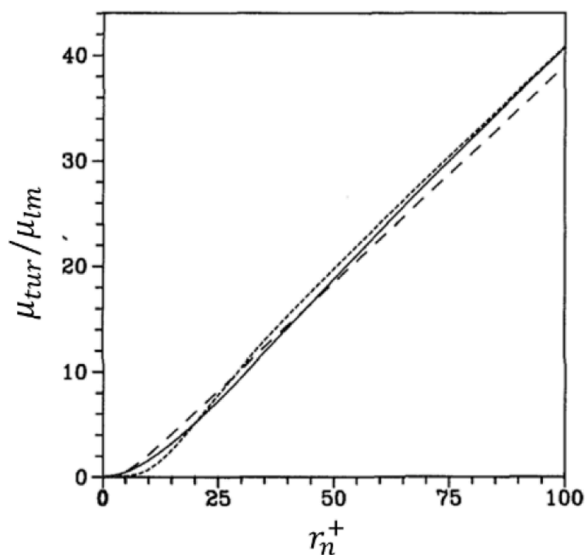


Fig. 20. Variation of μ_{tur}/μ_{lam} with dimensionless distance from cylinder wall r_n^+ , from the work of Yang & Martin [158]. (Reproduced with permission from Journal of Heat Transfer, ASME.)

4.5. Chemical kinetics

As combustion is a chemical process, the rate at which the reactions occur refers to chemical kinetics. This concerns the rate of creation/destruction of individual species, and thus influences the thermodynamic state in a zone. This arises because oxidation of the complex fuel molecule to its simpler combustion products of H_2O , CO , CO_2 and NO_x occurs in a sequence of elementary reactions over several intermediate species. The kinetic processes and the elemental reaction rates depend on the prevalent thermo-physical and chemical conditions and are to be modelled accordingly. Thus, the chemical kinetic mechanism contains information regarding the elementary reactions, species involved, the rate law and rate constants. From the perspective of implementation, data from the mechanism file is supplied to Eq. (58), which determines the net production rate of species i . ν'_{ij} and ν''_{ij} are the forward and reverse stoichiometric coefficients and j indexes the reactions. r_j is net reaction rate obtained according to Eq. (59), where X_i is the molar concentration of species i . k'_j is the forward rate constant which can be obtained, for instance, from the Arrhenius relation, and k''_j is the reverse rate constant which may be obtained basing on equilibrium constant. The heat released as a result of change in composition is contained within the internal energy term (left-hand side) of Eq. (2). Upon expansion, (Eq. (60)) the last term on the right-hand side is mainly responsible.

$$\dot{\omega}_i = \sum_{j=1}^{nR} (\nu'_{ij} - \nu''_{ij}) r_j \quad (58)$$

$$r_j = k'_j \prod_{i=1}^{nS} [X_i]^{\nu'_{ij}} - k''_j \prod_{i=1}^{nS} [X_i]^{\nu''_{ij}} \quad (59)$$

$$\frac{dE}{dt} = \frac{dm}{dt} e + m \left(c_v \frac{dT}{dt} + \sum_i^{nS} e_i \frac{dY_i}{dt} \right) \quad (60)$$

Simple methods of modelling combustion employ a global single-step or a two-step reaction approach [159,160]. These facilitate fast computing but lack the sophistication required to determine the sensitivities of ignition delay, HRR profile and emission levels to IVC conditions of mixture strength, temperature, pressure and EGR levels. Thus, information regarding elementary reactions and intermediate species are crucial with combustion proceeding along multiple reaction pathways. Detailed chemical kinetics models have been used extensively to

interpret fundamental phenomena occurring in shock tubes and flow reactors [161]. Also referred to as 'reaction mechanisms', chemical kinetics models of varying levels of detail [162] have become an important tool in combustion analyses through phenomenological or detailed CFD modelling [97]. Their importance lies in prediction of onset of ignition and/or knock, negative temperature coefficient (NTC) behaviour, combustion phasing and pollutant species production [163].

As noted above, the chemical processes associated with combustion rely on favourable thermal conditions for initiation and subsequent propagation throughout the cylinder. It therefore becomes crucial for the reaction mechanisms in LTC combustion prediction models to accurately represent this temperature dependence in order to model auto-ignition behaviour. LTC applications have been shown to be dominated by chemical kinetics [78,101]. Development of chemical kinetics models for combustion can be considered a study topic in its own right, and IC engine combustion modelling studies do not usually include this. Instead, researchers incorporate readily available reaction mechanisms developed by validating (ignition-delay computations, for example) against shock tube or rapid compression machine experiments. Where desired, studies can also implement simplified mechanisms derived from much larger parent mechanisms. Some investigations include a combination of different readily available reaction mechanisms to include species-related information and reaction pathways for multi-component fuels [78] or prediction of emissions such as CO_2 or NO_x . The chemical kinetics models used in these studies are considered suitably validated for the use cases.

Generally, the trend in multi-zone model-based engine research is to incorporate a suitable mechanism that has been pre-tuned or validated specifically for the chosen fuel(s) and operating conditions. Inclusion of relevant fuel species in the mechanism dictates the choice of chemical kinetics model used, while the balance between accuracy and computational effort is also a key factor. To understand this within the MZM context, Tab. 3 lists a few relevant LTC-MZM works that incorporate chemical kinetics in the overall modelling framework. This list is selective, aiming to paint a general picture of the types of mechanisms, fuels, surrogate(s) and level of detail included in model-based studies of LTC.

MZM studies have largely focused on HCCI combustion, evidenced by the higher incidence of works including data on chemical mechanisms that were used. Table 2 groups these works together, along with other combustion concepts for reference. Other concepts such as PCCI and RCCI are yet to be studied as extensively and this applies to the inclusion of detailed chemistry in the modelling framework. As expected, common fuels such as gasoline and diesel, represented by their surrogates iso-octane and n-heptane respectively, form the bulk of the studies. This is attributed to the existence of well-established chemical kinetics models for these fuels and the fact that they allow direct comparison with conventional IC engine concepts. As complex hydrocarbons, both gasoline and diesel sometimes necessitate additional representative molecules or surrogates to enable accurate combustion prediction. The work by Ogink & Golovitchev [93] included aromatic (toluene (C_7H_8)) reaction pathways to the n-heptane and iso-octane combination to represent gasoline in their previously presented chemistry model (109 species, 506 reactions), modified from [164]. This 'skeletal' model resulted in enhanced CO_2 emissions prediction thanks to inclusion of toluene to model the fuel, which otherwise comprises only aliphatic components. While the improved CO_2 predictions were approximately 2 % lower than the measured values, the modified reaction scheme with additional fuel species included still performed better than its parent reaction mechanism. Similarly, to model different compositions of diesel in their study to model PCCI combustion, Hergart et al. [78] used a combination of n-decane and alpha-methylnaphthalene in their 118-species, 1000-reactions detailed reaction mechanism. This new model was shown to better represent ignition delay behaviour in the low-temperature regime. The enhancement of this prediction was a result of the inclusion of n-decane, which,

Table 3
Overview of chemical kinetic models implemented in LTC-MZM literature

Fuel	Surrogate or fuel representative species	Level of detail	No. of species	No. of reactions	Regime	Reference	Chemistry model – source / basis
Gasoline	i-C ₈ H ₁₈ , toluene & n-C ₇ H ₁₆	Skeletal	109	506	HCCI	Ogink & Golovitchev [93]	Modified from Ogink & Golovitchev [164]
Gasoline	i-C ₈ H ₁₈	Skeletal	291	875	HCCI	Kozarac et al. [97]	Chen & Chen [166]
Gasoline	i-C ₈ H ₁₈	Reduced	199	386	HCCI	Flowers et al. [83]	Curran et al. [167]
Gasoline	i-C ₈ H ₁₈	Semi-detailed	84	412	HCCI	Komminos et al. [71]	Golovitchev [168]
Gasoline	i-C ₈ H ₁₈	Detailed	859	3606	HCCI	Aceves et al. [76]	Curran et al. [167]
Diesel	n-C ₇ H ₁₆	a) Semi-detailed	a) 137	a) 633	PCCI	Egüz et al. [100]	a) Andrae et al. [169]
		b) Reduced	b) 159	b) 770			b) Seiser et al. [170]
		c) Skeletal	c) 48	c) 248			c) Peters et al. [171]
Diesel	n-C ₇ H ₁₆	Detailed	177	1638	HCCI	Guo et al. [134]	Seiser et al. [170] & GRI-Mech 3.0 [172] for NO _x
Diesel	n-C ₁₀ H ₂₂ and alpha-methylnaphthalene	Detailed	118	1000	PCCI	Hergart et al. [78]	Hergart et al. [173]
PRF20	n-C ₇ H ₁₆ and i-C ₈ H ₁₈	Reduced	32	55	HCCI	Tzanetakis et al. [67]	Tanaka et al. [174]
PRF20	i-C ₈ H ₁₈ & n-C ₇ H ₁₆	Detailed	480	19000	HCCI	Bissoli et al. [96]	CRECK Modeling Group (PoliMilano) [175]
PRF90	i-C ₈ H ₁₈ & n-C ₇ H ₁₆	Detailed	1036	4238	HCCI	Angelos et al. [98]	Curran et al. [176]
Diesel	n-C ₇ H ₁₆	Reduced	17	21	HCCI	Orlandini et al. [74]	Peters et al. [171]
Gasoline	i-C ₈ H ₁₈	Reduced	26	37	HCCI	Orlandini et al. [74]	Golovitchev [168]
Diesel & gasoline	i-C ₈ H ₁₈ & n-C ₇ H ₁₆	Reduced	41	130	RCCI	Eichmeier et al. [58]	Ra & Reitz [177] Ra & Reitz [177]
Diesel & gasoline	i-C ₈ H ₁₈ & n-C ₇ H ₁₆	Semi-detailed	137	633	RCCI	Egüz et al. [141]	Andrae et al. (2008) [169]
Methane	CH ₄	Detailed	53	325	PCCI	Babajimopoulos et al. [79]	GRI-Mech 3.0 [172]
Diesel	n-C ₇ H ₁₆	Detailed	57	290	HCCI	Neshat & Khosbakthi Saray [87]	Golovitchev et al. [178] Golovitchev et al. [178]
Methane	CH ₄	Detailed	53	325	HCCI	Neshat & Khosbakthi Saray [87]	GRI-Mech 3.0 [172]
NG	CH ₄ , C ₂ H ₆ , C ₃ H ₈ , n-C ₄ H ₁₀ , N ₂ , CO ₂	Reduced	179	1125	HCCI	Aceves, et al. [73]	Curran et al. [167] & GRI-mech [172]
NG	(CH ₄ , C ₂ H ₆ , C ₃ H ₈ , n-C ₄ H ₁₀ , N ₂ , CO ₂)	Detailed	60	349	HCCI	Babajimopoulos et al. [179]	Warnatz, J (1999) [180]
Diesel & NG	n-C ₇ H ₁₆ , CH ₄ , C ₂ H ₅ & C ₃ H ₈	Semi-detailed	65	354	RCCI	Mikulski & Bekdemir [101]	1) Peters et al. [171]
Diesel & NG	n-C ₇ H ₁₆ & CH ₄	Semi-detailed	76	567	RCCI	Lashkarpour et al. [95]	2) GRI-Mech 3.0 [172] Rahimi et al. [181]
Hydrogen	H ₂	Detailed	53	325	HCCI	Kongsereparp et al. [99]	Chemkin library [182]
NG	CH ₄ & C ₃ H ₈	Detailed	53	325	HCCI	Kongsereparp et al. [99]	GRI-Mech 3.0 [172]

according to the authors, is known to be the primary driver of low-temperature chemistry. This study also included revised reaction rates to match the shock tube experiments by Pfahl et al. [165].

Dual-fuel concepts such as RCCI, however, favour studies with natural gas (various compositions) as one of the fuels, as can be seen in Tab. 3. In such studies, the comprehensive GRI 3.0 (Gas Research Institute) mechanism [172], validated extensively for NG combustion, tends to be the primary reaction mechanism of choice. This detailed mechanism contains information about several hydrocarbon species that are typically constituents of natural gas. The GRI mechanism is usually complemented for dual-fuel applications by separate reaction mechanisms for diesel or gasoline. For example, Mikulski & Bekdemir [101] combined the GRI 3.0 mechanism with a skeletal n-heptane mechanism by Peters et al. [171], creating a semi-detailed chemistry model containing 65 species and 384 reactions. The authors replaced the C₁-C₃ part of the n-heptane mechanism with information from the GRI 3.0 mechanism, which also provided NO_x reaction pathways. This approach enabled tracking of the intermediate species from n-heptane oxidation to give an accurate trend-wise prediction of RCCI combustion across different loads. The reaction mechanism used was not developed exclusively for RCCI combustion, but the authors justify its use based on the good predictive capabilities shown by their multi-zone model [56][101]

[183], where the negative temperature coefficient (NTC) behaviour described by the n-heptane mechanism is apparently of sufficient fidelity. However, there is a need to develop dedicated combustion reaction mechanisms for RCCI applications, where chemical kinetics assume even more importance as the combustion proceeds without flame propagation. The emergence of HPDI-RCCI concepts makes understanding the complex reactions even more crucial. This recent study on HPDI-RCCI (NG-diesel) [184] focused on constructing a chemistry model for the specific fuel combination and combustion mode. Detailed and reduced kinetic mechanisms, based on experimental and numerical studies, seemingly show good agreement in simulated pressure trace from CFD calculations. However, the document cited here does not provide more information about the mechanism itself, and its performance within phenomenological multi-zone models is yet to be understood. While such studies are ongoing, it seems to be common practice to use mechanisms studied or developed for HCCI or other older combustion concepts.

Table 4's 'Level of detail' column categorises reaction mechanisms based on their method of generation. This is also an important parameter in determining the speed of computation and accuracy of results. This column's terminology follows that commonly used in literature. The work by Zheng et al. [162] provides concise definitions for types of

Table 4
Categories of chemical kinetic models [162]

Category	Description	No. of species	No. of reactions
Detailed	The latest comprehensive reaction set	100s	1000s
Lumped	Uses a lumped description for larger species	100s	1000s
Reduced	A subset of the detailed model	10s	10s-100s
Skeletal	Employs class chemistry and lumping concepts	10s	10s
Global	Utilises global reactions to minimise reaction set	<10	<10

reaction mechanisms (Tab. 4) and readers are encouraged to refer to this work for more detail on the classification. The works included in Tab. 2 generally adhere to this nomenclature, but note that the table presents the model type as listed by the publication's authors.

Detailed chemical kinetic models include all important elementary reactions and species, using the highest quality of thermochemical and rate parameter information available. They are inherently large and therefore demand highest computational effort. Reduced models are derivations of these, culled to form a subset of the comprehensive model. They contain only the most important elements of the parent mechanism. Identification of these important elements is based on several established algorithmic procedures [185]. Reduced kinetic models aim to reproduce accuracy levels close to those of detailed models but with far less computational effort, focusing only on parts of the detailed mechanism applicable to the chosen combustion regime. Skeletal models can be considered a type of reduced models, where species deemed unnecessary are eliminated following a sensitivity analysis (as described by Bissoli et al. [96]). The skeletal models definition is slightly different in Zheng et al. [162]'s work, which states that these models are constructed using a sequence of composite kinetic steps representing the progress of the reaction. While definitions vary and nomenclature is open to interpretation, skeletal models in general offer the lowest level of detail but the fastest computation. Comparing Tab. 3 and Tab. 4, one can see a contradiction in the number of species used to classify these models. In Tab. 3, the models used by Ogink & Golovitchev [93] and Kozarac et al. [97] are labelled as 'skeletal', although containing more species than a supposed 'semi-detailed' gasoline reaction mechanism used by Komninos et al. [71]. This illustrates that using only the number of species or reactions included is not a robust method of determining a model's level of detail.

While skeletal or reduced models with fewer species and reactions generally tend to compute faster, there is a limit to how much the model can be reduced before computation times become longer. Take, for example, the skeletal model for gasoline described by Kozarac et al. [97], reduced from Chen and Chen [166] in order to model ignition timing and HC and CO emissions for HCCI. The skeletal model contains 291 species and 875 reactions, yet takes three times as long as the detailed PRF20 model used by Bissoli et al. [96] containing 480 reactions and 19000 reactions. While other aspects such as number of zones, fuel combination, etc. also affect total simulation time, the chemistry solver, like other ordinary differential equation (ODE) solvers, is impacted by the models overall stiffness. The system of chemical equations may become stiff if the model is reduced too much, potentially giving rise to solution stability issues [163]. The timescales with which free radicals approach pseudo steady-state and steady-state are vastly different and timescales of the chemical processes generally are very different from the timescales of the engine cycle. Due to these vagaries, reducing the chemistry information too much results in model stiffness and computation takes infinitely longer. Discussion of strategies to overcome stiffness are beyond the scope of this work, but readers are encouraged to consult works by Miller & Kee [163] and McNenly et al. [186] addressing this subject in the context of combustion modelling. It is

important to state that reducing the overall size of the chemistry model is possible in certain cases, as shown by Flowers et al. [82] (elimination of NO_x reaction pathways). The same is true in the case of modular reaction mechanisms, such as the one developed by Ra & Reitz [177], which enable users to choose only the parts of the mechanism pertinent to the fuel species studied.

The above-mentioned aspects are illustrated well in the work by Egüz et al. [100], which compared three types of reaction mechanisms for PCCI application. Interestingly, the skeletal mechanism by Peters et al. [171] used in this study appeared to provide better results than the more detailed ones by Seiser et al. [170] and Andrae et al. [169], also studied in this work. The difference in the speeds with which the different reaction mechanisms proceed significantly impacts the production of CO emission species, because the time available for complete oxygen conversion in the CO₂-rich zones dictates the emission levels. Such qualitative differences among different types of reaction mechanism impose difficulty in determining the suitability of mechanisms, so a global heuristic approach to select a mechanism is not straightforward. As indicated by [100], skeletal models sometimes perform better than detailed models. Tunér [123] proposes a phase-optimised-skeletal-mechanism approach to improve performance of skeletal models, even using a sensitivity analysis to determine which species are necessary for a given phase in the HCCI combustion cycle. By relaxing the necessity value of any species and selectively optimising an existing skeletal combustion mechanism for different combustion phases, Tunér illustrated (as a best-case scenario) computation times three times faster than a standard reaction mechanism, with deviations less than 0.1%. Such approaches can be considered for chemical kinetics implementation in multi-zone models of the future.

4.6. Crevice and blow-by modelling

The following sub-section consolidates the modelling assumptions for the crevice and blow-by phenomena. In the context of MZM, crevice usually refers to the piston-top land crevice, although it may be extended to the ring pack [91]. Appropriate approaches to capture the crevice region improves engine out emission predictions. According to Komninos et al. [71], at TDC 10-12% of the charge is located within crevice volume, of which around 5% is fuel. After the main phase of combustion, the unburnt charge flows back from the crevice to the in-cylinder area. Apart from being a source of UHC, Komninos & Hountalas [139] notes that the crevice is also source of CO, and the mechanism is 2 fold. The first is due to quenching effect causing partial combustion. Secondly, UHC leaving the crevice undergo partial oxidation further producing CO. A sensitivity analysis by Easley et al. [94] showed that if crevice volume was increased by 50%, the UHC emissions increased by 11%, CO emissions increased by 1.5% and NO_x emissions decreased by 9%.

Modelling of crevice region is usually by adding a dedicated zone. The size of this zone is fixed and is typically 1-3% crevice volume. To ensure quenching effect, the zone is prescribed as isothermal, with temperature fixed to that of cylinder wall, but Guo et al. [134] used the IVC temperature for this purpose. On the other hand, heat loss may be applied as in the work of [71], but with the heat transfer coefficient scaled up to ensure the thermal state is close to that of the cylinder wall. Crevice zone is usually shaped as a thin ring and located below the boundary layer zone. It is imperative to have mass transfer communication with the other zones to capture the phenomenology of emissions formation. Due to its location, mass transfer occurs through the BL zone. According to the scoped literature, mechanism of mass transfer has popularly been the P_{EQ} based. However, Bissoli et al. [96] proposed an alternative approach based on pressure difference, as in Eq. (61). ζ_{crevice} is a calibration constant. In fact, all remaining zones of the configuration exchanged mass with the crevice, and the quantity was based on pre-assigned weights. Tuning of $\zeta_{\text{crevice},z}$ was based on a non-reactive CFD simulation. As a consequence of this approach, Bissoli et al. excluded crevice zone from the pressure equalization condition. Ultimately, the

authors observed that the pressure difference was usually less than 1%, and that their MZM showed little sensitivity to $\zeta_{crevice}$. Nevertheless, their model was able to replicate trapped mass in the crevice, with a peak of 2.25% total mass at TDC.

$$\zeta_{crevice} \dot{m}_z = -\zeta_{crevice} \sqrt{|P_{crevice} - P_{cyl}|} \quad (61)$$

Blow-by on the other hand, refers to gas flow from the combustion chamber that gets past the piston rings into the crankcase [132]. It results in loss of mass and energy (enthalpy) and typically is driven by the pressure difference between the cylinder and crankcase. In the recent analysis by Koszalka & Hunicz [187] blow-by energy loss in HCCI mode was observed to be nearly twice the amount occurring in SI combustion. They noted that losses varied from 3 % to 8 % for HCCI, with lower losses associated with high-load operation. Based on conventional engine analysis, they showed that 60 % of the work losses attributed to cylinder friction was the contribution of blow-by.

From the modelling perspective, blow-by is influenced by in-cylinder conditions, piston ring-pack design and lubrication condition. The sophisticated approaches [187–189] model the effects of the piston ring dynamics by obtaining the gap through which the flow occurs. Other approaches [190] have determined blow-by at the post-processing stage. Nevertheless, most MZ implementations follow the conventional view in neglecting this approach. The works by Tzanetakis et al. [67] and Visakhamoorthy et al. [138] are exceptions.

The MZM for HCCI combustion by Tzanetakis et al. [67] considered blow-by, using the simplified approach of Ferguson [191]. The model implemented the enclosed zonal configuration and did not include a crevice zone. According to their approach (Eq. (62)), every zone contributed to blow-by, and the rate was proportional to the zone mass and engine speed (N_{eng}). In addition, the authors accounted for the enthalpy loss associated with the mass flow $^{BB}\dot{m}_z$. The ζ_{BB} in Eq. (62) is a calibration constant tuned by matching the pressure curve.

$$^{BB}\dot{m}_z = -\zeta_{BB} \frac{m_z}{N_{eng}} \quad (62)$$

Although this model was able to predict the blow-by in the best case within 10% error, the authors suggest the need for a detailed piston ring-pack model. The model was unable to capture the physics of low blow-by after occurrence of peak pressure via flooding of lubrication oil into the ring pack. Such limitation in predictivity was also substantiated by Visakhamoorthy et al. [138], who experienced poor predictions in the misfire region.

5. Simulation procedure

With discussions on modelling of all the terms in the governing equations complete, the focus now shifts to practical matters regarding implementation. This addresses aspects relevant to setting up and running the MZ simulations, including approaches to solve the ODE, prescribe the initial conditions and calibration procedures. We do not consider it relevant to explicitly discuss the implementation environments. Ultimately, differences between Matlab [92,99], C/C++ [96], Fortran [94,140], Java [58] or any other programming language come down to syntax. Choice of a particular environment may be dictated by available libraries and toolboxes, including selection of solvers, integration with external software packages and development time. Indeed, this encompasses applications that handle thermo-kinetic databases including dedicated solvers and analysis routines for chemical kinetics. The majority of the research works incorporate readily available packages such as Cantera [192,92,125] or Chemkin [182,71,134]. So, we proceed without further discussion, save for minor comments where needed.

5.1. Solution methodology

The equations that govern the dynamics of a multi-zone model constitute a coupled, non-linear and stiff system (section 3.1). They are relatively simple (first-order ODE) and straightforward to implement. Nevertheless, there are options for computational algorithms, solver choices and coding/implementation of equations which can affect simulation time and solution accuracy. The following text provides a brief overview of these choices.

McNenly et al. [186] note that stiffness in MZ models arises due to two contributions. The first is the well-known problem of solving chemical kinetic, where rate of change of species is spread over a large timescale. The second is coupling between the zones, governed by the constraint of equivalent zonal pressures Eqs. (4) and (5). Both issues can be handled by implicit solvers like LSODE [193], VODE [194,195] and their variants, which have been popularly employed in many MZM works. Even so, simulation time of a typical 10-zone model can last up to a couple of hours [97], depending on the size of chemical mechanism. That is not beneficial for control development and optimisation applications, so there have been many efforts to cut simulation time. These are summarised in the following text.

One way of improving simulation speed is based on the time-splitting approaches [196], popularly used in reactive simulations [197]. In the context of MZM, an adaptation of a first order splitting scheme, called the segregated approach [76], has been prevalent. It obtains the solution in two steps, i.e., chemistry step and flow step. First, the chemistry solver is advanced by a time step, by disregarding interzonal interactions. The obtained heat release information is fed back to the zones in the second step, where energy balance is performed up to the same time interval. Interzonal interactions and heat loss are considered in this step, but species change is disregarded. The algorithm then repeats, as summarised in Fig. 21.

Importantly, special attention needs to be given to the pressure equalisation condition. In the chemistry step, heat release in the zones is obtained as independent constant volume reactors. Consequently, by the end of step one, the zone would have developed different pressures. Thus, between the chemistry and flow step, ‘pressure correction’ [81] needs to be performed to satisfy the energy equation and ideal gas law. Fig. 22, taken from the work of Tzanetakis et al. [67], shows an example of the algorithm. The steps within pressure correction is analogous to the algorithm of P_{EQ} mass transfer (Fig. 19) where thermodynamic state of each zone is adjusted such that overall energy balance is satisfied. Note that Tzanetakis et al. did not model interzonal mass transfer.

The computation time, in theory [81], scales according to $[nZ \bullet (nEq)^3]$ as opposed to $[nZ \bullet nEq]^3$ for the non-segregated algorithm. nEq

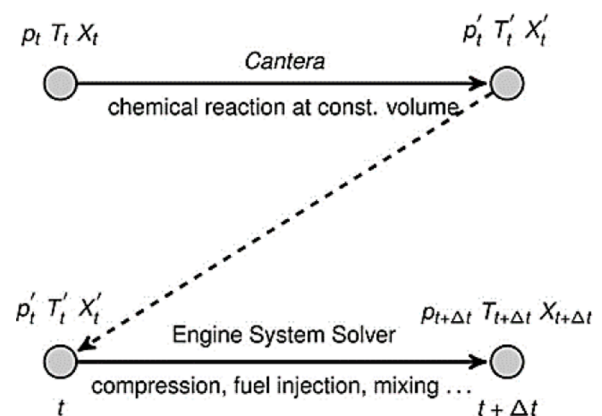


Fig. 21. Segregated solving algorithm implemented by Eichmeier et al. [58] with Cantera used to perform the chemistry step and the flow step handled using engine system solver coded in Java (Reproduced with permission from SAE International)

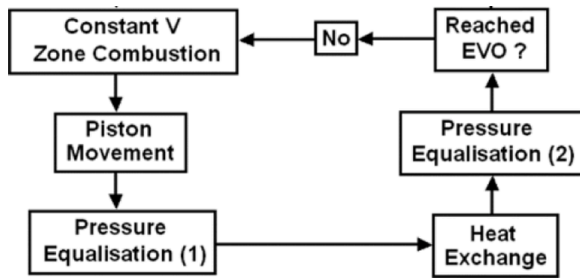


Fig. 22. Implementation of pressure correction by Tzanetakis et al. [67] (With permission from International Journal of Vehicle Design, Inderscience)

refers to the number of equations per zone. However, computation resources are wasted in integrator restarts. Specifically, this arises from the implicit integrator used in solving the chemistry step. The restarts happen in every loop of the segregated algorithm, and is connected to the numerical (approximation) Jacobian computation. This issue with the time-splitting approach is well known: interested readers are directed to the work of Sandu et al. [198].

On the other hand, the structure of the segregated approach offers a huge benefit in that it naturally facilitates parallel computing. This is because the zones are treated as independent constant volume reactors during the chemistry step. In the work of Visakhmoorthy et al. [138], for instance, a simulation time of about a minute was reported for a 10-zone model. Eichmeier et al. [58] developed their model in a Java environment as they claimed it eased parallel programming. They attained a simulation time of 12 s for a 31-zone simulation.

Furthermore, a segregated solver's algorithm structure was used to good effect in [71], capturing interzonal mass transfer. Specifically, this relates to the P_{EQ} based approach (section 4.3), where the pressure differences developed between zones at the end of every chemistry step, drive mass transfer. The present algorithm needs to be supplemented and the details were described in section 4.3.

While the above efforts focused on efficient usage of a given implicit solver, another group of research works explored improved solvers. At this point it is important to recognise that the governing set of equations (section 2.1) forms a differential algebraic equations (DAE) system. As is evident, equation of state (Eq. (4)) and volume constraint (Eq. (5)) are in fact algebraic equations. For use in traditional ODE solvers, the two equations should be combined (as in Eq. (6)), then differentiated, as Eq. (63). However, newer solvers like DASSL [199], or DSL48S [200], allow algebraic equations to directly coded. Although, it is typically known that solution to DAE systems are more challenging than (explicit) ODE [201], the difference in performance is of negligible concern to modern solvers [202].

$$\frac{dP}{dt} = \frac{R_u}{V_{cyl}} \left(\sum_{z=1}^{nZ} m_z T_z \sum_i^{nSp} \frac{1}{W_i} \frac{dY_i}{dt} + \sum_{z=1}^{nZ} m_z \frac{dT_z}{dt} \sum_i^{nSp} \frac{Y_{z,i}}{W_i} + \sum_{z=1}^{nZ} \frac{dm_z}{dt} T_z \sum_i^{nSp} \frac{Y_{z,i}}{W_i} - \frac{1}{V_{cyl}} \frac{dV_{cyl}}{dt} \sum_{z=1}^{nZ} m_z T_z \sum_i^{nSp} \frac{Y_{z,i}}{W_i} \right) \quad (63)$$

Approaches such as that of Bissoli et al. [103] make best use of the DAE structure in order to use the solvers efficiently. Their approach was based on the previously mentioned fact that pressure equalisation among zones burdens the computation. Instead of having a single, global equation of pressure such as Eq.(63), they implemented two additional equations for each zone. One pertained to pressure of individual zones

(Eq. (64)); the other was a so-called 'G' equation [96]. G was considered a pressure-weighted accumulated volume, as shown in Eq. (65). As can be seen, these equations take the form of algebraic constraints. With this particular formulation of the equations, the authors reasoned that a clear tri-diagonal block sparsity pattern of the Jacobian was achievable. Although simulation times were not presented in their work, in our opinion the improvement in speed could scale as (nZ) , following the analysis of McNenly et al. [186].

$$G_z = \sum_z^{nZ} P_z V_z \quad (64)$$

$$P_z = P_{z-1} \quad \text{for } z = 1, \dots, nZ - 1$$

$$P_z = \frac{G_z}{V_{cyl}} \quad \text{for } z = nZ \quad (65)$$

Along similar lines, use of advanced solvers in MZ literature has been aimed at easing the effort in Jacobian construction and the ensuing (iterative) solution of a linear system. Together, they account for nearly 95 % [81,186] of the computation resource per time step. Among earlier studies, Mehl et al. [135] employed a stiff solver from the BzzODE [203] package, attempting to reduce the number of function evaluations needed to construct the Jacobian, in addition to leveraging on Jacobian sparsity. McNenly et al. [186] conducted a detailed analysis of how to reduce the associated cost of Jacobian construction. A highlight of their work is their use of a run of non-interacting constant volume reactors as a preconditioner for the Jacobian factorisation, which was incorporated using a Krylov-type solver [204]. Ultimately, the authors reported a 75-fold decrease in computation time for a 20-zone simulation, compared to the regular (dense Jacobian factorisation) approach. This methodology was implemented later by Kodavasal et al. [81], who similarly reported a speed improvement of up two orders of magnitude for a 40-zone run.

5.2. Initialisation

This section discusses the common assumptions and methodologies employed to initialise MZ models. The essence stems from the nature of the governing equations, which being ODE, require well-defined initial conditions to draw out the desired solution. Regardless of the fidelity of the modelling approach, the accuracy of results depends on properly prescribed initial conditions, as highlighted in section 1.1. Broadly, there are two points to be considered: when the MZ simulation is initialised; and what constitutes the set of initial conditions.

Discussion of the former point is trivial if the engine's valve timing is fixed, because MZM are relevant only within the closed/trapped part of the four-stroke cycle. When the study involves an engine with variable

valve timing, the start (IVC) and end (EVO) crank angles need to be additionally specified. Furthermore, nuances exist, depending on the combustion model and MZM type. Fathi et al. [142] advocated MZ simulation should start after the direct injection event (EOI), stating that it had no observable influence on model predictivity, which they carried out for DI-HCCI. Therefore, it is evident that their approach can reduce computation effort. A similar approach can be found in the work of Orlandini et al. [74] for DI-HCCI, and [77] for PCCI. In the case of

Eichmeier et al. [58], the model was initialised at the moment of SOI, since it was the spray-MZ type.

Turning to prescription of initial conditions, the question concerns choice of information necessary to set the thermodynamic state of the system. Commonly used properties are pressure, temperature, mass and composition. However, difficulty lies in obtaining them without considerable uncertainty, as discussed well in literature [67,138]. For example, initial temperature is impacted by flow over the hot valves [58] and mixing with residual burnt gases. Indeed, determining initial composition can be troublesome due to influences of both external and internal EGR. The prominence of this cannot be understated, due to the high sensitivity of chemical kinetics-initiated combustion, as explored in many studies [58,94].

While correlations exist to estimate the IVC conditions [108, 252], the popular mitigation measure involves coupling with gas exchange models, such as simple valve flow models [130] or detailed air-path models. Examples of the latter include GT-Power, Ricardo Wave, AVL Boost, which are based on one-dimensional-quasi-steady-compressible-flow modelling. Typically, the gas exchange models are implemented on a single-zone framework. An exception is the work by Fiveland & Assanis [91,145], who ran their MZM even for the open cycle to obtain appropriate initial values (at IVC) for their turbulence and boundary layer submodels. 3D-CFD models have also been used to model gas exchange [79]: although this approach provides detailed results, evidently it is computationally demanding.

Nevertheless, the technique is to run the MZ and gas exchange models sequentially in closed-loop iterations [134] (cycle-to-cycle connection) to achieve results less impacted by experimental uncertainties. This is especially useful for VVA simulations. When dealing with negative valve overlap (NVO), Mikulski et al. [86] used an SZ-valve flow model coupled to their MZ RCCI simulation tool, as illustrated in Fig. 23. The methodology enabled them to study the influence of fuel injection during the NVO phase (fuel reforming) and the ensuing IVC conditions set-up for the following cycle. Section 6.2 has further discussion on this particular application. The authors mentioned that their simulation required six to eight iterations to arrive at converged results.

Further comments are made after acknowledging that MZ models, by nature, necessitate a set of initial conditions consisting of both cylinder-averaged quantities and zonal (local) quantities. The governing assumption common to all MZ models states that zones are homogeneous in pressure, so initialisation is naturally with cylinder-averaged value. The remaining quantities are usually dissimilarly initialised across the zones, especially T and/or λ , which are highly influential in many LTC strategies. However, the distribution cannot be straightforwardly obtained from experimental data, and so assumptions and empirical approaches are applied. As discussed above, although CFD is an apparent answer [100,141,179], its use may not justify the computational effort. Therefore, the following text elaborates on available

approaches from literature, while keeping in mind the predictive capability of multizone simulations.

5.2.1. Zonal temperatures

Most onion-skin MZM simply prescribe a uniform temperature across all zones, equal to the initial cylinder-averaged value [71,87,142]. Zonal thermal inhomogeneity is then captured by appropriately modelling interzonal heat exchange and wall heat loss. Still, specifying an appropriate temperature distribution at initialisation phase is shown to affect predictions [72,137]. For balloon MZM, on the other hand, initial zonal temperature distribution is key to capturing in-cylinder inhomogeneity (section 3.1). Specifically, sequential CFD-balloon models rely on the methodology of T-m mapping for initialisation. The T-m distribution is obtained from CFD simulation, and essentially provides information on what portion of the in-cylinder mass lies at a certain temperature. The procedure first involves post-processing CFD results of the motoring operation in a manner that associates the spatial distribution of in-cylinder mass to the temperature field, as shown in the centre of Fig. 24. Next, the area under the distribution is apportioned into bins (green-coloured grid), with the number of bins corresponding to the number of zones. Alternatively, the cumulative T-m distribution may also be used. In either case, the mean value of temperature and total mass of each bin is used to initialise the zones. Assignment to the zones is in order of increasing temperature. Fig. 24 summarises the procedure.

Apportionment of the T-m distribution into bins is based on identifying representative regions of the in-cylinder space. For example, Aceves et al. [73] assigned five from a total of 10 bins to represent the colder regions of BL and crevice. The five bins totalled 5 % of in-cylinder mass, each containing 1 %. Since the remaining 95 % mass was coarsely divided among the other five bins, in a follow-up [75] they attempted to redistribute this mass among the smaller bins in order to obtain a better heat release profile. Six of the 10 zones were used to describe the cold BL region, amounting to 12 % of in-cylinder mass. This is summarised in Tab. 5. Similar proportions were used in by Flowers et al. [82] and Babajimopoulos et al. [79]. However, Jia et al. [85] conducted a detailed analysis of the binning strategy, comparing two distributions while keeping the total bins to 10. The first distribution followed the proposal of Aceves et al. [73]. For the second, 0.5 % of in-cylinder mass was assigned to a bin representing the crevice; 11.5 % mass to a bin representing the BL region; 34 % representing the outer core region; and the remaining 56 % mass was evenly distributed in bins representing the hottest core region. Employing both distributions for their MZM, Jia et al. identified no difference with respect to P_{max} and CA(10-90) predictions, with sensitivity showed by HC and CO emissions.

In the case of stand-alone MZM (mainly onion-skin type), initial distribution of temperature is assumed to follow a certain profile. Starting with the simple, linear profile, two pieces of information in order to be applied. There are different ways of setting it up. Ogink &

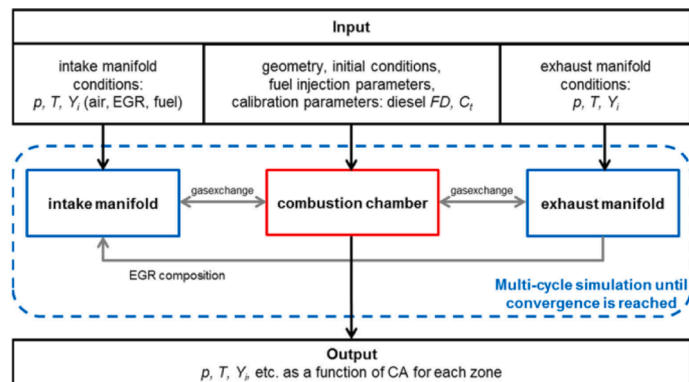


Fig. 23. Simulation framework for cycle-to-cycle connectivity of MZ-gas exchange model from the work of Mikulski and Bekdemir [101]. Beside cylinder-specific initial conditions, manifold conditions were also used for MZM initialization. (Reproduced with permission from Applied Energy, Elsevier)

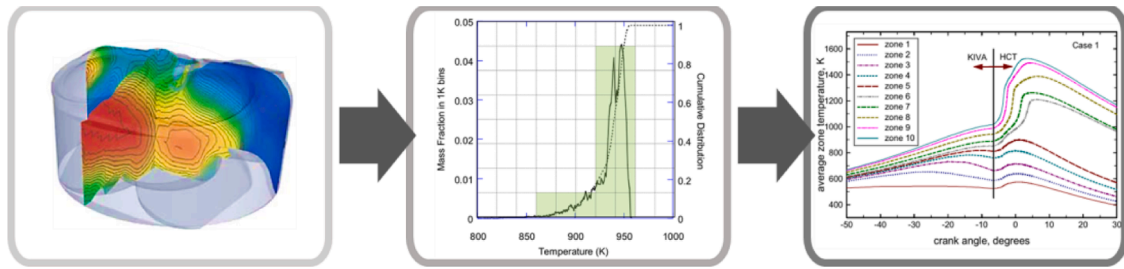


Fig. 24. Procedure for temperature-mass mapping adopted from [113, 79] and [75]. CFD results (left) are post-processed to produce a T-m distribution (middle), which then, based on binning, is assigned to the zones for MZM simulation (right).

Table 5

Initial zone mass fractions obtained from temperature-mass distribution of the coupled CFD-balloon MZ approach. Tabulated set of values are adopted from the works of Aceves et al. [73,75,77]

refs	[73]	[75]	[77]	Temperature Increase ↓
#z	zone mass %			
1	1	2	2	
2	1	1	2	
3	1	1	2	
4	1	1	5	
5	1	2	6	
6	2	5	10	
7	6	10	12	
8	17	18	15	
9	30	25	20	
10	40	35	25	

Golovitchev [93] used cylinder-averaged temperature, and a constant, ΔT , being the temperature difference between subsequent zones. To achieve predictivity, they determined a relation between engine load and ΔT , based on several simulation runs. Within the explored load range of 1.9 – 3.8 bar, they observed that for high loads $\Delta T=4K$ and low loads $\Delta T=6K$ gave best fits of the pressure and HRR traces. Additionally, the cylinder-averaged temperature was obtained from a detailed air-path model, and set to the middle zone. Thus, the BL zone and core zone are at the lowest and highest temperatures respectively.

Also for HCCI, Guo et al. [134] established a linear profile using manifold temperature (T_{iman}) and a cylinder- averaged temperature (T_{avg}), obtained from a valve-flow model. It was assumed for all operating cases that $T_{avg} > T_{iman}$. They set the outermost (BL) zone to T_{iman} and the middle zone to T_{avg} . Thus, temperature of the remaining zones was evenly distributed. In a similar vein, Tzanetakis et al. [67] used T_{IVC}

and T_{wall} , where T_{IVC} was set to the innermost zone and T_{wall} to the outermost zone. This exact approach was also used by Visakhamoorthy et al. [138].

On the other hand, Kongsereparp & Checkel [89] prescribed an S-shaped profile among the zones, as shown in Fig. 25, with temperature increasing from BL to core zone. The core zone temperature was ΔT above the BL zone temperature, which was computed based on a simple relation Eq. (66). T_{iman} is the intake manifold temperature and K_T is a tuning constant, set to 0.75. The model's predictions corresponded well with experiments, with small errors in CA10, 35 % in CA(10-90) at most and a maximum of 40 % for P_{max} . The approach was also used in work by Orlandini et al. [74]. However, it is difficult to further evaluate this approach, since the sensitivity of the profile on MZM results was not isolated. Furthermore, the authors did not provide a mathematical description of the profile. Nevertheless, in our opinion, an S-shape might be a poor representation of the temperature profile. Looking at the work of Bissoli et al. [103] or Komninos & Kosmadakis [104], the shape might resemble a square root's profile. And the previous linear approximation may be better in providing a simpler and practical approach.

$$\Delta T = \frac{T_{IEGR} - T_{iman}}{K_T} \tag{66}$$

5.2.2. Zonal fuel distribution

Fuel distribution appears to be a prominent topic for LTC concepts exploiting direct fuel injection, such as DI-HCCI [74], PCCI [100] or RCCI [92,95,141]. Fuel injection is used to restore (indirect) control over ignition timing and in moderating HRR [101,142,205]. It is worth noting that according to the phenomenology of LTC, early SOI provides adequate time for mixture formation, satisfying the requirement of (relatively) premixed and lean combustion. Consequently, all or at least the bulk of the injected fuel evaporates by the time combustion initiates. In other words, the lengthy ignition delay allows sufficient time for chemical kinetics to dominate in driving the start of combustion (SOC).

From a modelling perspective, the bulk effect of fuel injection, relevant to LTC is to be accounted for. Fundamentally, this pertains to the spatial inhomogeneity in mixture strength (ϕ or λ), analogous to

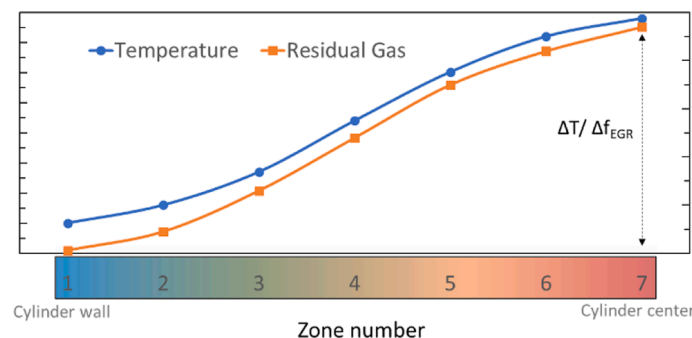


Fig. 25. Assumed S-shaped profile for zonal temperature and EGR by Orlandini et al. [74] and Kongsereparp & Checkel [89]. Colour bar represents the variation in thermal state across the zones.

thermal stratification. In other words, the current approach aims to establish a distribution of ϕ across the zones by the time fuel injection is completed. To this end, the popular modelling approach uses the assumption that fuel injection and combustion are decoupled. As a result, the complex processes of fuel break-up, evaporation, air entrainment, etc. are omitted from MZM applications. Instead, fuel is introduced directly to the zones in a vapour state. In the works of Egüz et al. for PCCI [100] and RCCI [141], diesel vapours were introduced between SOI and EOI to all zones, based on an imposed ϕ distribution. On the other hand, works such as Orlandini et al. [74] initialised their MZ simulation after EOI, with the zone imposed by a λ distribution.

The question then pertains to the shape of the fuel distribution. In sequential CFD-balloon models for simulation of PCCI combustion, Aceves et al. [77] employed an approach analogous to T-m mapping. Following the methodology of Babajimopoulos et al. [179], Aceves et al. processed the CFD results to produce a so-called T- ϕ distribution. This gave information on T and ϕ , corresponding to the distribution of the in-cylinder mass, as illustrated in Fig. 26. Apportionment of the T- ϕ distribution into bins first follows the procedure of binning in T-m approach. Aceves et al. identified representative regions by assigning the coldest 6% of in-cylinder mass to three bins, the warmest 25% mass to a single bin, and distributing the remaining mass among the other six bins. Following this, each T-m bin was further divided (equally, on mass basis) into a predetermined number of bins (four) along ϕ . This gave a total of 40 bins, which were accordingly assigned to the zones. Simplified for the purpose of illustration, the lines in Fig. 26 represent division of the T- ϕ distribution into 12 bins.

Lashkarpour et al. [95] initialised their onion-skin (annular) MZM by sequentially coupling it to a CFD model. The difference with their approach was that the time evolution of the spatial distribution of fuel vapours was processed from CFD results. This was then imposed onto the zones of the MZM until combustion initiated. The fuel vapour history was obtained from a CFD run under motoring operation, and tracking spatial regions that corresponded with the zones of the zonal configuration. A large portion of the fuel fraction was assigned to the innermost/central zone for two reasons. First, the size of the innermost zone was relatively large, at 14%–18% of the in-cylinder volume in an 11-zone MZM. Second, the injector cone angle was narrow, at 80°.

For a stand-alone approach, Egüz et al. [100] initialised their annular MZM by observing the spatial distribution of evaporated diesel mass

from a CFD model. Over a range of SOI, the distribution of diesel vapours was such that rich regions were located towards to the cylinder liner and lean regions near the cylinder centre. This stratification was observed at the instant before SOC. It is worth noting that the particular injector had a broad cone angle of 153°. The authors then generalised the shape of diesel stratification for all operating conditions, to a monotonic distribution with the outermost zone assigned as richest. They arrived at this deduction based on a sensitivity analysis. However, this approach to fuel distribution was not predictive and required user input of fuel mass fraction in each zone. To this end, Mikulski et al. [92] set up the distribution (analogous to [74]) by applying two tuning parameters: fuel concentration in the last zone ($\zeta_{\lambda nZ}$) and gradient in lambda starting from the last zone ($\zeta_{\nabla\lambda}$). Thus, the distribution shape was linear in λ over the zones. Since this approach required tuning on a case-by-case basis Mikulski et al. created a map to obtain $\zeta_{\lambda nZ}$ and $\zeta_{\nabla\lambda}$, characterised by operating parameters such as load, SOI, N_{eng} etc. Section 5.4 gives further details of the calibration procedure.

Orlandini et al. [74] used a functional form (Eq. (67)) to initialise their onion-skin model for DI-HCCI simulations. It relied on two tuning parameters, $\zeta_{\lambda,rich}$ and $\zeta_{\lambda,lean}$ to help determine how the overall fuel mass (λ_{cyl}) was distributed among the zones. With indexing starting from the outermost zone, the shape of fuel stratification was monotonic, with the innermost zone being fuel-rich. The authors attempted to make the simulations predictive by specifying two sets of values for the tuning parameters, based on the operating load. For $\lambda_{cyl} < 2$, $\zeta_{\lambda,rich}$ and $\zeta_{\lambda,lean}$ were set to 0.35 and 20 respectively. For $\lambda_{cyl} > 2$, $\zeta_{\lambda,rich}$ was 0.45 and $\zeta_{\lambda,lean}$ was 4. It is apparent that this approach disregards SOI's influence on fuel stratification. Furthermore, the calibration procedure behind the choice of tuning parameters was not presented, and the authors seemed to have used the approach as part of a parametric analysis of fuel stratification.

$$\lambda_z = \zeta_{\lambda,rich} + \zeta_{\lambda,lean} \exp\left(\frac{-z}{\lambda_{cyl}}\right) \quad (67)$$

One potential aspect to consider here is the effect of fuel evaporation on thermal stratification, as in the work of Egüz et al. [100]. The latent heat of evaporation was introduced along with the injected fuel mass in the zones, and the quantity of evaporative cooling in each zone followed the zonal λ distribution. Mikulski & Bekdemir [101] later shown that such introduced thermal stratification plays a significant role in making RCCI MZM predictive in terms of injection parameters.

Spray-based MZM by design capture the injection event in much more detail. With each zone initialised with fuel droplets during the injection event, the rate of spray evaporation, enthalpy flux and air entrainment are modelled. Fuel stratification is implicitly captured within the model. To this end, discussion of the modelling approach and the limitations were presented in section 3.3. Furthermore, the authors are aware of attempts [206] to use 1D-spray models coupled to MZM [92] to establish a zonal λ distribution. That work used the model of Musculus & Kattke [207] and captured the effects of spray-wall interaction. The approach generally required extensive tuning, and ultimately did not prove advantageous over simpler and faster implementations of using $\zeta_{\lambda nZ}$ and $\zeta_{\nabla\lambda}$, explained above. Furthermore, phenomena like wall impingement, relevant in early injection LTC concepts, have not yet been considered in MZM simulations. The above isolated examples suggest that direct coupling of a 1D-spray model with MZM is still considered relatively uncharted territory and can be a relevant development path.

5.2.3. Residual gas distribution

While accounting for residual gas (internal EGR) is crucial for model predictivity [86], its inhomogeneity distribution has secondary influence in comparison to thermal and fuel stratification [137,179]. Even in the case of VVA strategies (such as [56]), good estimates of the cylinder-averaged value seem sufficient for trend-wise results. To this

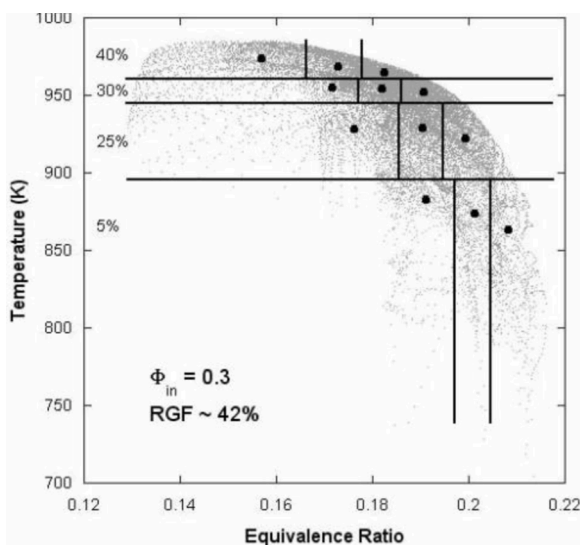


Fig. 26. The T- ϕ distribution at 30 CAD bTDC from the work of Babajimopoulos et al. [179]. The lines indicate limits of the bins and the dots indicate the average temperature and equivalence ratio (ϕ) of each bin. The percentages show the fraction for each temperature bin by mass, which is further divided into three ϕ bins. (Reproduced with permission from SAE)

end, valve flow or detailed air-path models are coupled to simulate the gas exchange phase, as explained above. Still, there are a few studies which attempt to initialise an iEGR distribution, aiming for predictive simulations.

In the sequential CFD-balloon approach, the aforementioned T- ϕ distribution was used by Babajimopoulos et al. [179] to investigate the influence of iEGR on HCCI operation (using NVO – see section 6.2). Details of the T- ϕ distribution have been explained above, but it is also worth noting that ϕ was based on fuel/O₂ ratio. The authors justified this choice by stating that the iEGR gas contained a significant composition of O₂. By comparing results of T-m-based initialisation against T- ϕ , the authors concluded that the latter approach better represented the phenomenon.

In the light of the above findings, Kongseerearp & Checkel [89] developed an approach to account for iEGR stratification in their onion-skin model. In particular, the conclusion relevant here is the correlation between iEGR and T distributions. As noted in [179], regions with lower temperatures also showed low concentrations of iEGR, such as near the liner. Similarly, higher concentrations of iEGR were observed in the central region of the combustion chamber. Thus, Kongseerearp & Checkel applied this pattern by assuming an S-shaped profile (Fig. 25), comparable to the zonal temperature distribution explained above. Δf_{EGR} is the cylinder-averaged residual gas fraction, which the authors obtained by a simple relation. Nevertheless, once determined, it is distributed among the zone, based on the shape.

5.3. Zoning calibration

The compromise between solution accuracy and computational effort is determined via an analysis analogous to the grid independence study, used to assess the influence of number of zones and the size/volume distribution of zones. Prescribing a low zone-count causes an over prediction of ignition angle [99] and HRR. Traces of cylinder pressure and temperature are bumpy or choppy [137] due to sequential auto-ignition of the zones. However, a higher zone count does not always imply better simulation results. For instance, Somers et al. [208] noticed that although smoother HRR were obtained with increasing zone count, a clear converging trend was not observed with respect to ignition angle. Aceves et al. [73] observed that their model was relatively insensitive for the tested zone counts of 10 and 20. This was reinforced by Hergart et al. [78] and Egüz et al. [100], who observed that very small changes in results were observed when the number of zones was beyond 10. The most popular zone count found in literature is around 10 (see Tab. 7).

The general procedure to determine the required zone count is to vary the number until simulation results match experimental data, or converging trends [100] on certain indicators are observed. Ideally, suitable indicators include a combustion phasing quantifier and one for emissions. Egüz et al. [100] used both CA10 and CO predictions, while Kongseerearp et al. [99] used only CA10. Flowers et al. [82] used burn duration (CA90-CA10) and position of peak heat release. A fit to experimental pressure trace has also been used, for instance by Voshtani et al. [102], and works [78,81] also used HRR profile. More extensive calibration was performed in [82], using other synthetic performance quantities such as indicated gross thermal efficiency and gross IMEP, plus emissions species UHC, NOx and CO₂ [87,95].

It is worth noting that the number of zones required for a certain accuracy level depends on fidelity of the MZ approach, with interzonal heat and mass transfer being particularly influential. For instance, in the balloon approach of Flowers et al. [82], a zone count of 40 was required to predict CO emissions, which still differed from experiments [209] by almost an order of magnitude. The authors noticed that CO emissions were particularly sensitive, as opposed to other emission indicators. Also, a lack of convergence in trends of CO with zone number was indicative of needing more zones. On the contrary, enabling interzonal flows in onion-skin models like [87,101] made it possible to achieve

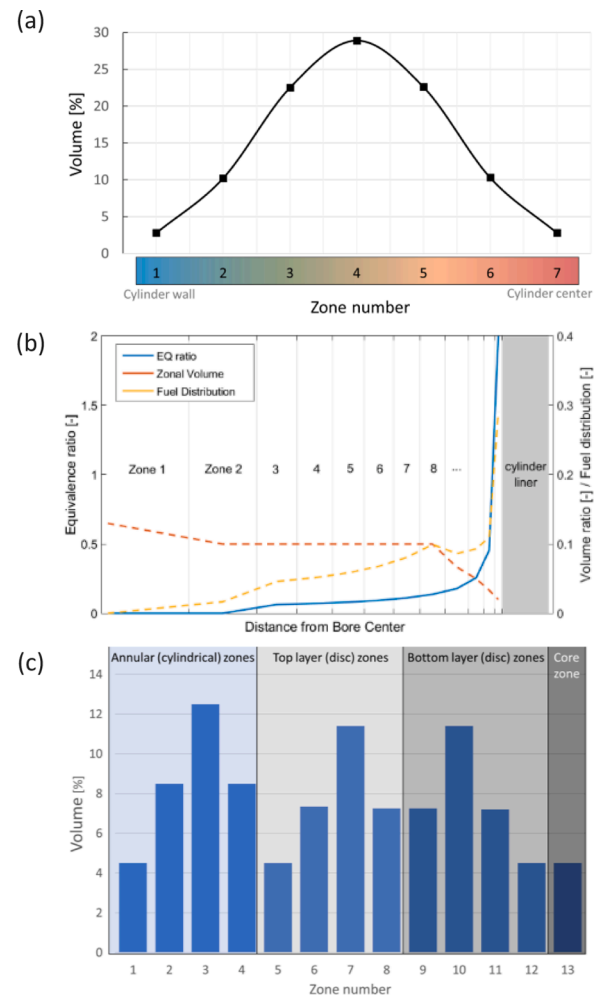


Fig. 27. Initial zone size distribution as a fraction of cylinder volume at IVC; (a) from Orlandini et al. [74] (b) from Mikulski et al. [92] (with permission from authors) (c) from Kongseerearp & Checkel [89]

trend-wise results of CO with only around 10 zones. Furthermore, the disproportionate sensitivity of CO to zone count was also reduced [95, 100].

Size distribution of the zones also must be considered in the calibration procedure. Discretisation naturally demands that regions of large (property) gradients need to be better resolved. Bissoli et al. [96] notes that appropriate characterisation of the gradients only where needed allows reduction of computational effort without affecting combustion behaviour. For sequential CFD-balloon models (Tab. 5), nearly half of the zones [75,77,79] are resolving regions of BL and crevice, which amounted to around 5% of total mass. The hottest gases located in the core zone were 25%–40% of total mass. However, the approach of Orlandini et al. [74] used a Gaussian distribution for zone size (Fig. 27a), since they aimed for a stand-alone predictive MZ model. The standard deviation of the distribution was arrived at the value of 1.4, fixed for all operating conditions. As mentioned by Aceves et al. [84], since interzonal flows are usually excluded in these approaches, sufficient zones need to be located in the crevice and BL region to capture the process of CO and HC production. Equally, there must be enough zones in the core region to obtain a smooth heat-release curve.

Jia et al. [85] conducted a comprehensive study of zone size distribution. Considering onion-skin models, the authors investigated the approaches of Komninos et al. [71] and Easley et al. [94], focusing on how interzonal mass transfer influences choice of zonal size distribution. While both models were of enclosed zonal configuration, that of

Komninos had a large core zone with approximately 40 % of in-cylinder mass, and smaller zones moving towards the BL. Easley's model divided the core mass (55 %) among seven zones, each around 8 % of total mass, and assigned a coarser BL with 20 % of total mass. Both models had same number of zones, similar inputs and had other similarities. Results showed significant difference between the approaches, especially for combustion phasing and emissions. Easley's model performed better for combustion duration and HC emission predictions, while Komninos' model performed marginally better in CO predictions. On the other hand, the comparison was not completely fair, as the seven core zones of Easley's model were constant-mass zones; only the outer core, BL zone and crevice zone transferred mass among themselves.

In case of annular MZM, as in Egüz et al. [100], the in-cylinder volume was divided evenly among the zones. In order to capture thermal and fuel stratification near the liner region, Mikulski et al. [92] prescribed a finer distribution moving towards the liner (Fig. 27b). In a follow-up study [101], the authors modified the distribution slightly by reducing volume in the core zone (Fig. 27b) to better reflect CH₄ emissions in their diesel-NG simulations. With a large core zone, the model exhibited a largely binary behaviour in this respect. The zone either did not combust due to insufficient mass and heat transfer from burning neighbours, or it combusted completely and under-predicted CH₄ and CO emissions. Neshat & Saray [87] followed a different approach, as described in section 3.2.1. Referring to Eq. (68), the user inputs required were size of core zone (Δr_{core}) and thickness of BL zone (Δr_{BL}). Then, the remaining in-cylinder volume was distributed evenly among the remaining zones. Furthermore, the authors considered a crevice zone with constant volume of 3 % clearance volume, which was also accounted for in the calculation. Thus, in their studies [95,131], the core zone was prescribed a volume of around 40 % of the bore, corresponding to 14 %-18 % of the in-cylinder volume. The BL zone was set with a thickness of 3 % of the bore (combustion chamber dimensions). The remaining volume of 70-75 % was distributed evenly among the remaining eight zones.

$$\Delta r_z = \frac{B/2 - \Delta r_{core} - \Delta r_{BL}}{nZ - 2} \quad \forall z, z \neq \text{core, BL zones} \quad (68)$$

Among enclosed-zone models, in the earlier work of Bissoli et al. [103] the size of the zones was initialised using volume. A normalised weighting factor was applied to make successively smaller zones approaching the cylinder walls. For instance, the outer zone was 1.5 % of V_{IVC} and core zone 50 % of V_{IVC} . In a similar vein, Tzanetakakis et al. [67] employed a calibration constant $\zeta_{\Delta w}$, defined as a factor by which volume of subsequent zones were reduced, approaching the outer zone. Specifically, $\zeta_{\Delta w}$ functioned as the common ratio in a geometric progression formed with the zonal volumes. The same approach was used by Nobakht et al. [140], who set $\zeta_{\Delta w}=0.3$ and V_{core} as 20 % of V_{IVC} . Since Komninos et al. [71] implemented a 'thickness' parameter (Δw_z) in defining geometry of their zonal configuration (section 3.1), they used the clearance height (S_{min}) as a reference to initialise the dimension of the zones. From Eq. (69), Δw_z was assigned equally to all zones. This is the volume remaining after subtracting the core zone's volume from the combustion chamber volume. It is the understanding of the authors of the present study, that core zone volume would then follow Eq. (70). In a later study, Komninos accommodated the changing thickness of boundary layer with boost pressure, by employing the correlation shown in Eq. (71). The subscript *ref* indicates the baseline operating conditions, i.e., naturally aspirated. This was necessary since they used a physics-based approach to model heat loss (Section 4.1).

$$\Delta w_z = \frac{S_{min}}{2 \cdot nZ} \quad \forall z, z \neq \text{core zone} \quad (69)$$

$$r_{z=core} = \frac{B}{2} - \Delta w(nZ - 1) \quad \& \quad h_{z=core} = h_{cyl} - 2\Delta w(nZ - 1) \quad (70)$$

$$\Delta w_z = \Delta w_{z,ref} \left(\frac{P_{IVC,ref}}{P_{IVC}} \right)^{0.511} \quad (71)$$

5.4. Submodel calibration

Calibration of the zonal configuration (zoning) and that of the submodels usually can be treated in a decoupled manner. For example, the zero-dimensional turbulence submodel implemented by Eichmeier et al. [58] was calibrated using CFD results of turbulence quantities such as turbulent kinetic energy and turbulent length scale. The focus was to capture the trends during compression and fuel injection, so used motoring condition data. As such, the cylinder-averaged quantities were used and thus did not depend on a perfectly turned zonal configuration. The fundamental heat loss submodel used by Bissoli et al. [96] was tuned using wall heat flow data from non-reactive CFD simulation. Since the conditions pertained to the BL zone, calibration could be conducted independent of a tuned zonal configuration. However, this was not the case in the model of Komninos [88]. The nature (section) of their fundamental heat loss meant that it consisted of no tuning parameters, but relied on calibration of the zonal configuration, as explained in section 5.3. This also can be the case [92] for submodels of interzonal heat and mass flow.

The following section examines procedures for selection of the tuning parameters/calibration constants of the discussed submodels in section 4. This separated from the text in the submodel section because certain calibration procedures [92] deal with tuning of multiple submodels at once. In addition, Tab. 6 provides a holistic view of the typical range of tuning parameters of submodels, comparing tuning procedures across different approaches.

5.4.1. Wall heat transfer

For use in their spray-based MZ model, Eichmeier et al. [58] assessed the performance of several correlation heat-loss models using CFD results. Their choice included models by Chang et al. [126], Hensel [212], Hohenberg [128] and Woschni [129]. The comparison was based on cylinder pressure, temperature, HRR and wall heat flow data for a low-load (3.2 bar) operating point. Their initial assessment showed that each of the models produced different trends during the different phases of the cycle. For instance, during the compression stroke, Woschni's predictions were lower among the tested models and CFD data. However, Woschni's predictions were considerably higher than the others during combustion. Thus, to maintain consistency for the purpose of comparison and calibration, the heat loss coefficient of all the correlations were scaled by matching the compression curve of wall heat flow. Chang's model was set to a factor 1.1, while Hensel's and Woschni's were set to 1.75. Ultimately, Chang's model was chosen, based on closeness to wall heat flow data of the CFD model. Working along similar lines, Komninos & Hountalas [139] calibrated the Annand correlation by matching to the compression pressure curve from experimental data.

The elaborate approach of Kodavasal et al. [81] leveraged on the correlation correlation-based heat transfer coefficient to set up thermal stratification across the zones of their MZM. This was performed achieved by using individually tailored scaling factors (c_z) for each zone, explained in Section 4.1, by Eqs. (14) – (16). Eq. (14) relied on external means of obtaining c_z by using results of motoring CFD simulation. The procedure was based on T-m mapping, where regions of the CFD grid were associated to zones of the MZM. The regions' temperatures were captured at TDC and then mapped to the zones. Observing Eq. (14), c_z was obtained straightforwardly from the CFD results without any need for tuning. Ultimately, the MZM results were not significantly better than simplistic implementations of HL correlation (explained in Section 4.1), so a follow-up study by Garcia-Guendulain [213] attempted to improve results by modifying Eq. (14). Specifically, T_{adb} was replaced by a tuneable temperature parameter they called T_{ref} . The tuning procedure entailed matching the zonal temperature distribution at TDC against

Table 6
Summary of the calibration procedure and typical values of the tuning parameters of all the submodels

Submodel	Approach	Calibration parameter	Meaning	Range	Procedure	Ref.	
Wall heat transfer	Correlation	Heat loss multiplier	Scaling factor for h in each zone	0–3	Eq. (14)	[81]	
		Scaling factor	Constant multiplied to h	1.1	Wall heat flux from CFD data	[58]	
		Scaling factor	Constant multiplied to h	0.9–1.5	Compression P curve	[89]	
	Fundamental T_{wall}	ζ_{wall}	Wall friction velocity	Wall friction velocity	0.3–0.83	In-cylinder T field or wall heat flux	[96]
		Surface temperatures	—	—	$T_{linr} = 422$ K $T_{head} = 478$ K $T_{pist} = 437$ K $T_{linr} = 440$ K $T_{head} = 420$ K $T_{pist} = 420$ K $T_{linr} = T_{head} =$ T_{pist}	—	[73,75]
		Area-averaged wall temperature	—	—	430 K	Exp. data of head + ΔT linear, interpolation between 20 K and 50 K	[97]
		—	—	—	430–440 K	Estimated based on T_{in}	[88]
		—	—	—	400 K	Eqs. (29) & (30)	[81]
		—	—	—	440 K	—	[93]
		—	—	—	400 K	—	[103]
		—	—	—	$T_{wall} = T_{cool}$	Experiment	[58]
		—	—	—	375 K	—	[99]
		—	—	—	350 K	—	[133]
	—	—	—	373 K	—	[138]	
	Boundary layer	BL zone size	—	—	390 K	—	[67]
			—	—	453 K	—	[210]
			—	—	0.9 mm	Match T, P, HRR	[97]
			—	—	3 % Bore	—	[131]
			—	—	15% (m/m)	Literature [145]	[135]
			—	—	0.1 mm	Literature [132]	[93]
			—	—	16.6% (V/V)	Match P	[67]
			—	—	19.6% (V/V)	Match P	[138]
			—	—	4% (m/m)	—	[134]
—			—	0.045–0.088 mm	Match emissions	[88, 104]	
—			—	1.5% (V/V)	—	[140]	
Interzonal heat transport	Heat transfer potential	ζ_{HTP}	Heat transfer time	1.0 e ⁻³ s	Match T, P, HRR	[97]	
	Interzonal mass transport	Diffusion	ζ_{mix}	Scaling factor for axial and radial entrainment rate	—	Match combustion P curve	[58]
Turbulence		Yang & Martin	ζ_u	Characteristic velocity	0.19 0.05 – NA 0.1 – boost 0.03–0.06 0.057 0.05 0.03–0.24 based on engine 0.32	Match P curve — Match peak heat flux from CFD data — — Match CFD mass flow rate —	[71] [88] [104] [133] [134] [96] [87]
Fuel stratification	—	Scaling factor	Turbulent diffusivity factor	10–1900	Optimising performance quantifiers with experiment data	[92, 141]	
		Single k eqn	ζ_{rd} ζ_{diss} ζ_{inj} $\zeta_{\lambda nZ}$ $\zeta_{\nabla\lambda}$ $\zeta_{\lambda,rich}$ $\zeta_{\lambda,lean}$	$k_{production}$ k_{diss} k_{inj} Φ in outer zone, gradient of Φ in outer zone	—	Motoring CFD	[58]
		—	—	0.4–0.8	Optimising performance quantifiers with experiment data	[92]	
		—	—	1.5–3	P curve (2 OPs tested)	[74]	
		—	—	0.35–0.45	—	[93]	
Crevice	Crevice zone size	—	—	4–20	Literature [132]	[93]	
		—	—	1.25% $V_{clearance}$ 2.5% m_{cyl} 3% $V_{clearance}$	—	[134]	
		—	—	1.5% $V_{clearance}$	Literature [132]	[71, 139]	
		—	—	—	Literature [132]	[88, 104]	
		—	—	3% $V_{clearance}$ 3% $V_{clearance}$	—	[95]	
		—	—	0.825 cm ³	Literature [211]	[131]	
		—	—	2.8% $V_{clearance}$	geometry (piston) geometry (piston)	[97] [96]	
Blow-by	Crevice mass flow	$\zeta_{crevice}$	Crevice flow constant	1.5×10^{-4}	Match ΔP (CFD)	[96]	
	—	ζ_{BB}	Blow-by rate constant	5.5 s ⁻¹ 6 s ⁻¹	Match compression P curve Match compression P curve	[67] [138]	

that obtained from CFD, using T-m mapping. The authors included a terse validation section, involving qualitative comparison against an experimental pressure curve, indicating that peak pressures were within ± 2 bar. Nevertheless, they said improvement in results was not apparent.

Using a physics-based wall function model [144], Bissoli et al. [96] conducted a detailed evaluation of their heat loss submodel. This pertained to the constant ζ_{wall} in Eq. (21). They calibrated their model mainly by using wall heat flux data from CFD models which were operated under motoring condition. This was done across three engine geometries and different operating points. Furthermore, they verified the predictivity of their model, based on piston surface heat flux data from literature [214,215]. Additionally, results of the temperature profile along the axial direction was assessed (from literature [216]) to ensure optimal calibration and predictivity.

The wall temperature model of Mikulski et al. [92,141] required information regarding mean value bulk gas temperature and heat transfer coefficient (gas to wall). Due to the interconnectivity between T_{wall} and bulk gas temperature, their MZ model was run in cycle-to-cycle connectivity until converged results were obtained. They validated the results against GT-Power's predictive wall temperature solver [51], and achieved T_{wall} within ± 7 K. This approach did not require case-dependent tuning, nor calibration to a particular engine. Running the model over a convergence loop was not considered a drawback because the integrated gas exchange submodel also needed the same step. Four to six iterations usually were needed for converged results.

Size of the BL zone usually follows from observations of bulk thickness of the boundary layer. Guo et al. [134] fixed the BL zone thickness to 0.1mm citing data from literature [132] of conventional engines typically 0.04 – 0.2mm. The work of Fiveland and Assais [145] has also been a popular reference for setting BL zone size, as followed in [135]. Tzanetakis et al. [67] tuned the BL zone volume by matching with experimental data of peak pressure and pressure trace of expansion stroke. The onion-skin MZM of Kongseereparp and Checkel [89] consisted of 3 BL zones (Tab. 1) and each was specified 4.5% IVC volume. The model of Komninos et al. [88,104], used emissions measurements to calibrate their zone size. Since they implemented a fundamental approach for wall HL, fine resolution of the boundary layer region was necessary. The calibration procedure was to progressively make the BL zone thinner, starting from a size equal to the other zones. The

simulation that best resulted a match in CO and HC emissions was chosen.

5.4.2. Interzonal flows and turbulence

The implementation by Kozarac et al. [97], discussed in section 4.2.1, used the heat transfer time parameter (ζ_{HTP}) to tune interzonal heat flow. The straightforward procedure assessed the sensitivity of ζ_{HTP} on pressure trace, HRR and temperature trace. Ultimately, they selected a constant value of $1e-3$ s for all operating conditions (λ sweep). Their MZM was able to attain qualitative trends in CO, UHC, η_{comb} and fitness to pressure trace.

Tuning of the popularly used Yang & Martin turbulence model (section 4.4) is based on the sole parameter ζ_{ub} pertaining to the characteristic velocity. As noted in the works [96,104], ζ_{u} is a global tuning parameter implying that retuning is required if the engine geometry changes. Regarding the means for tuning, Komninos et al. [71] initially stated that the experimental cylinder pressure during combustion was used for tuning, and the resulting value was 0.19. In a later study [104], Komninos & Kosmadakis conducted an extensive analysis and validation of their fundamental heat loss submodel, using wall heat flow data from a CFD model. They assessed the model over three different engines with the value ranging from 0.03 to 0.06. Bissoli et al. [96] employed a non-reactive CFD model, specifically designed to tune their MZM. The procedure involved tracking the evolution of an initially segregated N_2/Ar mixture under adiabatic conditions and under closed cycle operation. ζ_{u} was then adjusted so that the MZM (initialised similarly) matched the results of the CFD model.

Eichmeier et al. [58] based their spray-MZ combustion approach on a zero-dimensional, single equation k model for turbulence. Tuning of the model mainly pertained to Eq. (49), using the parameters of ζ_{tur1} , ζ_{tur2} , ζ_{tur3} and ζ_{tur4} . ζ_{tur1} was for turbulence generation, ζ_{tur2} for turbulence dissipation and C_{tur3} for turbulence induced by direct injection. ζ_{tur4} was for scaling the turbulent length scale. The tuning process employed a CFD model, where the results of concern were the cylinder-averaged turbulent kinetic energy (k), turbulence intensity (ν) and turbulence length scale (l_t). The simulation was performed over four representative load points of varying engine speed, diesel injection timing and diesel-gasoline mixture. Thus, the tuning procedure encapsulated matching the MZM results to CFD by adjusting the three tuning parameters. The results are shown in Fig. 28.

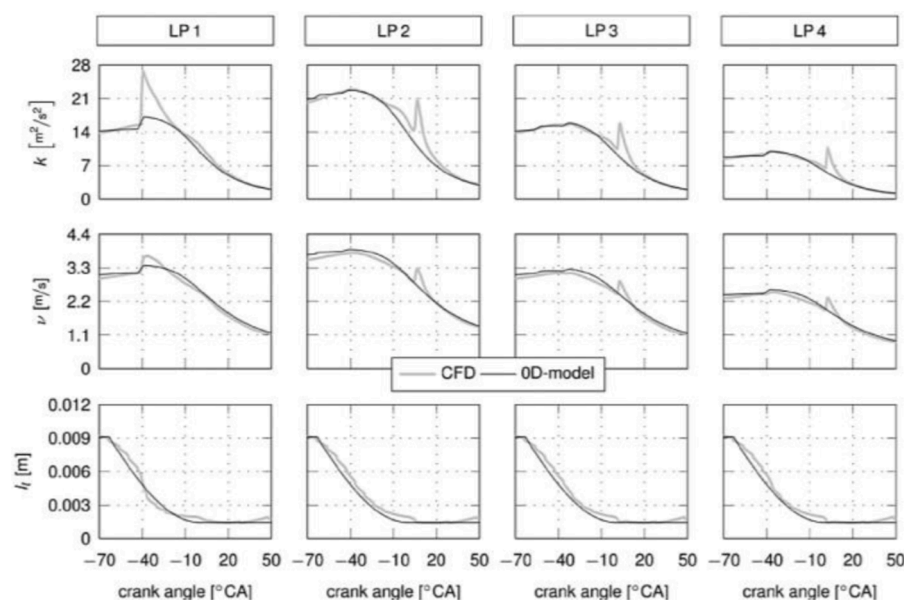


Fig. 28. Calibration and functional verification of zero-dimensional turbulence submodel by Eichmeier et al. [58], based on evolution of turbulence kinetic energy, turbulence intensity and turbulence length scale. RCCI combustion in diesel-gasoline engine across four operating conditions. (Reprinted with permission from SAE international)

The MZM of Mikulski et al. [92] simulated NG-diesel RCCI combustion, and presented three case-dependent tuning parameters. One (ζ_r) pertained to the turbulence submodel and two ($\zeta_{\lambda nZ}$, $\zeta_{\nabla\lambda}$) were associated with the initial diesel stratification, as discussed in sections 4.4 and 5.2.2 respectively. The authors devised a single tuning procedure to handle all three parameters, by creating a map of the tuning parameters for different operating conditions. To this end, they selected four representative load points (of varying fuel mixtures, SOI_{diesel} and EGR), and optimised the values of ζ_b , $\zeta_{\lambda nZ}$ and $\zeta_{\nabla\lambda}$ for each case. Optimisation was based on matching simulation results to experimental data of CA10, CA50, P_{max} , IMEP and UHC. Ultimately, ζ_t varied from 10 to 1600 between low and high loads. $\zeta_{\nabla\lambda}$ varied between 1.5 and 3, and $\zeta_{\lambda nZ}$ between 0.4 and 0.8, for changes in SOI and NG-diesel mixtures. In a follow-up study, Mikulski & Bekdemir [101] also included the influence of NG (low-reactivity fuel) stratification, ultimately resulting in five case-dependent tuning parameters. Nevertheless, their work was an explorative study and the tuning procedure was extended to accommodate the additional parameters.

5.4.3. Crevice and blow-by

Size of crevice zone is usually of fixed volume and specified as fraction of clearance volume ($V_{clearance}$). The value ranges between 1.5 – 3% and the choice is cited from literature [132]. Since crevice usually refers to the piston top-land crevice, the volume can be directly computed if piston geometry is available, as in [97]. As mentioned in Section 4.6, mass flow via the BL zone is based on the mechanism of P_{EQ} . However, Bissoli et al. [96] modelled mass flow according to square root of pressure difference as in Eq. (61). The constant $\zeta_{crevice}$ was calibrated from non-reactive CFD simulation. Essentially the difference between crevice and bulk cylinder pressure was matched. The value of $\zeta_{crevice,z}$ turned out to be 1.5×10^{-4} .

The simplified blow-by model in Tzanetakakis et al. [67] was tuned using the proportionality constant ζ_{BB} , as in Eq. (61). A single operating point with $\lambda = 1.51$ and EGR = 13.5 % was chosen for calibration, and the process involved matching the compression pressure curve from experiments. With a global calibrated value of 5.5 s^{-1} for the blow-by constant, the authors observed around 18 % loss in the trapped residual mass at IVC. Although seemingly high, this loss was in line with measurements on their target platform, which indicated 20 – 30%, by TDC.

6. Model application and validation

6.1. Accuracy of the modelling approaches

The goal of validation is to ensure a simulation model can produce consistent results within predefined accuracy requirements. These requirements differ according to application, depending whether the model is used for control purposes or for insight into a specific phenomenon, as discussed in the following subsection. This will define the appropriate scope (what quantities) and range (how many operating points) to validate the model. Finally, the MZM can be validated against experimental data (from full-metal or optical engines) or against a more detail model (CFD), assuming this already has been validated experimentally. The latter approach has some added value since the high-fidelity modelling provides additional insight into the phenomena, allowing comparison with parameters that are difficult to obtain directly from engine measurement. However, note that some studies have relied on literature data to validate the MZM model. Tab. 7 sets out validation methodologies and assesses MZ approaches, based on accuracy and versatility for operating regimes.

Balloon MZ models account for 77 % of the reviewed literature, with the one-way coupled CFD-balloon model comprising a significant proportion of those. The models were mainly validated against HCCI operation. A few works [77,78,112] were oriented towards PCCI combustion, but they lacked adequate validation and focused instead on

exploratory or model model-sensitivity studies. Regarding accuracy, the coupled CFD-balloon approaches models perform well in terms of qualitative reproduction of the pressure curve and combustion phasing predictions. A good example is the work of Babajimopoulos et al. [79], where in the best-case, peak pressure prediction was within 5 % of the experimental reference, while predictions in CA10 and CA50 was were within 1CAD. On the other hand, CFD-balloon models typically provide poor predictions of emissions, with lack of interzonal heat and mass flows being the main reason. This can be observed (Tab. 7) in the work by Aceves et al. [73,75,76,84,218]. Section 5.3 expands on this problem, which is based on the analysis by Flowers et al. [82]. It is worth noting that NO_x and PM quantities were usually ignored in these modelling approaches, since these emissions already were considered ultra-low for HCCI, both from the experimental and simulation side. Regarding simulation time, these models were reportedly slow, despite ignoring the CFD simulation at initialisation phase. A possible explanation is their use of relatively large chemical mechanisms (such as for propane [167], with 179 species and 1125 reactions) running on the early computer machines (such as DEC Alpha). However, in the follow-up works they were able to accelerate this by using parallel computation, reducing simulation time by a factor of 100, as explained in section 5.1. Consequently, data regarding the calculation speed/accuracy trade-off must be viewed with a historical perspective, since these works were the first to deal with MZ thermo-kinetic HCCI simulations. Finally, note that few stand-alone balloon models [74,135,210] were explicitly meant for trend prediction only, and there are very few data on their quantitative validation.

Among onion-skin models, the enclosed type has been used solely in the context of HCCI simulations. Komninos & Kosmadakis [104] performed extensive validation of their MZM including that for their fundamental wall heat loss submodel (described in section 4.1). It is worth acknowledging that the heat loss submodel could not be validated by a decoupled approach since it was intrinsically tied to the zonal configuration and interzonal heat transport. Nevertheless, CFD models of three different engine geometries were constructed and after validating with experimental data, served for MZM model validation. The conditions covered variations in rpm and compression ratio, and the simulation runs were under motoring conditions. Overall, the validation outcome is that the authors' in-house fundamental heat loss model better matched wall heat flow than single-zone results based on the Annand correlation. There also was good agreement with the near-wall temperature profiles. The authors [88] also conducted an overall model validation to reflect HCCI engine operation under boosted conditions. Variations in P_{IVC} , T_{IVC} and λ were considered over nine operating points. The models predictions showed good correspondence with experiment data with respect to qualitative pressure trace and trends in emissions. Specifically, the average error in NO_x emissions was 0.005 g/kWh, 1.72 g/kWh for HC and a rather large 3.6125 g/kWh for CO. In our opinion, the works of Komninos and his group present a most thorough validation of the MZM approach, and the process of the workflow is inspirational. However, considering the intended applications of MZM, the large investment in effort and resources may not be justified.

Other authors validated their HCCI-oriented onion-skin models directly on full-metal engine experiments. Table 7 shows their most relevant validation results. The scope of validation in the works of Neshat et al. deserves attention: the authors tested their HCCI model with different fuels, including, n-heptane, NG [87], PRF mixture, RG blending [219], and over a range of EGR rates and compression ratios [95]. Voshtani et al. [102] used reformer gas-HCCI experiments to validate their model. Fathi et al. [142] validated their HCCI combustion MZM (with a direct injection predictive submodel, discussed in sub-section 5.2.2) by exclusively varying SOI (146–61 CAD bTDC), covering over 10 operating points. The sophisticated MZM of Bissoli et al. [96] demanded validation in two stages. First, its fundamental heat loss model was validated, using heat flux measurements under motoring

Table 7
Accuracy and validation of different modelling approaches

Reference	Model type	Concept	Engine type	Range of validation	nZ	Simulation time	Model performance			Remarks	
							In-cylinder pressure /HRR	Percentage error Combustion indicators	Emissions		
Aceves et al. 2000-2005	[73]	CFD-balloon	HCCI	NG $V_D = 1600 \text{ cm}^3$ $B = 120 \text{ mm}$ $cr = 21:1$ 6-cyl to 1-cyl (flat piston)	#OP = 3 $P_{intake} = 1-3 \text{ bar}$ $\phi = 0.26-0.38$	10	12 hrs MZ only	$P_{max} \leq 5\%$	CA10-90 $\leq 10\%$ $\eta_{th} \leq 10\%$ $\eta_{ind} \leq 10\%$ $\eta_{comb} \leq 1\%$	UHC $\leq 55\%$ CO $\geq 70\%$	NO _x ignored because too small, closed cycle
	[75]		HCCI	C ₃ H ₈ $V_D = 1378 \text{ cm}^3$ $B = 114 \text{ mm}$ $cr = 18:1$ 6-cyl to 1-cyl (flat piston)	#OP = 3 $N_{eng} = 1000-1800 \text{ rpm}$ $T_0 = 340-342 \text{ K}$ $\phi = 0.17-0.36$	10	12 hrs (40 hrs total) DEC-Alpha 450 MHz	$P_{max} \leq 5\%$	CA10-90 $\leq 8\%$ $\eta_{th} \leq 5\%$ $\eta_{ind} \leq 5\%$ $\eta_{comb} \leq 4\%$	UHC $\leq 35\%$ CO $\leq 70\%$	Improved emissions predictions
	[76]		HCCI	i-C ₈ H ₁₈ $V_D = 1378 \text{ cm}^3$ $B = 114 \text{ mm}$ $cr = 10.5:1$ 6-cyl to 1-cyl (bowl in piston)	#OP = 2 $N_{eng} = 1010-2007 \text{ rpm}$ $T_0 = 381 \text{ K}, 413 \text{ K}$ $\phi = 0.346-0.348$	10	2 days MZ only DEC-Alpha 450 MHz	$P_{max} \leq 2\%$	CA10-90 $\leq 20\%$ $\eta_{th} \leq 2\%$ $\eta_{ind} \leq 2\%$ $\eta_{comb} \leq 1\%$	UHC $\leq 30\%$ CO $\leq 90\%$	Segregated solver
Babajimopoulos et al. 2003	[79]	CFD-Balloon	HCCI	NG $V_D = 4310 \text{ cm}^3$ $B = 170 \text{ mm}$ $cr = 21:1$ 1-cyl	#OP = 3 $P_0 = 1.5-2.0 \text{ bar}$ $\phi = 0.25-0.3$ $T_0 = 391-444 \text{ K}$	10	—	$P_{max} \leq 5\%$	CA10 $\leq 0.3\%$ CA50 $\leq 0.5\%$ CA90 $\leq 0.5\%$	—	CFD: BL grid coarse full cycle VVA parametric study, results compared against simulations in [91]
Fiveland & Assanis 2001	[145]	Onion-skin	HCCI	NG $V_D = 1600 \text{ cm}^3$ $B = 120 \text{ mm}$ (flat piston)	#OP = 2 $\phi = 0.26-0.31$ $cr = 17:1, 19:1$	2	—	$P - q_{lt}$	—	—	Assumed valve profile and flow coeffs, comparing CK [172] & [180], parametric study of HL models [129, 217]
Ogink & Golovitchev 2002	[93]	Onion-skin	HCCI	RF-08-A-85 (97 RON) $V_D = 487 \text{ cm}^3$ $B = 83 \text{ mm}$ $cr = 13.2:1$ 1-cyl	#OP = 3 $N_{eng} = 1450-2000 \text{ rpm}$ $\lambda = 0.99-1.56$	9	20-30 min	$P - q_{lt}$ HRR - q _{lt}	IMEP _{net} $\leq 13\%$	UHC $\leq 100\%$ CO $\leq 88\%$	Full cycle, coupled to AVL Boost
Guo et al. 2009	[134]	Onion-skin	HCCI	n-C ₇ H ₁₆ $V_D = 612 \text{ cm}^3$ $B = 82.5 \text{ mm}$ zariaible cr 1-cyl	#OP > 25 $AFR = 45-55$ $cr = 10:1-14:1$ $N_{eng} = 600-1400$	8	—	$P - q_{lt}$	—	q _{lt} : CO vs. AFR- fair NO _x vs. AFR- good NO _x vs. cr - poor	Calibration of T ₀
Komninos et al. 2005-2009	[71]	Onion-skin	HCCI	i-C ₈ H ₁₈ $V_D = 1600 \text{ cm}^3$ $B = 120 \text{ mm}$	#OP = 3 $\lambda = 2.66-3.23$	11	40 min (Pentium4 3GHz)	$P - q_{lt}$ HRR q _{lt}	—	—	$\zeta_u = 0.19$ (not explicit calibration)

(continued on next page)

Table 7 (continued)

Reference	Model type	Concept	Engine type	Range of validation	nZ	Simulation time	Model performance			Remarks	
							In-cylinder pressure /HRR	Combustion indicators	Emissions		
[88]	Onion-skin	HCCI	cr = 17:1 6-cyl to 1-cyl i-C ₈ H ₁₈ V _D = 1600 cm ³ B = 120 mm cr = 17:1 6-cyl to 1-cyl	#OP = 9 P ₀ = 1–3 bar λ = 2.67–4.44	16	40 min (Intel Core2duo)	P – qIt HRR – qIt	—	qIt: CO vs. λ, p ₀ – fair UHC vs. λ, p ₀ – fair NO _x vs. λ, p ₀ – good	ζ _{it} = 0.05, 0.1, T ₀ = 80, 105°C, calibration V _{zone} = f(p)	
[104]	Onion-skin	HCCI	Fairbanks-Morse diesel (a) B = 79.4 mm Triptane (b) B = 76.2 mm Perkins engine (c) B = 98.4 mm	#OP = 9 (a) motoring cases cr = 8:1–14:1 (b) N _{eng} = 750, 1500 rpm (c) N _{eng} = 705–2395 rpm	16	—	Heat flow – qIt	—	—	Validation of fundamental HL model, thickness of zones is generated automatically by the code	
Kongsreeparp et al. 2005	[99]	Onion-skin	HCCI	V _D = 612 cm ³ B = 82.5 mm cr = 17:1 (NG), 11.5:1 (n-C ₇ H ₁₆) 1-cyl	#OP = 3 For NG+RG RG = 16%–40% For C ₇ H ₁₄ +RG Φ = 0.3–0.6	12	30 min	P – qIt PRR _{max} ≤ 20%	CA10 ≤ 3% CA10-90 ≤ 25% IMEP ≤ 25% η _{th} ≤ 20% η _{th, ind} ≤ 20%	—	Comparison with single-zone model
Egüz et al. 2013	[141]	Onion-skin	RCCI	n-C ₇ H ₁₆ + i-C ₈ H ₁₈ V _D = 2097 cm ³ B = 130 mm cr = 14.9:1 bowl in piston 6-cyl to 1-cyl	#OP = 12 BR = 0.7–0.9 SOI = 60–90 CAD bTDC	10	1 hour	P-V (log-log) – qIt	CA10 ≤ 5 CAD CA50 ≤ 5 CAD	—	Good trend-wise CA50
Mikulski et al. 2016	[92]	Onion-skin	RCCI	NG + n-C ₇ H ₁₆ cr = 14:1 flat piston	#OP = 4 BR = 0.6–0.85 GR = 0–48%	12	30 min	P – qIt HRR – qIt CHR – qIt P _{max} ≤ 10 bar	CA10 ≤ 3 CAD CA50 ≤ 3 CAD IMEP ≤ 0.5 bar	UHC ≤ 50% CO ≤ 30% NO _x ≤ 1130%	—
Mikulski et al. 2018	[56]	Onion-skin	RCCI	NG + n-C ₇ H ₁₆		13	45 min	—	—	—	Different geometry, VVA
Neshat & Saray 2014	[87]	Onion-skin	HCCI	CH ₄ , n-C ₇ H ₁₆ V _D = 612 cm ³ B = 82.5 mm 1-cyl	#OP = 6 cr = 12.7:1, 21.5:1 λ = 2.05–3.87 EGR = 0–40%	11	—	P – qIt HRR – qIt	—	UHC ≤ 20% CO ≤ 2% NO _x ≤ 100%	nZ calibration
Lashkarpour et al. 2018	[95]	Onion-skin	RCCI	CH ₄ + n-C ₇ H ₁₆ V _D = 612 cm ³ B = 82.5 mm cr = 17:1	#OP = 6 BR = 0.978–0.984 m _{air} = 2.63–3.89 g/s SOI = 10–25 CAD bTDC EGR = 0–30%	11	—	p – qIt HRR – qIt P _{max} ≤ 2.8%	CA10 ≤ 200% CA50 ≤ 25%	UHC ≤ 35% CO ≤ 20% NO _x ≤ 67%	nZ based on emissions
Eichmeier et al	[58]	Spray MZ	RCCI	i-C ₈ H ₁₈ + n-C ₇ H ₁₆ V _D = 477 cm ³	#OP = 4 N _{eng} = 1500–2300 rpm	30	12 s (operator splitting, parallel)	P – qIt HRR – qIt (fundamentally different)	—	—	CFD for calibration

(continued on next page)

Table 7 (continued)

Reference	Model type	Concept	Engine type	Range of validation	nZ	Simulation time	Model performance			Remarks
							In-cylinder pressure /HRR	Percentage error Combustion indicators	Emissions	
			$B = 82\text{mm}$ $cr = 16.7:1$	Single & double injection $BR = 0.7\text{--}0.9$			characteristics)			

qlt = qualitative validation; OP = operating point; cr = compression ratio; V_D = displacement volume; $\eta_{th, ind}$ = indicated thermal efficiency

conditions, sourced from literature covering three different engine geometries: Fairbanks-Morse [214,220], GM Tripane [214,220] and Perkins [220]. This first stage validation confirmed that the submodel enabled qualitative capture of the profile of heat flux with CAD, across changes in engine speed and engine geometries. The second validation stage was of the MZM as a whole and was conducted under firing conditions with data from literature [221,222]. Results showed that the model was qualitatively able to follow the profile of pressure and cumulative heat release rate (CHR) over varying boost pressure [221]. With in-cylinder intermediate species data available, [222] the model overestimated the concentration of molecules such as formaldehyde, alkenes and CO during the main combustion event. The authors attributed this to residual gases residing in the crevice zone. However, further comments cannot be made since validation results regarding emissions were sparse. Nevertheless, the results show the potential of Bissoli et al.'s predictive simulation tool, applying physics-based submodels for inter-zonal heat and mass flow, turbulence and wall heat loss.

Looking at onion-skin MZM validated for dual-fuel RCCI operation, the most thoroughly validated is the approach first proposed by Egüz et al. [100]. In their original work, the authors provided qualitative validation of in-cylinder pressures (P-V plots) for several sweeps of gasoline-diesel blend ratios (BR) and SOI. Their Fortran-code model was concluded to be trend-wise predictive for relevant combustion indicators like IMPE, P_{max} , PRR and CA10/50. The absolute simulation error for the latter was rather large, however, at 5 CAD. Emissions were not considered as a validation factor. The code of Egüz was further modified by Bekdemir et al. [183] to the Matlab-Cantera coupling and after several upgrades, including (but not limiting) initialisation with a valve-flow submodel and a predictive wall-temperature submodel, validated directly on a multi-cylinder, heavy-duty NG-diesel RCCI engine in subsequent works by Mikulski et al [56,92,101]. The upgrades also resulted in greater detail for the zonal configuration, including 13 zones, and simulation time was halved to around 30 minutes per cycle.

The validation in [92] targeted reproduction of in-cylinder pressure trace within cycle-to-cycle variations, which transferred to the same target for IMEP, CA10/50 and P_{max} . Experimental and simulated emissions were also compared. The results summarised in Tab. 7 are expanded for selected operating points in Fig. 29 and Fig. 30 for better comprehension.

It is noteworthy that in their later works Mikulski et al. [56,86] proved that their MZM (XCCI), when combined with a zero-dimensional valve-flow submodel, can predict the RCCI combustion response to various variable intake valve actuation strategies. The experimental validation involved different piston geometry and injector alignment (Mexican hat with squish; narrow injection umbrella-angle), compared to the original calibration's set-up in [86] (flat piston; wider umbrella). Those changes meant absolute values of CA10/CA50 were off by as much as 4 CA, but this difference was consistent when varying intake valve timing, proving high scalability and transferability of the model to different hardware platforms. Other, less complete validation endeavours for onion-skin RCCI MZM were made, amongst others, by Lashkarpour et al. [95]. The model was conceptually similar to the earlier-mentioned models by Egüz et al. [100,141] and the TNO team (Bekdemir et al [183], Mikulski et al. [92]). The zonal division and NG-diesel kinetic mechanism involved were much coarser than those of Mikulski et al, which resulted in a large error in CA10 prediction. Emission prediction accuracy was similar to that of other onion-skin models.

Summarising Tab. 7's data regarding onion-skin model validity, it can be concluded that the models can predict control-relevant combustion indicators both qualitatively (trends) and quantitatively (absolute values). Absolute differences in combustion phasing (CA10/50) and IMEP do not exceed 3 CAD or 0.5 bar respectively. Emissions are trend-wise predictive and particular focus is on calibrating CO and HC as they influence IMEP. Outside the calibration spectrum, onion-skin MZM typically capture these emission indicators with an error of 30 %. NO_x emission is reported as ultra-low, the same as in LTC experiments, and

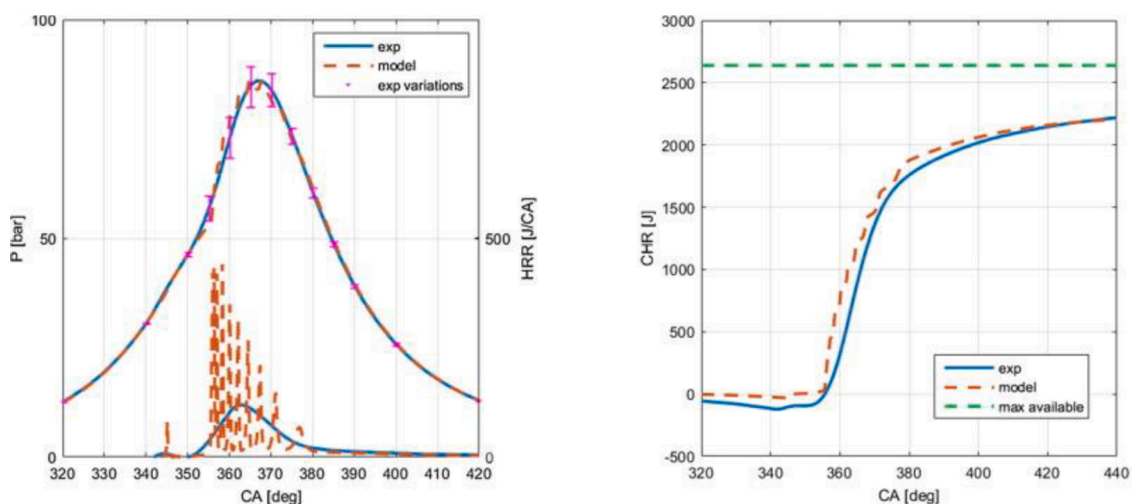


Fig. 29. Experimental and simulated in-cylinder pressure and heat release rate (left) and cumulative heat release as a function of CA for selected RCCI case (mid-load) [101]. Cycle-to-cycle variations of the measured pressure are indicated with the bars. (Reproduced with permission from Applied Energy, Elsevier)

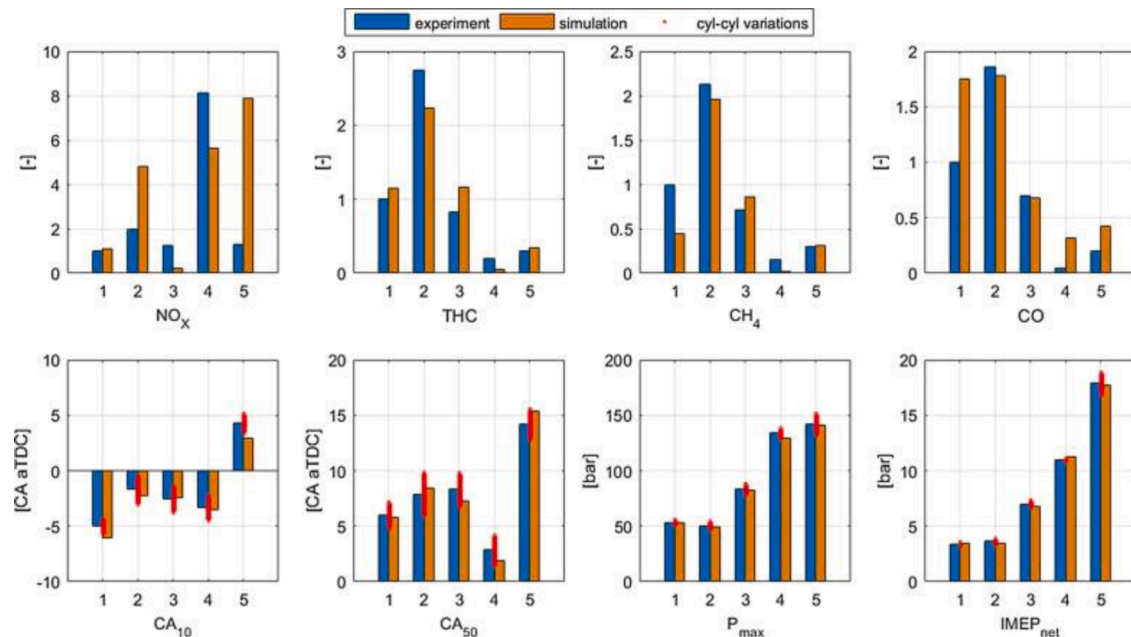


Fig. 30. Engine-out emissions and control-related parameters: model (brick) vs. experiment (blue) for several validation cases (x-axis) [101]. Error bars indicate mean cylinder-to-cylinder variations when such data were available. Emission values are given relative to the experimental value of case 1. (Reproduced with permission from Applied Energy, Elsevier)

though the relative differences may be up to 70 %, with such small values these differences are within emission measurement accuracy. Finally, simulation times on a single CPU are consistently reported as between 30 minutes and one hour, with differences in performance due to different levels of fidelity, ways of initialisation, solver, and, of course, the simulation platform. As the latter factor is not always reported, one should take in to account that newer studies bring progressive improvement in computational power. Thus, the actual computation time probably converges around the lower value of the reported span, assuming models are benchmarked on a common up-to-date hardware platform.

Validation data from other MZM categories are scarce. The spray-based MZM of Eichmeier et al. [58] was validated against CFD results of gasoline-diesel RCCI combustion. The authors also presented it against experimental data, sourced from [223]. The operating conditions spanned four load points (IMEP: 3-5 bar), various fuel blends and different SOI. The authors claimed qualitatively good fit of in-cylinder pressure traces, but in-depth analysis of HRR suggests a fundamentally different combustion regime in the model (separate combustion of diesel and gasoline fractions) compared to the RCCI experiments. The good fit was obtained probably by over-constraining the physics with tuning, a pitfall of all simplified physics-based approaches. This, and the fact that emission prediction validity was not reported, make it doubtful that spray-based approaches can be useful to predict RCCI. This is despite spectacular computational speed (a matter of seconds – see Tab. 7) and ability to straightforwardly connect to multi-injection strategies and other diesel fuel modes.

6.2. Applications

This section reviews the application domains of MZM. They range from fundamental-level studies that support understanding of in-cylinder processes in LTC, through applied-level research into combustion concept design and optimisation, to direct control-development applications. The section is divided accordingly and may be inspirational in highlighting how different MZM approaches can suit particular applications. This focus on application, coupled with the previous sections' review of submodel structure, accuracy and simulation times,

should provide input to the final discussion about what makes the optimum application-tailored MZM.

6.2.1. Fundamental studies

One of the advantages that engine modelling has over full-metal engine tests is the possibility to isolate selected parameters and then identify the model's response to a single factor. This is especially important for LTC combustion concepts, where in-cylinder thermodynamic parameters, chemical composition, combustion and emissions usually are cross-related, both within a single cycle and on the cycle-to-cycle basis. This complexity is magnified if thermal and compositional stratifications are taken into consideration. Therefore, MZ models proved to be useful tools for various parametric studies aiming to provide deeper understanding of the phenomena.

The works focused on fundamental understanding of LTC phenomenon are summarised Tab. 8. In this section, we do not comment on the modelling details or validation, focusing instead on approaches to solve particular problems and their results. As a side note, the cited results are arranged so that they start with general statements and move to more detailed conclusions.

6.2.1.1. Stratification. Thermal and compositional stratification, after chemical kinetics, is the second-most important phenomenon shaping LTC performance. Here, the work of Kongseeraparp et al. [99] is worth mentioning, because it decoupled the effects of thermal and compositional stratification in a hydrogen-fuelled HCCI engine. The stratification of Φ was found to have modest effect on SOC and combustion duration. With homogeneous mixture ($\Phi = 0.3$) as a reference, 50 % stratification span with higher fuel concentration in the core zones advanced SOC, but in a limited range of less than a single CAD. At the same time combustion duration was lengthened by 20 %. Quantitatively, the opposite effect was observed for both combustion indices when fuel was more concentrated in the outer zones. In contrast to excess air, the effect of thermal stratification was found to be much more pronounced. When the temperature span between inner and outer zones at IVC was set to 60 K, auto-ignition was advanced by 4 CAD. At the same time, combustion duration increased by a factor of six. Examination of the isolated effect of residual gas inhomogeneity, where up to 35

Table 8
Application of MZM to fundamental studies

MZM type	Ref.	concept	Application	Approach	Highlights	Comment
Stratification						
Balloon	[77]	PCCI CH ₄ , n-C ₄ H ₁₀	Study of Φ stratification Applying T- ϕ mapping for PCCI	Four hypothetical Φ stratification cases (profiles). Profiles are only in radial direction, and linear in ϕ Two fuels tested Results verified against CFD simulation	Steepest profile with rich zone on cylinder axis – earliest auto-ignition Gradient of profile has little effect on burn duration and NO _x .	ϕ is fuel/O ₂ equivalence ratio Results influenced by transition angle Discussion focuses more on transition angle
Onion-skin	[99]	HCCI H ₂ , NG	Parametric study: fuel (Φ) compositional stratification, compositional EGR stratification, thermal effect of EGR Isolation of the individual effects Light-duty engine	Different Φ in zones: from homogeneous to 50 % variability Variable residual concentrations between zones from uniform to 40 % difference Temperature differences between zones at IVC from 0 to 60 K	Modest effect of fuel stratification on SOC and CD; 1 CAD advance of SOC, 20 % longer CD Moderate effect of EGR stratification: 1.5 CAD advance of SOC, 35 % longer CD Substantial effect of temperature stratification	Potential of thermal stratification in HCCI control
Onion-skin	[101]	RCCI n-C ₇ H ₁₆ + NG	Parametric study: low- reactivity fuel (NG) stratification Heavy-duty NG-diesel RCCI	NG stratification by tuning parameters: $\Phi(1.3)$ and $\Delta\Phi$ Combustion performance evaluated on CA10, CA50, P _{max} , PRR _{max} IMEP _{net} , $\eta_{c,net}$, η_{comb} & emissions of NO _x , UHC, CH ₄ , CO	Increase in NG stratification affects η_{comb} improvement at low load THC & CH ₄ emissions decrease at low & mid loads P _{max} , PRR _{max} & NO _x increase in general	Shape of stratification – linear in phi space
Onion-skin	[145]	HCCI NG	Influence of P _{IVC} on BL thickness and wall heat transfer coefficient	Fundamental heat loss and BL model	Within a cycle, BL thickness increases during compression Heat transfer coefficient increases with P _{IVC} BL thickness decreases with P _{IVC}	—
Balloon	[209]	HCCI i-C ₈ H ₁₈	Influence of Crevice size on combustion performance	V _{crevice} = 1.26, 6.2, 10.26 cm ³ Rc maintained at 17:1 Influence of λ (2.5→4.5) also included Results verified against experiments	Smallest V _{crevice} showed lowest CO & HC emissions and highest η_{comb} CO increases with λ , & η_{comb} decreases HC emissions insensitive to λ	MZ model [76] captures trends of results very well nZ = 40 used.
Turbulence effect						
Balloon	[75]	HCCI C ₃ H ₈	Influence of swirl, T _{wall} and crevice volume on emissions (CO & HC) reduction potential Applying MZ model of [73] to propane fuelling	Two swirl ratios tested: 4.3:1 & 0.43:1 Two T _{wall} tested: 440K & 600K Five out of 10 zones are considered adiabatic	Swirl has little effect. CO & HC change by < 3% T _{wall} has significant effect CO & HC reduce by 75%	Hot walls effects – by correlation... Only 2 'states' for V _{crevice} influence – base and 0
Balloon	[84]	HCCI	Influence of piston bowl shape on combustion and emissions Sensitivity of piston induced turbulence on combustion	Flat vs. square piston bowl Influence of T _{IVC} (429K ↔ 451K) also investigated Results verified against experiments	Square piston bowl causes higher CO & HC, as well as lower η_{comb} HC emissions relatively insensitive to T _{IVC} , as opposed to CO & η_{comb}	CO predictions are poor (underpredicted, error ≈ 0.9) Trends in HC & η_{comb} with T _{IVC} is not captured well Trends in burn duration captured well
Fuel Reforming						
Onion-skin	[224]	HCCI n-C ₇ H ₁₆	H ₂ blending with n-C ₇ H ₁₆	Isolating chemical & dilution effects by artificial inert species approach H ₂ : 0 → 20 (%m/m)	CA50 retards with H ₂ CA10-90 first decreases then increases with H ₂ η_{th} , ind first increases then decreases with H ₂ Indicated specific UHC & N ₂ O emissions increases with H ₂ Influence of H ₂ decreases with EGR%	Interzonal mass transfer considered for crevice zone
Onion-skin	[225]	HCCI	Reformer gas (RG) blending with NG, n-C ₇ H ₁₆ , i-C ₈ H ₁₈	Isolating thermodynamic, chemical & dilution effects by artificial inert species approach [224] Interaction effect between artificial species also studied RG = 0.75H ₂ + 0.25CO RG: 0→50 (%m/m)	CA10 advanced for NG, retards for n-C ₇ H ₁₆ , slightly advances for i-C ₈ H ₁₈ with RG% Peak ROHR increases for all fuels with RG % Thermal effect of RG advances CA10 for all fuels Chemical effect of RG causes different behaviour in SOC for fuels	No interzonal mass transfer Influence of RG composition not studied
Onion-skin	[219]	HCCI PRF	Reformer gas (RG) blending with PRF [226] additional investigation on influence of supercharged condition	Isolating thermodynamic, chemical & dilution effects by artificial inert species approach [224] RG = 0.5H ₂ + 0.5CO (%V/V) RG: 0→30 (%BR) Varying PRF % Varying RG-PRF blends ROPA	Influence of RG decreases with i-C ₈ H ₁₈ % P _{max} , PRR _{max} , IMEP & NO _x emissions reduces with RG CA10, CD, UHC & CO emissions increases with RG Chemical effect most prominent, followed by dilution effect, then thermodynamic effect	—

(continued on next page)

Table 8 (continued)

MZM type	Ref.	concept	Application	Approach	Highlights	Comment
Onion skin	[227]	HCCI NG	Detailed study into the effects of water addition	Water addition to fuel up to 10 % Separation of thermal and chemical effects of water addition	Low-temperature H abstraction reactions rate decreases with RG RG has strong influence on LTHR Thermal effect of water is dominating over chemical effect. Thermal effect of water addition can effectively control SOC Water addition reduces reaction rate but not reaction pathways	Water injection can be used as an additional control tool for HCCI combustion
Second Law analysis						
Onion-skin	[228]	HCCI i-C ₈ H ₁₈	Exergy analysis Optimisation	Exergy analysis by varying P _{IVC} , Φ, rpm & V _D 300 simulation cases	Exergy efficiency increases with P _{IVC} , Φ, rpm Exergy efficiency highly sensitive to Φ, & low sensitivity to N _{eng} Optimal combustion timing to maximize exergy Optimal strategy to control load	Balloon, low no. of zones, emissions, no interzonal heat & mass transfer
Onion-skin	[229]	HCCI n-C ₇ H ₁₆	Availability (exergy) analysis of RG blending	Closed cycle analysis Isolating thermodynamic, chemical & dilution effects by artificial inert species approach [224] RG = 0.5H ₂ + 0.5CO (V/V) RG: 0 ↔ 20 (%BR) EGR: 0 ↔ 46 (%m/m)	Availabilities of chemical, thermomechanical, work, wall heat transfer & destruction decreases with RG % η _{II} insensitive to RG % Dilution effect of RG more influential on availability terms than chemical & thermodynamic effects Utilisation increases with RG %	Influence of RG composition not tested
Variable valve actuation						
Onion skin	[56]	RCCI	Parametric study: VVA (IIVO, eIVC, 2EVO) Heav- duty NG-diesel RCCI	IOCV & EOCV Combustion performance evaluated on T _{IVC} , T _{EVO} , CA10, CA50, P _{max} , PRR _{max} IMEP _{net} , η _{t,net} , η _{comb} & emissions of NO _x , UHC, CH ₄	EIVC – high load extension (by limiting P _{max} , PRR _{max}) LIVO – improved at η _{comb} low load 2EVO – improved η _{comb} & thermal management	—
Onion skin	[86]	RCCI	Parametric study: VVA (NVO) NVO + fuel injection (high reactivity) IIVO, eEVO, eEVC late IVO for validation Heavy-duty NG-diesel RCCI	Combustion performance evaluated on T _{IVC} , CA10, CA50, IMEP _{net} , η _{th,net} , η _{comb} & emissions of NO _x , UHC, CH ₄	NVO w/ eEVO + eEVC 15 % reduction in CH ₄ emissions Improved thermal management	—

CD = combustion duration; η_{II} = second law efficiency

% of air and exhaust was unmixed, also showed that the effects on combustion depended on the direction of stratification. When residual content in the core zone was increased, SOC was retarded by 1.5 CAD and combustion duration reduced by about 35 %. The trends were reversed for greater concentration of residuals in the boundary region. The common conclusion of the study is that increase of fuel concentration in the core zone advances SOC, independently of the diluent, i.e., air or residuals. However, combustion duration lengthens because more diluted fuel in the outer zones, which ignite later, burns slower. In a more realistic scenario, Kongsereparp et al. provided the results for combined compositional and thermal effect of residuals inhomogeneity. The results showed that the thermal effect dominated. Repeating the same research plan with NG revealed lower sensitivity, presumably due to lower NG ignition energy, but following the same trends.

Mikulski & Bekdemir [101] investigated the effects of low-reactivity fuel stratification in a Diesel-NG RCCI engine, as a response to difficulty of realising high-pressure gaseous fuel injection experimentally. At this point it should be noted that, in contrast to HCCI, where auto-ignition first appears in the centre of the combustion chamber, in RCCI more reactive diesel-like fuel is distributed in the outer regions, which ignite earlier. Therefore, unlike HCCI, in RCCI combustion there is usually incomplete burning in the combustion chamber's core zone. The investigations compared even distributions of NG with stratified cases, but with increasing fuel concentrations towards outer zones. The results showed that at low load, NG stratification improved combustion efficiency because the core zones contained less fuel, which usually is not completely burnt due to the quenching effect of temperature drop.

6.2.1.2. Influence of in-cylinder flow field/turbulence. The effect of in-cylinder flow field was studied mainly within the context of one-way coupled CFD-balloon approaches. Aceves et al. [75] conducted a limited study of how initial swirl number affected HCCI combustion characteristics for a low-load case. They changed swirl number by a factor of 10 (i.e., from 0.43 to 4.3), for which UHC and CO emissions changed by approximately 7 %. In a follow-up study [84] the authors used the same model for a detailed analysis of the influence of squish flow and turbulence on HCCI combustion. They tested two shapes of piston bowl: a flat one, and a square bowl shape with a surface area of its top land increased by a factor of 1.66. Results indicated that combustion duration was prolonged with the square bowl, with an advance in CA10 by about 6 CAD. However, this was accompanied by a 5 % drop in combustion efficiency. Although CO and UHC results were presented, it is difficult to make comments, since CO was underpredicted by a factor of 3-10, and good trend-wise results in CO and HC were not seen.

In the above methodology, information regarding flow field modelled by CFD was contained within the T-m history. Thus, by disregarding interzonal flows, the balloon MZ model had little to do with the sensitivity of the results. On the other hand, sophisticated MZ approaches [58,103] with predictive turbulence submodels, although capable, have not yet been used in the context of such studies.

6.2.1.3. Fuel composition/reforming effects. Guo & Neill used their eight-zone model [134] to study hydrogen enrichment on n-heptane-fuelled HCCI combustion [224]. The influence of H₂ blending on engine performance was analysed by isolated its effect on chemistry, dilution and

thermodynamics. To do so, artificial species were introduced to the chemical mechanism, substituting the corresponding components of reformer gas. Their MZ model was of the onion-skin type and included a dedicated boundary layer and crevice zone. Interzonal mass transfer was mainly considered for the crevice zone. The blending of H₂ was quantified as a fraction of total fuel mass (% m/m). Results show that CA50 retards with H₂ blending, with the dilution effect being most influential. Combustion duration first decreases and then increases with percentage of H₂, and is mainly influenced by its chemical effect. Indicated thermal efficiency increases with percentage of H₂ at fixed CA50. In terms of emissions, indicated specific quantities of UHC and N₂O increase with percentage of H₂, but N₂O sensitivity reduces with delayed CA50.

The influence of reformer gas (RG) blending was explored mainly in the context of HCCI. RG being a hydrogen-enriched gas [133], it was modelled as mixtures of H₂ and CO. Due to the chemical kinetics-driven nature of LTC, RG acts as an additive to affect combustion characteristics, and its influence depends on the type of baseline fuel used. The analysis to identify the influence of RG blending is along the lines of chemical, dilution and thermodynamic influences, similar to the previously mentioned artificial species methodology [224]. Reyhanian & Hosseini [225] performed a comprehensive analysis by including NG, n-heptane and iso-octane fuelling in a study mainly focused on RG blendings influence on combustion timing. NG showed an advancement in CA10 with increasing percentage of RG; n-heptane showed retardation; and iso-octane showed advancement, although less sensitive. The peak value of heat release rate increased for all fuels with RG blending. The thermal influence of RG causes advancement in CA10 for all fuels, owing to its high ratio of specific heats (γ). Dilution effect has a large influence on n-heptane. The chemical effect is the main reason for discrepancy in SOC behaviour between fuels. Individual contributions of CO and H₂ revealed both act to advance SOC for n-heptane, but for NG they act oppositely, with H₂ being more influential.

The study of Neshat et al. [219] focused on influence of primary reference fuel (PRF) composition coupled with RG blending. They used a similar methodology as the above, and fixed RG composition to a 50/50 H₂-CO₂ mix. RG blending with PRF was quantified on an energy basis, as in Eq. (72). The authors noticed that increasing RG percentage generally caused a retardation in combustion phasing; decrease in P_{max}, IEMP and NO_x; and increase in combustion duration, UHC and CO. Although some of these trends might not agree with the previous study, it is worth noting the difference in RG composition and the maximum levels to which RG-PRF blending was studied. Furthermore, analysis of chemical kinetics by rate of production analysis (ROPR) revealed that RG had a strong influence on low-temperature heat release (LTHR) of n-C₈H₁₈, by reducing rate of H abstraction reactions.

$$ER_{RG} = \frac{\dot{m}_{RG} LHV_{RG}}{\dot{m}_{RG} LHV_{RG} + \dot{m}_{PRF} LHV_{PRF}} \quad (72)$$

Ahari & Neshat [227] simulated addition of water vapour to an NG-fuelled HCCI engine, aiming to identify the mechanisms of water's effect on combustion and emissions. Generally, water additive up to 3 % increased thermal efficiency and substantially decreased NO_x emissions. Greater additions of water resulted in delayed and incomplete combustion, with high CO and UHC emissions. The use of the artificial inert species method enabled the authors to identify the effects of water. The most pronounced water function was its high heat capacity. Water's effects on combustion chemistry were negligible.

6.2.1.4. Second-law analysis. The goal of these studies was to investigate the mechanisms and sources of thermodynamic irreversibilities which otherwise would not be possible based on the first law alone. In combining the first and second laws, they assess the quality of energy content and identify potential for efficient resource utilisation. Saxena et al. [228] set out to investigate the influences of intake pressure, equivalence ratio, engine speed and displacement volume on the mechanisms of exergy losses. They used a one-way coupled CFD-balloon

model for the investigation on a gasoline-fuelled HCCI engine. They set up a simulation matrix consisting of 300 cases to accommodate variations of all input parameters, with quantities varied from four to six steps. Their analysis used the quantity exergy efficiency (η_{ex}), defined as the ratio between total indicated work and total exergy in fuel. Results indicated that η_{ex} in general increased with intake pressure, equivalence ratio and engine speed, but remained relatively insensitive to engine size. Importantly, the authors concluded that optimal combustion timing, according to exergy efficiency, occurred when unburnt species losses surpassed that of wall heat transfer. Thus, the optimal strategy to control load in HCCI engines mainly was to vary P_{IVC} during high-load operating points, while maintaining a constant value of Φ . Only for low-load operation was Φ to be varied, but minding that combustion phasing occurred before the point that induced a sharp increase in unburnt species.

Another example is the study by Neshat & Asghari [229], which analysed how reformer gas blending affected the various mechanisms of irreversibilities. Their baseline was an n-heptane HCCI engine, and RG composition was a fixed 50/50 (%V/V) mixture of H₂ and CO. For blending with n-heptane they used an energy-based quantifier, blend ratio, similar to the Eq. (71) and essentially used two operating points (0 and 20 BR %) to delineate the influence of RG blending. They used the quantifier of utilization factor, which was defined differently from η_{ex} . It was defined as the ratio of total availability utilised to the availability supplied to the engine. It included contributions of rejected heat to cylinder walls and exhaust gas on the output side, and accounted for availability of in-cylinder charge at IVC, apart from the chemical availability of the fuel. Results showed that chemical and work availabilities decreased with percentage of RG, and so did availability loss due to heat transfer. They observed that the irreversibilities decreased with percentage of RG, leading to an increase in utilisation factor, by approximately 1 % for every 10 % increase in RG. However, second-law efficiency (η_{II}) remained relatively insensitive. In terms of isolating the individual effects of RG blending, they used the [224] artificial inert species methodology. They discovered that the dilution effect was most influential and led to a decrease in thermomechanical availability.

6.2.1.5. Understanding variable valve actuation (VVA) effects. Regarding the application of variable valve actuation for LTC, readers are referred to the works by some authors of this current article [56,86]. These studies are of importance because, unlike most other studies in literature, they focus on prediction of RCCI combustion rather than HCCI applications. Both cited investigations used an onion-skin type multi-zone model and the VVA concepts were tested for NG-diesel combustion in RCCI mode. The primary focus in [56] was extending the operating range of RCCI. Three different VVA measures were studied, two of which were also realised on a heavy-duty RCCI test-engine hardware platform. Early intake valve closing (EIVC) simulations demonstrated that extending full-load operation up to 23 bar IMEP was possible while adhering to maximum cylinder-pressure limits, but with the observation that increasing load beyond 21 bar IMEP resulted in reduced thermal efficiency. On the other hand, late intake valve opening (LIVO) was observed to offer potential for moderate combustion efficiency improvement for low-load RCCI operation, where the improved combustion efficiency (in simulations) from higher blend-ratio operation could be countered by higher pumping losses in a real engine. Additionally, the authors also used the model to investigate the exhaust valve double lift (2EVO) strategy on the same platform. This entailed opening the exhaust valve for a short duration during the intake stroke to promote internal EGR and increase intake charge temperature. It was investigated in a one-way coupled simulation set-up where the multi-zone combustion model was coupled with a GT-Power engine model that simulated the gas exchange processes during valve flow. Simulation results indicated that it was possible to reduce engine-out methane emissions by as much as 98 %, along with up to 100 K

increase in exhaust gas temperature for better thermal management at low loads.

Continuing the theme of enhancing low-load RCCI combustion, the research presented in [86] focused on investigating the effects of negative valve overlap (NVO) and on-board fuel reforming by direct diesel injection. In this simulation study, the MZM presented in [56] was modified to represent the reduced valve overlap period and the partial fuel oxidation occurring in that phase. The timing and amount of diesel directly injected into the hot, recompressed exhaust gases was varied to modify in-cylinder thermo-chemical state prior to combustion. The strategy was studied in two cases: a high-EGR operating point and a lean-burn case. This VVA measure was shown to elevate the exhaust gas temperature to 850 K, enabling reformation of diesel and ultimately cutting methane emissions by as much as 15 %. At low loads, net indicated efficiency was also seen to improve, despite increased pumping losses from reducing the valve overlap. With these measures, the authors attempted to provide an outlook for RCCI operation across the full load-range, with emission reduction towards Euro VI limits. It must be noted that the simulation model used for these studies was best-suited

for trend-wise prediction of the combustion characteristics.

6.2.2. Application-oriented studies

Fast simulation times, comparable with high-fidelity 1D engine simulation, make the MZM particularly suitable for different applied-level studies. This refers mostly to finding/optimising the operating limits of the given LTC concept, as a prerequisite to detail control design, discussed in the next subsection. Tab. 9 gathers the works that used MZM to deal with defined application-oriented studies. The key findings and results are presented in the ‘Highlights’ column: the ‘Comments’ column lists aspects not directly mentioned in the publication or which provide related information outside the scope of the associated application.

Prediction of knock and misfire limits

True analysis of knocking conditions cannot be studied within the MZ framework, since its fundamental assumption of equal zonal pressure, breaks down. This is because the large-amplitude pressure waves associated with knock occur at speeds greater than that of sound.

Table 9
MZM use for application-oriented studies

MZM type	Ref.	Concept	Application	Approach	Highlights	Comments
Balloon	[230]	HCCI i-C ₈ H ₁₈	Knock limit prediction Misfire limit prediction	Based on analysing P and HRR using correlation Eq. (72) Results verified against data from literature Misfire: $\eta_{\text{comb}} < 93\%$	Formulated β correlation Knock mainly influenced by λ & EGR% Knock insensitive to T_{IVC} & P_{IVC} Knock occurs $\lambda > 1.8$ or EGR $> 30\%$	Influence of crevice on misfire limit not modelled Fixed N_{eng}
Balloon	[231]	HCCI i-C ₈ H ₁₈	Influence of T stratification on knock limit	Knock: ringing intensity $< 5 \text{ MW/m}^2$ MZM: five-zone, equal zone mass, adiabatic T stratification: linear (parametric variation)	To avoid knock: T stratification must increase with rpm. T stratification must increase with Φ Higher T stratification required for earlier CA50	Equal zone P assumption breakdowns No extensive validation of MZ model Heat loss ignored
Onion-skin	[67]	HCCI PRF20	Knock limits prediction	Comparing knock prediction methods: PRR_{max} [232] & β [230] Varied λ & EGR% Results compared against data from literature	For EGR $\leq 15\%$ both methods are similar PRR_{max} captures knock boundary better for EGR $> 15\%$ β not limited by solver time step size. But PRR_{max} is. Linear trend of knock boundary with λ Knock occurs at $\lambda < 1.8$ or EGR $< 30\%$	Fixed $N_{\text{eng}} = 700 \text{ rpm}$
Onion-skin	[57]	RCCI	Feasibility study: RCCI large-bore engine Optimising combustion performance over whole operating range	MZ decoupled air-path model Full factorial (5670 OPs) with variable EGR, T_{IVC} , λ , BR, SOI on stock hardware Optimising based on rc Constraints: $\text{NO}_x < 2.4 \text{ g/kWh}$ & $P_{\text{max}} < 180 \text{ bar}$ Large bore (B = 350 mm)	Peak $\eta_{\text{th}} \approx 47.8\%$ @ 75% load for stock hardware (rc = 12.2:1) Optimum @ $T_0 \approx 370 \text{ K}$, $\lambda \approx 2.6$, SOI $\approx 60 \text{ CAD bTDC}$, BR $\approx 83\%$ Peak $\eta_{\text{th}} \approx 51.8\%$ for rc = 15.2:1 within constraints of P_{max} & NO_x	Fuel stratification modelled from pre-tuned map Not validated on large bore 13-zone simulation time $\approx 20 \text{ min}$
Balloon	[213]	HCCI i-C ₈ H ₁₈	Generating performance map Identification of optimal operating region	Φ -iEGR performance map Constraints: $\eta_{\text{comb}} > 85\%$ & $\text{RI} < 5 \text{ MW/m}_2$ Constant speed operation Closed cycle MZ model	Optimum operating range at 25% $< \text{iEGR} < 55\%$ & $0.35 < \Phi < 0.65$ Optimum performance at 1 bar $< \text{IMEP} < 4 \text{ bar}$ & $28\% < \eta_{\text{th}} < 42\%$ Trend-wise results	Simulation time $\approx 10 \text{ min}$
Balloon	[98]	HCCI PRF90	Transient operation	Plant model: MZ+GEX Fuelling transient (step change in Φ from 0.9 to 1) rpm transient (step-change in N_{eng} from 1500 to 1250) Valve timing transient (Step- change in EVC by 6 CAD)		Step-change approximated by manual operation of actuators Step-change in rpm aided by fuelling change
Balloon	[112]	PCCI n-C ₇ H ₁₆	Transient operation Development of a dynamic time response plant model	Plant model: MZ+mean value+Wiener model [233] Controlled variables: IMEP, CA50 Actuators: SOI, EGR, m_{diesel} Response for step inputs in SOI, EGR & m_{diesel}	IMEP & CA50 are in very good agreement with experiment	Fixed fuel stratification imposed on all OP Simulation time of plant model $\approx 6 \text{ min}$ Constant speed operation

Nevertheless, MZ models can be used to predict propensity for engine knock, based on given operating conditions. The methodology relies on identifying when HRR exceeds the rate of pressure equalisation, which represents (localised) overpressure in a zone. To this end, Yelvington & Green [230] formulated a dimensionless parameter, Eq. (73) based on scaling analysis of the first law. In the equation, \dot{q} is the volumetric heat release rate and γ is ratio of specific heats. L_c is a characteristic length scale which was fixed to $B/10$. The parameter β is applied to all zones and knock is identified when $\beta \leq 1$. Basically, it implies that knock occurs when the HRR of any zone becomes greater than the rate of volume expansion of that zone.

$$\beta = \frac{L_c(\gamma - 1)}{\gamma P} \frac{\dot{q}}{v_{sound}} \leq 1 \tag{73}$$

Yelvington & Green conducted their study under constant-speed operation, and observed that λ and EGR were more influential than pressure and temperature at IVC. Results showed that knock occurred for $\lambda > 1.8$ or EGR $> 30\%$. In a following study, Tzanetakis et al. [67] observed similar results for the β criterion. In addition, they tested knock detection based on PRR_{max} , choosing a threshold criterion of 39 bar/CAD. However, for the PRR_{max} method, its value was sensitive to the size of the simulation's time step. After a sensitivity analysis, the authors settled with a value for time-step size of 10^{-6} s for 700rpm. Comparing both approaches, the authors noted that both performed similarly for EGR $< 15\%$, but the PRR_{max} method gave better predictions for EGR $> 15\%$.

Sjöberg & Dec [231] undertook a parametric study of the influence of thermal stratification on knock. They used the criterion for knock as ringing intensity $> 5 \text{ W/m}^2$, similar to [234]. This is shown in Eq. (74) where the unit of PRR_{max} is kPa/ms and for P_{max} is kPa. They employed a simple five-zone model and disregarded wall heat loss. Temperature stratification was set linearly across the zone, and the gradient was varied. They concluded that steeper thermal stratification reduced knock tendency. In other words, steeper thermal stratification was required to avoid the tendency to knock when operating at higher engine-speed or high equivalence ratio.

$$RI = \frac{1}{2\gamma} \frac{(0.05 PRR_{max})^2}{P_{max}} \cdot \sqrt{\gamma RT_{max}} \tag{74}$$

In terms misfire detection, the approach used thus far has been based on value of combustion efficiency. If combustion efficiency drops below a pre-calibrated value, it is considered that the engine operates in the misfire region. For HCCI, Yelvington & Green [230] followed this approach and selected the misfire limit as 92-94%. However, compared to their knock boundary predictions, the predictions of misfire did not

reproduce the experimental trends well enough. This may be attributed to the balloon MZM inherently producing poor emissions predictions (Section 5.3). In addition, their model did not capture the changes in IVC conditions well (by gas exchange model), due to large cycle-to-cycle variability during this unstable operation. Good estimates of IVC temperature and composition is shown to largely influence misfire predictions [235].

6.2.2.1. *Optimisation.* Due to the unique positioning of MZ models between simplified single-zone and detailed CFD models, they can be used as a reliable means of exploring the design space. Along these lines, Garcia-Guendulain et al. [213] focused on identifying the optimal operating region for an HCCI (i-C₈H₁₈) engine by generating a performance map. The design space was composed of ϕ and iEGR, and constrained by combustion efficiency and ringing intensity Eq. (73) thresholds of 85 % and 5 MW/m² respectively. They employed the MZ model of Kodavasal et al. [81] and did not incorporate a gas-exchange model. Thus, iEGR concentration was imposed, and the resulting T_{IVC} was estimated by using standard procedure [132]. With over 100 points in the design space, each run of their 40-zone model took about 10 minutes. The optimisation results were typical of Pareto front (Fig. 31), with optimal indicated thermal efficiency between 28 % and 42 %, and IMEP in the range of 1 to 4 bar.

Mikulski et al. [57] a performed an extensive study seeking the optimal performance region of a natural gas-diesel RCCI engine, with the goal to demonstrate its applicability as a mid-speed marine engine. Their hardware was based on a commercial, boosted, dual-fuel gas engine. They explored a vast design space composed of T_{IVC} , λ_{diesel} , BR, SOI_{diesel} , EGR concentration and across four representative load points. A total of 5670 cases were considered. The design was constrained by limiting NO_x to 2.4 g/kWh and peak in-cylinder pressure to 180 bar. The MZM employed was a detailed 13-zone, onion-skin (annular) type, extensively validated in their earlier works [56,92]. To improve computational efficiency, they ran a detailed air-path model which was decoupled from the MZ model. The sequence entailed first an optimisation run solely on the MZ model, followed by the air-path model simulation, with imposed burn rate from the previous run. The authors demonstrated that, based on the stock engine hardware, a peak indicated efficiency of 47.8 % was attainable at 75 % load, with CO and UHC emissions well below legislation limits. The optimum was located around T_{IVC} at 370 K, and λ , SOI and BR at 2.6, 60 CAD bTDC and 83 % respectively. In addition, they demonstrated the potential of hardware enhancements for RCCI performance. Their detailed analysis focused on compression ratio (r_c), showing a further improvement in indicated efficiency to 51.8 % at a r_c of 15.2:1. This was still within the previously

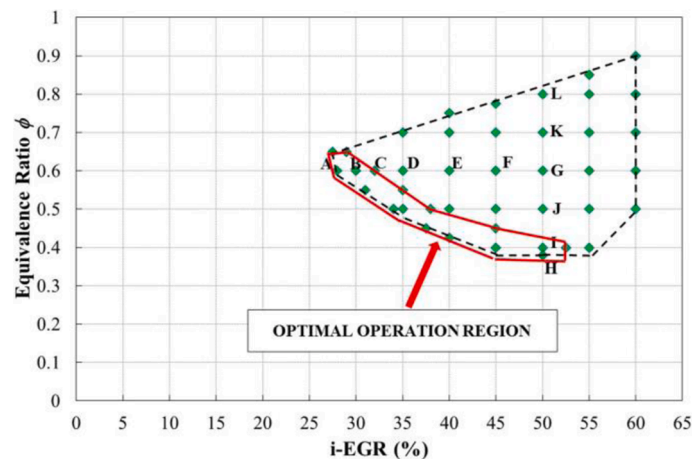


Fig. 31. HCCI operating region based, on optimisation for $\eta_{comb} \geq 85\%$ and $RI \leq 5 \text{ MW/m}^2$ from Garcia-Guendulain et al. [213]. (Reproduced with permission from International Journal of Engine Research, SAGE)

defined constraints, and was achieved by adjusting for optimal CA50 using T_{IVC} and BR.

6.2.2.2. Dynamic time response simulation. In an attempt towards creating transient simulation, Angelos et al. [98] developed a simplified approach. They created the plant model by coupling a two-zone to a detailed air-path model. The simulation was run in closed-loop cycles, each lasting seven or eight minutes, and requiring between 20 and 25 cycles to reach steady state. Transients were then introduced as step changes in the inputs, and the responses of $IMEP_{gross}$ and CA50 were monitored. For a step change in ϕ , from 0.9 to 1, the trend in transients of $IMEP_{gross}$ was captured well, with a small systematic 5 % over-prediction. Predicted response in CA50 was a 1.7 CAD drop, against experimental (mean) value of 0.7 CAD. The model was tested for speed transients (1500 to 1250 rpm) where a similar accuracy in $IMEP_{gross}$ as before was obtained. However, CA50 was largely underpredicted, around a value of 9 CAD. Finally, valve timing transients were introduced by earlier EVC by 6 CAD. The model was able to reproduce the response in CA50, which however was underpredicted by 7 CAD.

Felsch et al. [112] presented a comprehensive methodology for development of control-oriented, dynamic time response simulation, starting from 3D CFD results. Ultimately, their simulation toolchain followed the Wiener-type [233] approach, splitting the plant model into stationary and dynamic response parts. The stationary model consisted of an MZ and mean-value gas exchange model to capture steady-state operation, but also to well represent the non-linearities associated with LTC operation. The dynamic part was for transfer functions developed in the frequency domain. Considered inputs were SOI, EGR rate and m_{diesel} (mass of fuel injected); outputs were IMEP and CA50. Fig. 32 depicts the overall structure.

The MZM used was derived from a two-way coupled CFD-balloon model. It was made to operate as a stand-alone model by assuming a fixed zonal fuel distribution for all operating conditions. This was done,

based on the experimental matrix, which consisted only of an SOI sweep. Nevertheless, the overall simulation time for 15 zones was six minutes per cycle. The results (Fig. 32) were obtained for a square wave in SOI signal (between 20.7 & 30.7 CAD bTDC) while EGR and fuel mass injected were held at 30 % and 10.2 mg/cycle respectively. The integrated model captured the dynamics well, as shown by the responses depicted in Fig. 32. It is worth noting that experimental data were obtained via step response measurement in an HIL set-up.

6.2.3. Control development

All the combustion concepts discussed here lack a distinctive, fast-response ignition trigger. Since LTC is very sensitive to changes in IVC conditions and thermal and compositional stratification, closed-loop combustion control is believed to be a necessary pre-condition to maintain proper combustion onset [236]. The limited load-range originating from the low-load issues with combustion efficiency is another control problem for LTC, as is excessive combustion harshness at high loads, as discussed in the introduction. These issues make it difficult to cover the whole load-range with a single LTC strategy, so this usually calls for mode-switching towards more conventional (hot combustion concepts), leading to the need to develop proper control functions for this transition. Finally, overall LTC performance can be further improved by considering constrained or targeted (on-board extremum-seeking) control of emissions or/and efficiency. The control problem may be addressed with various actuators, usually involving fast thermal management (HCCI), combined with coordinated air/fuel path control strategies in stratified LTC concepts (PCCI, RCCI). Different LTC control approaches have been reviewed by, amongst others, Duan et al. [15], Li et al. [237], Pandey et al. [238], Rahul et al. [239]. Those works identify the proper combustion models as enablers for rapid prototyping of robust control, balancing system complexity with fast simulation. This section aims to give an overview of how MZ models fit this control-oriented application, revealing the benefits of a detailed,

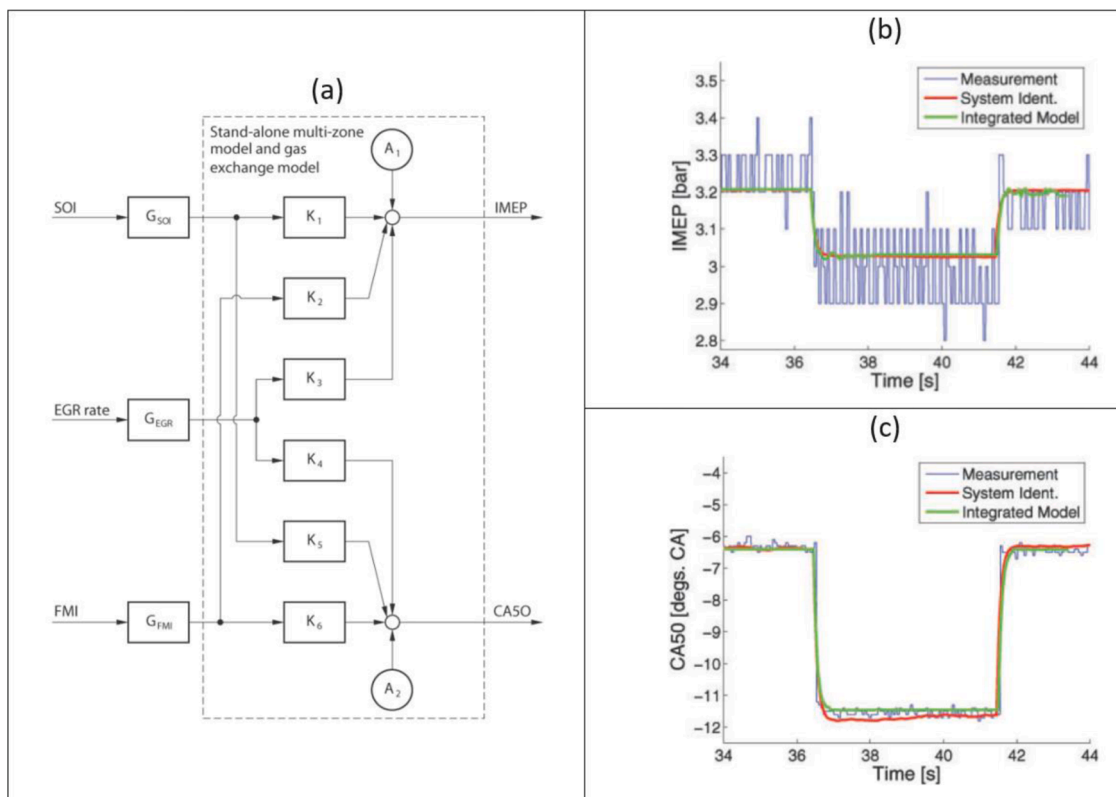


Fig. 32. Combined static and dynamic plant model (a) and comparison of measurements and simulation data for step SOI changes; IMEP (b), CA50 (c) from [112]. Data acquired for diesel engine operated in PCCI mode at moderate load. (Reproduced with permission from International Journal of Engine Research, SAGE)

Table 10
Application of MZM for controller development

Ref.	Concept	MZM reference model	Control model surrogate (COM)	Control strategy	Highlights
Map-based control					
[81, 213]	HCCI i-C ₈ H ₁₈	AMECS; accelerated 40-zone, 252 species & 1038 reactions balloon-type MZM	—	CA50 control; optimal control map for ϕ and iEGR	MZM model experimentally validated - the results show good agreement 10 min run on a single-core desktop computer
[240, 241]	HCCI ethanol	Six-zone, 58 species, 310 reaction MZM	—	CA50 optimal control map for N_{eng} , P_o & ϕ	Low nZ limits the emission prediction accuracy PRR cannot be predicted
[242]	HCCI ethanol	Six-zone, 58 species, 310 reaction MZM	Surrogate double Vibe model	CA50 control with 2 sets of input variables: VVA, EGR & VGT VVA, EGR, SC & VGT	Good correspondence between the double Vibe results and the MZM result – suitable for the system-level simulation study Double Vibe model computation time is 500 times shorter than the MZM
[59]	HCCI diesel	Five-zone model coupled with GT-Power model to simulate the whole engine process	NA	Dual PID control of IMEP and CA50; input variables: IVC & fuel flow rate	Concept demonstrating the cycle-simulation model to identify the PID controller parameters, and control design during transients in speed and load Controller performance is not considered
Model-based control					
[243, 244]	HCCI n-C ₇ H ₁₆ & ethanol	Single-zone, 38 species & 69 reactions	Reduced-order kinetics for resolving the ignition point and Vibe function for combustion	PID and MPC CA 50 controllers; comparison of two input variables: Fuel BR IVC	The physical COM model can be used as a base for feedback strategies for ignition control. Qualitative phasing behaviour is correctly reproduced at variations of input condition Model-based HCCI control entirely based on physical modelling has not been achieved Experimental results show both PID and MPC controllers are capable to track the reference and compensate for the disturbance
[65, 125]	HCCI i-C ₈ H ₁₈ & n-C ₇ H ₁₆	Six-zone, 64 species & 125 reactions MZM with inter-zonal heat transfer	0-D physics-based CA50 and IMEP model and ANN optimal CA50 and ANN minimum emission model	MIMO control (with three sub-controllers) of CA50, IMEP & emissions of CO + HC; input variables: fuel flow rate & ON (by BR).	COM model is validated by engine tests at steady-state and transient conditions with acceptable accuracy of CA50, IMEP, UHC, and CO The simulation time of the grey-box model on a 3.00GHz processor is about 0.1ms per cycle The controller is capable of tracking all desired set-points solely through load demand and rejecting the disturbances within three-five engine cycles
[64]	RCCI NG-diesel	XCXI; 13-zones, 354 reactions & 65 species, phenomenological heat and mass transfer	Nonlinear function fitted to approximate the MZM (the function is further linearised around the nominal operating condition)	MIMO combustion control of IMEP, CA10, NOx, and soot; input variables: SOI & BR	COM 99 % accurate versus detail MZM, but in limited range due to linearisation Robust control performance, effective decoupling, and fast settling time Control demonstration in MIL; MZM as a plant model
[62]	RCCI / CDF* NG-diesel	XCXI; 13-zones, 354 reactions and 65 species, phenomenological heat and mass transfer 2-zone model used for CDF mode	RCCI: nonlinear function fitted to approximate the MZM (the function is further linearised around the nominal operating condition)	Coordinated air-fuel path controller of IMEP, CA50, and PRR; input variables: VTG, EGR, SOI & BR	Robust combustion mode switching control developed (RCCI-CDF) Results demonstrated in MIL MZM and a two-zone model (CDF) coupled with MVEM (air-path) as plant model

predictive approach, and identifying the limitations.

Table 10 summarizes the most relevant research works that applied MZM to develop LTC control. In general, the control strategies can be divided into map-based and model-based approaches. We lead the following discussion accordingly, with a separate subsection for each of those control approaches. The schematic diagram in Fig. 33 should serve as a useful accompaniment to both subsections.

6.2.3.1. Map-based control. Currently, the most common way of engine control is the look-up table-based proportional integral derivative (PID) controller, where the controller adjusts the actuator's action to reach the reference condition. With the MZM model, a thorough simulation of all conditions can provide a preliminary optimal reference essential for this strategy. To this end, Kodavasal et al. [81] used an accelerated MZM model for engine cycle simulation (referred to as AMECS) which captures the closed cycle of the HCCI engine with initial condition obtained

from CFD analysis. The term accelerated refers to its use of block preconditioning of the multi-zone solver, reusing individual zone Jacobians over several time steps. The model was thoroughly benchmarked against detailed CFD simulation and HCCI engine experiments in [213]. The validation included two different engine designs and a variety of equivalence ratios. It proved in-cylinder pressure reproduction within experimental cycle-to-cycle variations and zonal temperature distribution within 4.4 K accuracy, comparing to the spatially averaged CFD results. The HC emission is underestimated, with the highest accuracy of around 65 %; CO estimation, in general, is underestimated, with the best accuracy of around 47 %. The validated model is further applied to generate a performance map where combustion timing CA50 is optimal for efficient and smooth combustion. This was performed by running the AMECS over 100 times for an engine controlled by equivalence ratio and internal EGR (iEGR) under single-speed, steady-state condition. Simulation results show that, with this map, when IMEP remains low, HCCI

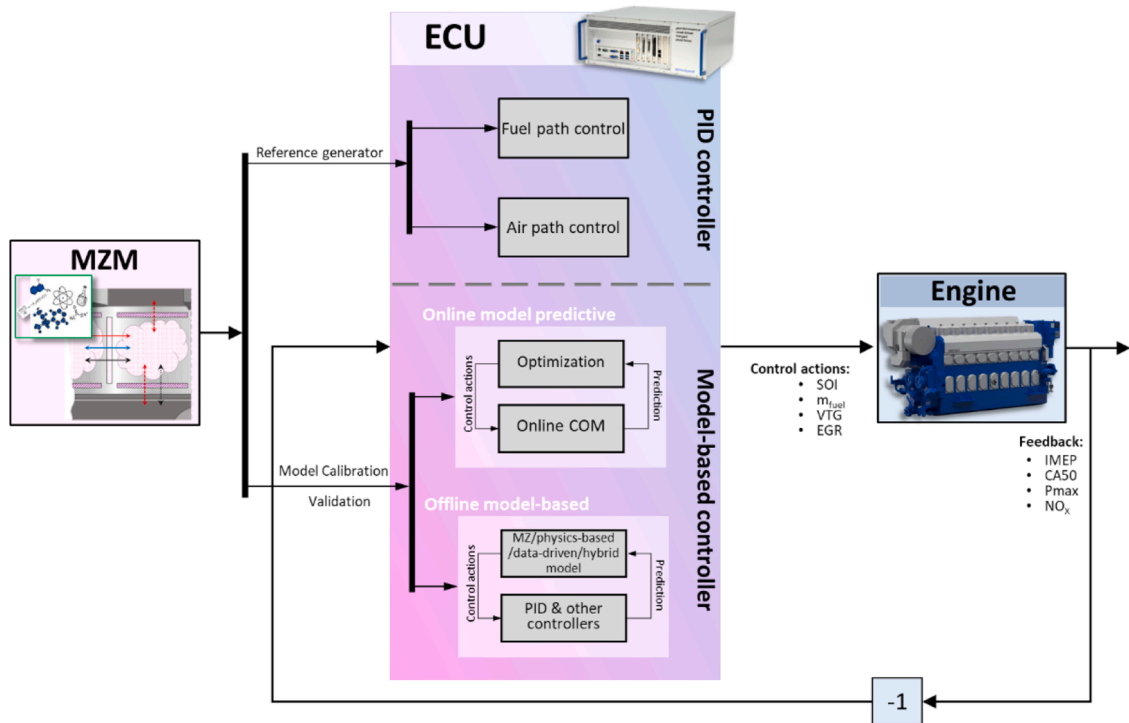


Fig. 33. MZM control design routines, including map-based and model-based strategies

operation can achieve high efficiency and low (essentially zero) NO_x and particulate matter emissions.

Pinheiro et al. [240], applied MZM full-cycle simulation to enable the high load to present the complete engine map for a boosted HCCI engine. They used a six-zone, balloon-type model incorporating inter-zonal heat and mass transfer and a kinetic mechanism with 354 species. The MZM simulation results match the experimental pressure traces with a small difference in the intake phase, while the combustion timing, and the average combustion rate match well and are suitable for the system-level simulation study. The engine map was built to ensure that powertrain systems are designed to achieve optimal performance, by defining the most efficient intake temperature, with the combination of variables: engine speed, intake pressure and equivalence ratio. Intake temperature is used to control CA50, thus the CA50 map is created further. The study identified the limitations of the control strategy, as the applied temperature actuation was not rapid enough for cycle-to-cycle engine control. Furthermore, the control map was created through the evaluation of steady-state conditions, so the effects of transient conditions on the performance map were not considered. Further limitations were identified on the model side. The use of only six zones meant the temperature gradient could not be properly captured, so the maximum PRR could not be predicted. At the same time, the emission predictions were unreliable, rendering the inclusion of emission-control strategies impossible.

Note that the authors also used the MZM presented in [240] to calibrate a fast-running combustion model (FRM) in [241]. A surrogate semi-predictive double-Vibe model was created, using parameters - the start of combustion, combustion duration and the shape parameter - extracted from the MZM. These parameters were obtained easily by means of a regression function for each one, found through DOE and the response surface method. The FRM showed good correspondence accuracy, and calculation time was 500 times shorter than the detailed MZM. However, such a model is engine- and fuel-specific and predictive only within the calibration range of the used training matrix, limiting its applicability.

This FRM model is further used as the combustion model in the full-engine model by Taritas et al. [242] to numerically study two different

charging strategies by a cycle simulation. The aim was to enable high boost-levels and high-load operation in an ethanol HCCI engine working across a wide speed range. The first set-up consisted of variable valve actuation (VVA), EGR and a variable geometry turbocharger (VGT) whereas the second one used VVA, EGR, a supercharger (SC) and VGT. To achieve CA50 of 8-10 CA ATDC, the two charging systems were compared, based on performance and efficiency. The approach of the cycle simulation model enables a relatively easy search for the optimal solution in a complex and large design space.

In work [59], a one-dimensional (1-D) GT-Power model was coupled with an external cylinder model which incorporates submodels for fuel injection, vaporisation, detailed chemistry calculations (Chemkin), heat transfer, energy conservation and species conservation. Modelling accuracy was improved by using a five-zone model to account for temperature and fuel stratifications in the cylinder charge. The predictions from the coupled model were compared with experimental data. The models prediction of the two-stage ignition phenomena and the start of combustion were fairly good. However, P_{max} was over predicted and there was a deviation from the experimental data during the expansion process. Inclusion of more zones in the multi-zone calculations as well as tuning the initial conditions for temperature and fuel-air distribution may offer improvements. Nevertheless, the predicted trends were generally in good agreement with the experiments. A dual PI-control (proportional, integral) simulation for simultaneous control of IMEP and CA50 by IVC timing and fuel amount was demonstrated. The controller parameters were identified by the integrated cycle simulation. The work mainly demonstrates that an integrated model can be used to develop closed-loop control strategies. However, the response time between control computation and actuation, and the effect of controller characteristics to capture cycle-to-cycle variations are two of the issues that were not considered.

6.2.3.2. Model-based control. The ever-increasing number of sensors and actuators in engines makes the feedback design more complex, due to the greater number of control parameters and couplings between control inputs and process variables. The conventional map-based controller works well for a single-input, single-output (SISO) system,

but there is no systematic way for a multi-injection, multi-input, multi-output (MIMO) system. Model predictive control (MPC) provides the solution for handling MIMO systems, especially in terms of constraints-handling ability and control optimization. MPC relies on the control-oriented model (COM) to predict the future system parameters from the current time step. The predicted process parameters are used to formulate a predefined optimization problem: by solving this problem the optimal control actions can be obtained, and this will eventually achieve the desired control objective.

Early works by the Combustion Engine Research Team from Lund University, Sweden, greatly contributed towards HCCI control [243, 244]. The model-based HCCI engine-control framework is well described by Bengtsson, Tunestal, & Widd [245,246]. The real-time capable HCCI control model was created by incremental simplification of the detailed MZM concept. The resolution was reduced to a single zone, and the reduced-order kinetics were maintained only for resolving the ignition point: combustion followed via a pre-calibrated Wiebe function. Such a model was used to train the controllers, which were designed from the result of direct control model linearisation. The controlled output was the combustion onset (CA50), and a fast thermal management system was used to obtain intake temperature actuation. Successful model-based control was accomplished for both the set-point tracking and disturbance rejection. Obvious limitations come directly from the used COM because its physics-based principle was too simplistic to provide MIMO functionalities in terms of combined emission-performance control.

Nazoktabar et al. [125] used a six-zone chemical kinetic mechanism with 125 reactions and 64 species to develop model-based HCCI combustion control. It included heat transfer between zones and assumed that blow-by is negligible and that all zones have the same pressure. The cylinder-pressure result from the validated MZM was very close to the experimental test and the model gave acceptable accuracy of emission estimation. Then the MZM was coupled with a genetic algorithm (GA) to find the optimal CA50 where normalized CO and UHC emission (NCHC) is minimum and IMEP are maximum at different engine-loads, with control variables of octane number (ON) and equivalence ratio. This methodology enables determination of the optimal CA50 for any load, and the data are used to train the artificial neural network (ANN) model for predicting the optimal CA50, based on IMEP trajectory and control variables. Afterward, the ANN model determines the minimum NCHC, employing optimal CA50 trajectory and control variables. The ANN optimal CA50 model and ANN minimum emission model, together with a physical CA50 and IMEP model, constitute a grey-box model, which acts as a virtual HCCI engine to track the main control variables. It was validated extensively with experimental data at steady-state and transient conditions from a Ricardo HCCI engine. The validation showed that the grey-box model was able to predict CA50, IMEP, NO_x, CO and UHC with average errors of 1.2 CAD, 0.4 bar, 10 PPM, 0.8 % and 394 PPM respectively. The simulation time of the grey-box model on a 3.00 GHz processor was about 0.1 ms per engine-cycle. In other work [65], the grey-box model is applied as a control model, where a MIMO controller has been designed to control CA50, IMEP and NCHC by fuel flow rate (FFR), fuel equivalence ratio (FER) and ON respectively. The disturbance effects of any sub-controller on the other ones were prevented by using two maps in optimum conditions. The controller was tuned and validated by using the MZM model, and it was concluded that the controller is capable of regulating and tracking the desired outputs in less than five engine-cycles and the controller can reject the disturbances within three to five cycles, with deviations within 0.04 bar, 0.5 CAD and 0.03 for IMEP, CA50 and normalized NCHC.

Indrajuana et al. applied an MZM-supported approach to investigate different RCCI control strategies [64,62]. The MZM, referred to as XCCI (discussed earlier in section 6.1), was used to develop dedicated control models, targeting a concrete strategy.

In [64] the detailed, 354-reaction, kinetic model, including 13 annular zones with a phenomenological heat and mass transfer model,

was approximated by a non-linear stationary function which described the cycle- individual combustion event, based on selected performance (CA10, IMEP and specific fuel consumption) and emissions (specific NO_x) indicators. Additionally, P_{max} and PRR were mapped by a separate function to predict if safety-priority mode should be enabled in control. The model was further linearised around the nominal engine operating conditions, which allowed reproduction of the detailed MZM results with over 99 % accuracy, however in a very limited range of parameter disturbances. The linearised model was further used to design the multi-input multi-output (MIMO) controller with start of injection and fuel values (of diesel and NG) as control actions. This cycle-to-cycle control strategy was tested on desktop simulations using the detailed XCCI MZM as the plant model, and it demonstrated robust and stable performance for the simulated disturbance rejection and reference-tracking cases.

In [62] Indrajuana et al. extended this RCCI combustion control concept into coordinated air-fuel path control, by combining static decoupling EGR ratio, pressure difference control with next-cycle CA50-IMEP-blend ratio control. The linearised XCCI model discussed earlier [64] and a two-zone thermodynamic conventional dual fuel (CDF) model are integrated into a mean-value engine model for the design of an RCCI-CDF mode-switching controller. Note that the CDF model was only trend-wise validated to show feasible sensitivities for diesel SOI and BR. In previous work [64], fuel-path control was applied here, with the decoupling method extended for coordinated air-fuel path control. An air-path feedback controller was designed, with EGR ratio and VTG as control actions. The closed-loop, mode-switching simulation showed all reference variables are reached within three seconds, indicating the stability and reference-tracking capabilities of the proposed controller. However, tracking errors occurred during a mode change: dynamic decoupling would be beneficial to reduce such errors.

7. Discussion and outlook

The present work encapsulates over 70 original works, aiming to create a concrete vision of MZM-based development of LTC engine concepts. This includes a review of 16 distinctive modelling approaches developed independently by numerous research groups over the past 20 years. These works are analysed, assessed and discussed, starting from modelling assumptions, and then moving through model composition towards model performance and application range. Table 11 presents a “big-picture” summary of the individual sections, helping to address the four research questions set out in the introduction and thus formulate a cohesive vision for MZM in LTC.

According to the core concept of phenomenological modelling, the detailed assumptions of the MZM will be tailored towards the given application, both in terms of the combustion concept to be simulated and engine development stages. Thus, it is logical first to answer the two research questions concerning application area (and Q4), and then address issues of optimum model configuration (Q1) and the accuracy/calculation-speed trade-off (Q2). The discussion follows this logic, and in addition to answering the research questions, also identifies specific knowledge gaps in the corresponding research areas.

7.1. Application of MZM with respect to combustion concepts and associated fundamental-level phenomena

As evident from Tab. 11, early MZ models were developed exclusively to tackle HCCI combustion, fuelled by the automotive industry's interest in this new combustion concept. The early toolchains were designed to support fundamental-level combustion studies, providing a solution to the simulation-speed issues of CFD simulation. A good example of such an approach is the Hydrodynamics, Chemistry and Transport (HCT) multi-zone model developed by the University of Michigan and Lawrence-Livermore National Laboratories [73,76,79]. The fundamental-level works covered various parametric studies

Table 11
Summary of most relevant works involving MZ models, grouped by the development team

Research Group / Model	References	Model highlights	LTC concept / fuels	Validity/ simulation speed	Applications
Lawrence Livermore National Labs, University of Michigan Massachusetts Institute of Technology HCT	Aceves et al.(2000)[73] Aceves et al.(2001), [76, 75, 209] Aceves et al.(2004)[218] Aceves et al.(2005)[84, 12] Flowers et al.(2002)[82] Babajimopoulos et al. (2002)[79] Babajimopoulos et al. (2003) [179] Yelvington & Green (2003) [230] Bedoya et al.(2012) [251]	One-way coupled CFD-balloon 10-40 zones T-m or T-φ map depending on application NG = (detailed) 179 species	HCCI Initially validated on NG i-C ₈ H ₁₈ , C ₃ H ₈	12 hrs (single- core) 2 hrs (parallelised) for 10 zones $P_{\max} \leq 5\%$	Fundamental: Crevice effects, piston geometry VVA (eEVC, 2EVO, NVO) Fuel stratification Applied: Knock limit analysis Optimisation
General Motors Corp. RWTH Aachen XOD	Hergart et al. (2005) [78] Felsch et al. (2007)[252] Felsch et al. (2009)[112]	One-way coupled CFD-balloon 15 zones IZMT (HL correlation) IZHT (enthalpy) T-φ map (detailed) 118 species	PCCI n-C ₇ H ₁₆ Initially validated on n-C ₁₀ H ₂₂ + α-methylnaphthalene	≈3 min In-cylinder pressure within cycle-to-cycle variations Trend-wise emissions	Fundamental: VVA (NVO) Applied: Dynamic time response simulation
University of Michigan University of Guanajuato AMECS (based on HCT)	Kodavasal et al. (2013) [81] Garcia-Guendulain et al. (2020)[213]	Balloon 40 zones Simplified thermal stratification by heat-loss multipliers (lumped) 252 species	HCCI PRF90	10 min (block preconditioning) $P - \text{qlt}$ HRR – qlt	Control dev: Map-based control
University of Michigan	Fiveland & Assanis (2001) [145] Fiveland & Assanis (2002) [91]	Onion-skin Two zones [145]; 17 zones [91] IZMT Heat loss (fundamental) Boundary layer submodel Turbulence (k-ε) (Detailed) 60 species	HCCI Initially validated on NG	$P - \text{qlt}$	Fundamental: Wall heat loss (BL phenomenon)
Ford Motors Corp. Chalmers University	Easley et al.(2001) [94] Ogink & Golovitchev (2002) [93] Orlandini et al. (2005) [74]	Onion-skin (enclosed) Six-nine zones IZMT (P_{EQ}) IZHT (enthalpy) ([74] disabled IZHT & IZMT) GEX (APM) (Skeletal) 109 species	HCCI, PCCI Initially validated on gasoline n-C ₇ H ₁₆ , i-C ₈ H ₁₈	≈30 min $P - \text{qlt}$ HRR – qlt	Fundamental: Fuel stratification
National Technical University of Athens	Komninos et al. (2005) [71] Komninos & Hountalas (2008) [139] Komninos (2009)[88] [256] Komninos & Kosmadakis (2011) [104]	Onion-skin (enclosed) 10-21 zones IZHT (diffusion), IZMT (P_{EQ}) Heat loss (fundamental) Turbulence (Yang & Martin) (Semi-detailed) 84 species	HCCI i-C ₈ H ₁₈	≈40 min $P - \text{qlt}$ HRR – qlt	Fundamental: Wall heat loss IZMT
University of Alberta Sharif University of Technology Babol University of Technology	Kongsereeparp et al. (2005) [99] Kongsereeparp & Checkel (2007) [133][89] Voshtani et al. (2014) [102] Reyhani & Hosseini (2018) [225] Fathi et al. (2017) [142]	Onion-skin (enclosed) [102,225] 11-13 zones IZHT (diffusion) Turbulence (Yang & Martin) GEX (valve flow) 53 species (GRI3.0)	HCCI, PCCI H ₂ , NG, n-C ₇ H ₁₆ , RG blending, PRF70	≈30 min $P - \text{qlt}$ PRR _{max} ≤ 20% Heat flow – qlt	Fundamental: T, fuel, EGR stratification Fuel composition effects (fuel blending, reformer gas)
University of Toronto University of Waterloo	Tzanetakakis et al. (2010) [67] Visakhamoorthy et al. (2012) [138]	Onion-skin (enclosed) 10 zones IZHT (HL correlation) Blow-by (Reduced) 32 species	HCCI PRF20, methane + hydrogen	≈1 min (parallelised) In-cylinder pressure within Cycle-to-cycle variations	Applied: Knock limit predictions Fundamental: Fuel composition effects (biogas fuelling)
National Research Council of Canada	Guo et al. (2009) [134] Guo & Neill (2013) [224]	Onion-skin (Enclosed) Eight zones IZHT (diffusion) Turbulence (Yang & Martin) GEX (APM) (Detailed) 177 species	HCCI n-C ₇ H ₁₆	In-cylinder pressure within cycle-to-cycle variations Trend-wise emissions	Fundamental: Fuel composition (H ₂ blending)

(continued on next page)

Table 11 (continued)

Research Group / Model	References	Model highlights	LTC concept / fuels	Validity/ simulation speed	Applications
University of Zagreb University of California	Kozarac et al. (2010) [97] Kozarac et al. (2010) [90] Kozarac et al. (2011) [241] Kozarac et al. (2014) [257] Taritas et al. (2014) [242] Pinheiro et al. (2015) [240]	Onion-skin Six zones IZHT (heat transfer potential) GEX (APM) (Skeletal) 291 species	HCCI i-C ₈ H ₁₈ initial validation	14-15 hrs (single- core) In-cylinder pressure within cycle-to-cycle variations Trend-wise emissions	Fundamental: VVA (NVO) Fuel composition (ethanol, biogas fuelling) Control dev.: Development of FREM Map-based control
Technical University of Eindhoven TNO Netherlands XCCI	Egüz et al. (2012) [100] Egüz et al. (2013) [141] Bekdemir et al. (2015) [183] Mikulski et al. (2016) [92] Mikulski & Bekdemir (2017) [101] Mikulski et al. (2018) [56] Mikulski et al. (2019) [86] Mikulski et al. (2019) [57] Indrajuana et al. (2016) [64] Indrajuana et al. (2018) [62]	Onion-skin (annular) 10-13 zones IZHT (diffusion) IZMT (diffusion) Turbulence (scaling const.) GEX (SZ valve flow) (Semi-detailed) 65 species	Mainly RCCI diesel-NG; Initial validation on PCCI	≈30 min cycle <i>P</i> – <i>q</i> _{lt} HRR – <i>q</i> _{lt} CHR – <i>q</i> _{lt} <i>p</i> _{max} ≤ 10 bar	Fundamental: Low-reactivity fuels stratification VVA strategies Applied: Design exploration and optimisation Control dev.: Controller design and mode- switching control
Sahand University of Technology ^{a,b} Islamic Azad University ^c	Neshat & Saray (2014) [87][131] Neshat & Saray (2015) [247] Neshat et al. (2016) [219] ^a Neshat et al. (2017) [226] ^a Neshat & Saray (2019) [258] Neshat & Asghari (2019) [229] Ahari & Neshat (2019) [227] Lashkarpour SM (2017) [95] Nazoktabar et al. (2018) [125] Nazoktabar et al. (2019) [65]	Onion-skin (annular) 11 zones IZHT (diffusion) IZMT (P _{EO}) Heat loss (fundamental) Turbulence (Yang & Martin) GEX (OD) Coupled CFD-MZM for fuel distribution 65-137 species, depending on fuel	HCCI, RCCI Initially validate on HCCI using n-C ₇ H ₁₆ & NG PRF mixtures, PRF/RG blend, NG	<i>P</i> – <i>q</i> _{lt} HRR – <i>q</i> _{lt}	Fundamental: Fuel composition (Reformer gas blending) Exergy analysis Water injection Wall heat loss (comparison of HL models) Influence of IZMT
Politecnico di Milano	Bissoli et al.(2013) [103] Bissoli et al.(2016) [96] Pelucchi et al.(2017) [248]	Onion-skin (enclosed) 10-15 zones IZHT (diffusion) IZMT (diffusion) Turbulence (Yang & Martin) Heat loss (fundamental) (Detailed) 480 species	HCCI Validated on PRF20 n-C ₇ H ₁₆ , methyl-hexanoate, methyl-decanoate	≈2 min (15 zones) <i>P</i> – <i>q</i> _{lt} PRR _{max} ≤ 20% Heat flow – <i>q</i> _{lt}	Fundamental Fuel composition (n-butanol, n-pentanol, TRF/ butanol blend) Applied: Extending engine performance map
Karlsruhe Institute of Technology	Eichmeier et al. (2014) [58]	Spray-based IZMT (diffusion) Turbulence (single eqn k) GEX (APM) (Reduced) 41 species	RCCI Gasoline-diesel	12s (parallelised) <i>P</i> – <i>q</i> _{lt} HRR – <i>q</i> _{lt}	—

gex = gas exchange model; APM = air path model; IZHT = interzonal heat transfer; IZMT = interzonal mass transfer

investigating, amongst others, the effects of piston geometry on HCCI performance and emissions [84,209], various fuels including different PRF [247], reformer gas blends [226] and natural gas blends [101]. These kinds of studies are still popular, because capturing the fuel compositional effects is inherited by the governing chemical kinetic submodels. Within the HCCI regime, they were recently picked-up, amongst others, by Politecnico di Milano on n-butanol and n-pentanol [248]. The potential of MZM fuel-sensitivity simulation spans towards other alcohols (ethanol [240]) bio-gas compositions [138] and supports the current interest in direct use of hydrogen in LTC engines, as

investigated by researchers from the National Research Council of Canada [224]. Regarding high reactivity fuels, the challenge lies in simulating the effects of biodiesels on LTC. MZM can capture those effects provided appropriate multicomponent mechanisms are able to reflect ignition properties of associated hydrocarbon chains. Examples of such biodiesel mechanisms may be Luo et al. [249] or An et al. [250], however, their application in MZM is yet to be seen.

More recently fundamental-level MZ modelling has leaned towards PCCI concepts more than HCCI. This supplements the bulk portfolio of HCCI explorations of thermal [72,81,99,135,251] and compositional

(EGR) [79,90,99,179], towards a better understanding of fuel stratification. These fundamental issues have been studied by almost all the development groups listed in Tab. 11 and both balloon and onion-skin type models have proved suitable for this purpose. However, we note that in many cases the authors silently hypothesised that models that were validated for homogenous combustion are ultimately valid in the PCCI domain too. One should bear in mind that, at least for simplest models without interzonal heat and mass transfer [77], the hypothesis may not hold, rendering the results questionable. The few dedicated MZ models created explicitly for stratified PCCI combustion include the onion-skin approach by Technical University of Eindhoven [100], and the balloon-type XOD model by General Motors Corporation [78].

MZ models applied towards dual-fuel RCCI are comparatively rare in literature. A singular spray-based MZM by Karlsruhe Institute of Technology [58] led to a paper reporting validation results, but the works did not follow up with publicly reported use cases. That apart, the only MZM thoroughly validated on RCCI is the XCCI toolchain by TNO Netherlands [92]. Note that this approach bases on earlier FORTRAN code designed in TU-Eindhoven for PCCI combustion [100].

Regardless of the combustion concept, one of the most prominent fields of explorative MZM simulations was understanding the effects of various VVA strategies on LTC [56,79,179,242,252]. After connecting with the gas exchange submodel, the inherited sensitivity of kinetic-based models to thermal and compositional effects make MZ models particularly suitable for this kind of application. Complex valving strategies incorporating fuel reforming effects during the NVO phase are also within the realm of MZM applications [86,252]. As proven by Mikulski et al [56,86], the results of VVA simulations qualitatively are valid for multiple engine platforms, without needing to re-calibrate the model. VVA control is commonly considered as an enabler for LTC, so this field of explorative research creates an important bridge for MZ models towards applied development, addressed in the next research question.

In summary, MZ models have been proven suitable for all “clean” LTC concepts, with RCCI being so far the least documented. In terms of PCCI and RCCI, the regimes on the boundary of conventional CI (like PPC) where diffusion flame plays an increasing role, the results are predicted with increased error. The only “hybrid” solution advertised to be capable of capturing the LTC and CI regime is the spray-based MZM by the Karlsruhe Institute of Technology [58]. However, it has not been thoroughly validated, nor confirmed in any direct applications. Consequently, one can say that the state of the art for MZ models’ use for resolving combustion regime change remains co-simulation with other phenomenological (diffusive flame and/or flame propagation) combustion models. In such a case, transition points are simulated independently by both models and a good approximation of actual engine performance and emissions can be achieved by weighted averaging of the results, as proposed by Indrajana et al. [62].

Turning to performance/emission simulation of LTC, the scope of confirmed fundamental-level applications of MZ models is similar to CFD, as long as insight of detailed dimensional and flow effects is not sought. Naturally, one must acknowledge the accuracy reduction in favour of covering trends from many more simulations, both on the individual operating-point bases or cycle-to-cycle basis. Apart from faster simulation allowing large-scale parameter sweeps, another undervalued advantage of low-fidelity simulation for fundamental-level research is that it allows easy decoupling of the governing mechanisms. When the goal is to understand those mechanisms, the targeted research produced with MZM can have potentially bigger archival value than largely generic CFD simulations. A good example of such highly-cited, fundamental-level research performed with an MZM is the paper of Mikulski et al. [101], investigating the effects of low-reactivity fuel stratification on RCCI combustion.

7.2. MZM and applied engine research

The reduced model complexity and focus on governing combustion mechanism make MZ models particularly suitable for applied-level research. The boundary between fundamental- and applied-level research is not explicitly defined. Naturally, the fundamental insight obtained from various parametric explorations, mentioned in the previous paragraph, provides the basis for efficient design of optimisation experiments and engine-control functions. This incremental type of research is therefore defined here as applied research. Accordingly, any research with a primary goal of a functional and robust LTC engine, basing on an established combination of an experimental set-up and MZM, is regarded as applied in this paper.

This maturity requirement narrows down the portfolio of such applications. Surprisingly, this review has revealed only two publicly available reports of MZ models being employed in large-scale LTC optimisation endeavours [57,213]. Neither of these optimum-seeking study has been verified experimentally, leaving a knowledge gap in MZM applications. This gap is significant, because these kinds of phenomenological combustion models are expected to solve the dilemma of the extensive calibration effort for next-generation engines. Only Mikulski et al. [57] attempted to couple the MZM with a detailed air-path model for fully resolved extremum seeking. This research had the potential to resolve another knowledge gap for MZM applications - namely its coupling with one-dimensional engine air-path models. The XCCI MZM, however, was not integrated with the GT-Power engine model used in this study, and IVC conditions were provided off-line without aiming for convergence.

Two research studies aimed to use MZ models directly for transient engine simulations [98,112], thus moving towards coupling MZM with engine models for a complete, system-level toolchain. However, Angelos et al. [98], as in the earlier-cited work by Mikulski, could not cope with the computation effort and so settled for coupling a simplified two-zone surrogate of his detailed MZM with a GT-Power engine model. Felsch et al. [112] coupled his full MZM, but the engine model was simplified to a mean-value approach. Thus, the full coupling of MZM kinetic codes with third-party engine-modelling software remains to be demonstrated.

MZ models have been widely used for HCCI control development. These were usually speed-oriented models (reduced zone number or simplified chemical kinetics mechanisms) used directly to generate a reference map for the controller [59,213,241,242]. Some researchers used an intermediate approach: Taritas et al. [242] used very narrow MZM-generated data to first train a much faster Wiebe function-based combustion model surrogate. This was then used to increase the control map resolution. In the light of bulk research using the direct approach, the additional effort of training a surrogate might seem questionable. But with typical simulation times of MZ models (~30 minutes), one needs to bear in mind that not all authors have access to high-performance cluster computing that allows direct generation of large-scale maps.

Such map-based control strategies have been successfully verified experimentally in many cases, providing solid proof of concept for MZ models as LTC-control design tools. On the other hand, most of these tackled relatively simple dual-input (equivalence ratio and EGR [213]; IVC timing and fuel amount [59])/single-output (CA50 [213,240,242]) control problems, excluding, for instance, emissions control. Their use of MZ models as map-generators was largely an academic exercise, since the workload of calibrating an MZM most probably would be no less than the experimental effort needed to create the controller maps experimentally using DOE techniques (refer to Fig. 8).

From this perspective, committed MZM development makes much more sense for more-demanding MIMO controls. These have been mostly realised as model-based control, where the controllers encapsulate the models. The controller model is a surrogate derived from the detailed MZM. These surrogates have been obtained by various measures, starting as simple nonlinear approximation around the operating

point [62] of interest, and moving towards the most sophisticated direct reduction of MZ models (single-zone Wiebe incorporating part of the kinetic mechanism to be predictive on SOC [244]). Coordinated air-fuel path control of RCCI is an emerging topic and MZ models have highlighted its usefulness. In this domain, the work of Indrajana et al. [62] represents the state of the art, although it has limitations of the controller and has only been confirmed in MIL simulations.

Considering the rapid progress in model-based control methodologies, MZM application in RCCI control is thus considered largely uncharted territory. With plenty of open questions concerning optimum controller design, model reduction techniques and real-engine validity, many more contributions are needed to advance LTC strategies towards market readiness.

7.3. Evolution of MZM

Chronological analysis of Tab. 11 reveals that balloon models are making way for onion-skin models. This trend is explainable when we look at the applications. Computational power has progressed rapidly in the past 20 years, along with computational techniques for reactive CFD. Thus, accelerating the reactive simulation stops being the primary goal for MZ models that evolve from largely CFD-dependent balloon models towards more generic and autonomous onion-skin models. The requirement for autonomy is relevant to the applied research discussed in the previous point. If the model should reduce the effort for engine calibration and control design, it should not be forced to rely extensively on experimental (or high-fidelity simulation) results for its own initialisation and calibration.

Onion-skin models are a better fit for autonomy. They can rely on simple yet reliable estimations of IVC conditions, derived, for instance, from isentropic valve flow correlations [86]. This provides the MZM with full-cycle simulation capability, while thermodynamic conditions at intake/exhaust port/manifold are used to initialise the model. Thermal stratification, a determinant for combustion phasing and emission formation in HCCI, can be resolved during the simulation, instead of imposing the T-m map as occurred in most early-stage balloon-type MZ models. For stratification to evolve during the simulation, the model needs to employ a proper mechanism of heat transfer to the environment and between the zones. In terms of the first submodel, there seems to be agreement that diffusion-based mixing better resembles the system phenomenology and is computationally more efficient than the P_{EQ} -based approach. Two concepts compete for modelling heat loss. Neshat & Saray [87] and Komninos et al. [104] advocated advantages of fundamental heat loss modelling over the empirical heat transfer correlations popularly used in other phenomenological models. The first approach mainly benefits from calculation efficiency, since in principle the same phenomena govern the interzonal interaction and zone-to-environment coupling, so calculation can be partially shared. On the other hand, the original correlations of Woschni or Hohenberg have been validated on a variety of engine classes (including LTC) and are well established in post-processing the experimental data. Thus, if used properly, they can reduce the amount of effort necessary for model calibration. However, it is necessary to stress that heat transfer correlations were used inconsistently in the studied works. Not all authors acknowledged that correlations were validated for bulk in-cylinder conditions. In principle, applying the same correlation to individual zones requires normalisation (in every time-step) so that the sum of heat losses per zone is equal to bulk heat loss, as postulated in Kodavasal et al. [81]. Still, very accurate modelling of heat loss coefficient has no real point if the cylinder wall temperature is not evaluated carefully, as this has a governing effect on overall heat transfer. In many studies this was just assumed from literature, forming an example of unjustified simplification. Relatively simple yet accurate methods exist for estimating wall temperature of various cylinder components, and their use with MZ models is recommended [96,94].

Applying physics-based heat transfer models assumes both laminar

and turbulent phenomena. The effect of turbulence has been neglected by some researchers, although its influence on transfer of heat and mass can be an order of magnitude greater than in steady-flow conditions. This example, together with the previous note on using heat transfer correlations, illustrates the pitfalls of creating phenomenological models. To this end, we consider phenomenological turbulence modelling to be crucial for predictive simulation at different engine- speeds, boost pressures or VVA strategies. Although traditional k- ϵ or K-k turbulence submodels have been used in MZ models, the Yang & Martin [158] approach now seems to be established in state-of-the-art onion-skin models. This mainly is due to its low demand for calibration, using a single tuning parameter to reflect differences in engine hardware.

Including turbulence will have a more pronounced effect in LTC concepts that include stratification of mass. Needless to say, MZ models for simulating PCCI or RCCI regimes should include a proper mass transfer submodel, as evident from Tab. 11. At each time step, reaction products from one zone will be transferred to their neighbours, reinforcing (highly reactive radicals) or suppressing (for instance, CO₂) reaction rates in these zones. Studies on RCCI modelling [101] show that without this mechanism in place, largely fuel-lean core zones have no chance of igniting, heavily underestimating the overall combustion efficiency. The mass transfer is usually handled according to the same principle as the interzonal heat transfer. For gradient-based approaches, individual species concentration is used as the driving force.

Sophisticated MZ models suitable for PCCI/RCCI include submodels for simple (imposed rate) fuel-injection and evaporation [100]. The initial fuel distribution between them is still imposed, from optical engine data or CFD studies [95], or as a calibration parameter [92,101]). So far, there is no successful attempt to couple an onion-skin model with a phenomenological spray formation submodel [206]. This remains a major gap to be filled in the drive for fully autonomous MZ models.

Leading-edge onion-skin MZ models have 6-15 zones and employ mechanisms for between 53 and 480 species (Tab. 11). Both parameters naturally are influenced by the accuracy/calculation-speed trade-off that is chosen: this point is pursued in the next subsection. It is important to stress that generally, more advanced LTC concepts will require more zones. They will also need more elaborate mechanisms to handle the complexity of fuel and the number of species that need to be captured. For example, initial studies with PRF require fewer species and thus fewer reactions than the studies that aim to capture fuel compositional effects. Here for instance the influence of different renewable diesels (compositionally complex mixtures) on LTC combustion forms a particular challenge that has not been yet addressed in MZM simulation. Similarly, dual-fuel RCCI combustion will require bigger mechanisms than single fuel HCCI or PCCI simulation.

The requirement for more zones stems from the need for better reproduction of stratification and chamber geometry effects. Again, simulation of stratified charge concepts usually involves grid-resolved simulation with a zone count above 10 [95,141], whereas six zones have proven sufficient for simple HCCI concepts with flat piston geometry [97,125]. Zone size distribution favours smaller zones towards the cylinder liner for optimum capture of influences on combustion timing and NO_x formation. Smaller zones are also preferable towards the cylinder centreline, where there are important influences on combustion efficiency and HC/CO emissions. To this end, smart zonal distribution, either imposed or generic, facilitates accurate simulations with fewer zones. In addition to the numbers mentioned above for forming a clean annular/enclosed zone structure, there is the need to reproduce the combustion chamber's geometrical features. A separate crevice zone is considered essential for accurate UHC/CO emission results, regardless of the combustion concept [71]. Then, depending on the target of the simulation, one can consider one to three zones to account for combustion chamber/squish zone, which would be useful for comparing different hardware. It may also be beneficial to have additional separate zones pertaining to the boundary layer, to investigate how thermal properties of cylinder components, such as the hot exhaust valve seat,

affect ignition and emissions. These additional special zones usually result in a hybrid annular/structure with more complex constraints applied on interzonal mixing models.

7.4. Accuracy and speed of MZM

As already outlined, the trade-off between accuracy and calculation speed will majorly depend on the task-tailored composition of the model. Many remarks on model accuracy have been already provided while addressing the research questions above. It is useful to address the issue of accuracy and simulation speed by first defining a certain benchmark. Then, by synthesising the knowledge from sections 4 (Relevant submodels), 5 (Simulation procedure) and 6 (Model application and validation), we will discuss the factors that have greatest influence on the trade-off.

Of the studies listed in this review, most that report in detail on model performance are works related to model calibration and validation. Usually, this step ultimately determines the grid-resolved zonal configuration beyond which additional zones do not lead to significantly better accuracy. This is confirmed in [Tab. 11](#), as practically all the models report accuracy in terms of in-cylinder pressure within the cycle-to-cycle variations, and aim to predict trends in emissions without ambitions to get the absolute level correct. The fact that this is reported regardless of the number of zones, size of mechanism or involved submodels, is partially explained by the fact that simpler combustion concepts require less-detailed models – a trend already discussed in the earlier research question. Finally, MZM accuracy will depend on how carefully the model has been identified and calibrated and in what range this has been done. Although authors usually claim that the model is valid outside the calibration space, none of the studies reported have verified this for the whole foreseen engine map – a shortcoming that needs to be addressed to establish trust towards the MZM family in general.

Aside from consistency in the claimed accuracy, individual research groups report largely consistent simulation times. This is also explained when we consider evolution of the MZ models. The models have gradually become more sophisticated to tackle more complex combustion concepts, but the growth in model complexity has been balanced by the progress in the computational power of the workstations.

Let us assume that the current state-of-the-art MZM is an onion-skin model with 13 zones, including intentional heat and mass transfer submodels, with a reaction mechanism involving a combination of six PRF and suitable for simulating a variety of combustion concepts, from HCCI to multi-fuel RCCI. The expected simulation time on a leading-edge personal computer will be around 30 minutes, depending on the exact assumptions and efficiency of implementation (coding, solver choice etc.).

From this reference, assuming proper calibration, increasing the zone number usually does not bring substantial improvement in the estimation of in-cylinder pressure trace and resulting combustion indicators, but does influence the emission calculation. On the other hand, every extra zone will increase the number of required operations by the factor of $[1 + 1/nZ]^3$. Thus, moving from 13 to 14 zones with a non-segregated solver increases the simulation time by 25 %.

The size of the mechanism affects calculation time but this is largely dependent on how well the solver can deal with the stiffness of the system. Typically, stiffness in the chemical mechanism is due to the large spread, highly coupled and non-linear rate of change of species, especially the rapid elementary reactions. Furthermore, overhead of memory usage increases with the size of mechanism, including computation expense for the thermo-chemical data-handling routines. There are many mitigation strategies for this: one potential approach yet to be explored in LTC MZM is tabulated chemistry. This has been implemented, for instance, in phenomenological models [[253,254](#)] for conventional SI, where it was reported to speed-up calculation by a factor of four or five.

Stiffness arises in MZ models due to the coupling among the zones, based on pressure equalisation. In comparison, diffusion-based interzonal mixing has secondary influence [[186](#)] on computational demand. A proven mitigation strategy is to use a segregated solver, whereby computational effort is $1/nZ^2$ of the non-segregated approach [[81](#)]. This acceleration reduces the typical simulation time to 30 minutes for a 13-zone model, as mentioned above. Further reduction techniques involve alleviating dense Jacobian construction. Perhaps the analytical Jacobian approach offers most promise: there is a report [[98](#)] of an order of magnitude decrease in simulation time of a two-zone model. Other approaches include tri-diagonal block sparsity in Jacobian [[96](#)] (via G formulation) and Jacobian preconditioning [[81,186](#)]. However, from a programming/implementation perspective, parallel computing has been shown [[58,138](#)] to reduce the time of a typical 10-zone simulation to the order of seconds. Furthermore, computing on graphical processing units reportedly [[255](#)] is able to cut simulation time by a factor of two to four, and this potential is so far unexplored in MZM studies for LTC.

7.5. Outlook

Although MZ modelling has been used for LTC simulation for over 20 years, the evolving development of LTC technologies sets new modelling challenges. Literature analysis indicates a recent revival of interest in these toolchains associated with maturing dual-fuel RCCI technology and its extensive needs for calibration and control. To this end, the above discussion has revealed multiple knowledge gaps in MZM development, application and techniques to improve calculation speed. The individual challenges ahead will be restated in the conclusions for clarity. In broader terms, there are two core issues that need addressing. First, there is no openly available MZM toolchain thoroughly validated for RCCI combustion. Second, there is no complete proof of concept that MZM can support the evolution of RCCI and other LTC technology throughout the complete engine development pathway foreseen in [Fig. 10](#). Overcoming these development challenges requires excellent infrastructure, substantial resources and strategic commitment, beyond the reach of the relatively small consortia (refer to [Tab. 11](#)) working in this field.

The recently established Clean Propulsion Technologies (CPT) [[259](#)] consortium has those mentioned resources and strategic commitment to developing MZM-supported RCCI combustion. This work will be in synergy with other highly promising powertrain technologies, including advanced aftertreatment and deep hybridisation with self-learning power management. The CPT consortium brings together the core of the Finnish powertrain industry and academia in a 15-million-euro project focused on the marine and off-road sectors. [Fig. 34](#) illustrates how CPT work packages (WP) 2 and 3 relate directly to MZM/LTC.

WP3 will apply the lessons learned from this review, developing a new MZM by taking it from the governing assumptions towards a fully autonomous simulation toolchain. The model identification and creation of dedicated submodels (spray/fuel distribution, turbulence) are supported by high-fidelity CFD simulation, validated on a state-of-the-art RCCI engine with variable valve actuation and using natural gas/diesel as the baseline fuel mixture. The final experimental validation of the MZM involves three engine platforms with cylinder bores of up to 310 mm and having different spray patterns. The developed MZM will be used to optimise the RCCI operating range and to develop the sophisticated multi-input/multi-output RCCI control. The latter's control parameters will include the fuel blend ratio, high-reactivity fuel injection, variable valve actuation and advanced thermal management. This will be implemented using a tailored, fast-running surrogate, maintaining the most relevant physics from the full model. Other use cases of the developed MZM in CPT involve coupling with a detailed one-dimensional model of the engine air-path to support optimisation studies. This coupled model will be further coupled with the dedicated aftertreatment submodel towards full (hybrid) powertrain/propulsion system-level simulations. Interested readers are encouraged to track the

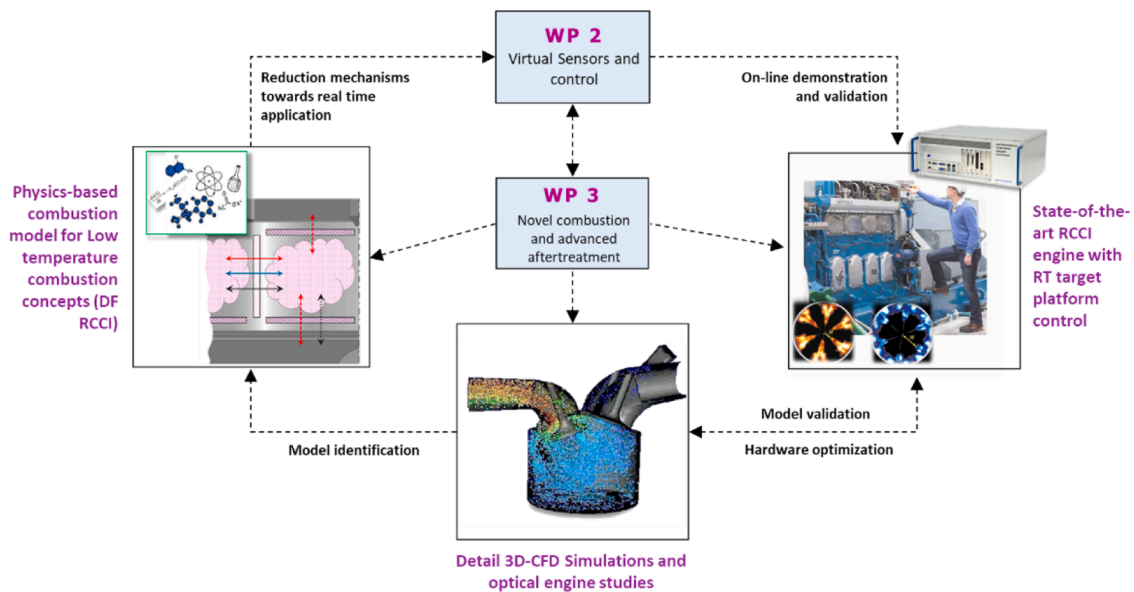


Fig. 34. Work packages 2 and 3 of Clean Propulsion Technologies have common workflow and support each other in model-based development of RCCI technology.

project website [259].

8. Conclusion

The following main conclusions can be drawn from this comprehensive review:

- Multi-zone models have proven their mandate for supporting LTC combustion. Current use cases gradually move from mono-fuel HCCI and PCCI modes towards more complex RCCI strategies. MZ models still figure prominently in fundamental-level, large-scale parametric investigations but their focus is gradually shifting to more applied research involving multi-parameter optimisation and transient simulation towards (indirect so far) applications in model-based control.
- Bearing in mind the above prospective applications, the current state of the art in multi-zone modelling is an onion-skin configuration with 10-15 zones and phenomenological heat and mass transfer sub-models with predictive in-cylinder turbulence. Recommended chemical kinetic mechanisms are of the semi-detailed or reduced-order type, involving 53-199 species, depending on the fuels used. Such a set-up calculates a single combustion cycle in roughly 30 minutes on a contemporary workstation, with single-core simulation.
- Looking towards fully autonomous and predictive simulation, the handful of submodels that exist are proven to couple well with MZM simulation. This involves zero-dimensional gas exchange models capable of capturing effects of variable valve actuation; wall temperature submodels enhancing the predictive capabilities in terms of thermal stratification; simple rate-driven injection and fuel evaporation routines; blow-by models; or knock prediction functions.
- Turning to direct control applications, most viable model-reduction strategies involve zone reduction and tabulated chemistry, avoiding operator splitting with dedicated implicit solvers. Further selectivity of the range of detailed kinetics to be resolved, in favour of covering the bulk part of the cycle with a (still physics-based) semi-predictive surrogate, brings real-time simulation within scope.
- The above development would open a new chapter for model-based RCCI control, ultimately making the final leap towards a robust combustion engine running in ultra-efficient and clean RCCI mode across the whole load-range.

Before the above can happen, however, the present study identifies

several knowledge gaps that need to be addressed. The most important are:

- Model predictivity – providing a robust way to couple multi-zone models with phenomenological spray formation models for fully predictive initialisation of fuel stratification
- Model applicability – developing stable and computationally efficient two-way coupling with commercial one-dimensional engine modelling toolchains
- Calculation speed – implement available techniques for reducing the cost of Jacobian construction and factorisation
- Model reliability – providing unbiased results of model validity outside the calibration space for a broad range of operating conditions

Author statement

Aneesh Vasudev: conceptualization, methodology, formal analysis, investigation, project administration, visualization, data Curation, writing – original draft, writing – review & editing **Maciej Mikulski:** conceptualization, methodology, funding acquisition, project administration, supervision, resources, writing – original draft, writing – review & editing **Xiaoguo Storm** investigation, writing – original draft, writing – review & editing **Praveen Ramanujam Balakrishnan:** investigation, visualization, writing – original draft **Jacek Hunicz** writing – original draft, writing – review & editing

Declaration of Competing Interest

The authors declare that they have no known competing financial interests or personal relationships that could have appeared to influence the work reported in this paper.

Acknowledgements

The work was conducted in the framework of the Clean Propulsion Technologies project with financial support from Business Finland (ref. 38485/31/2020). Jacek Hunicz also acknowledges financial support from the project Lublin University of Technology-Regional Excellence Initiative, funded by the Polish Ministry of Science and Higher Education (contract no. 030/RID/2018/19). Finally, we appreciate the invaluable contribution of Mr. David Wilcox in proofreading our

manuscript and providing his expert suggestions on stylistic points.

References

- [1] Stanglmaier RH, Roberts CE. Homogeneous Charge Compression Ignition (HCCI): Benefits, Compromises, and Future Engine Applications. *SAE Transactions* 1999; 108:2138–45. <https://doi.org/10.4271/1999-01-3682>.
- [2] Akihama K, Takatori Y, Inagaki K, Sasaki S, Dean AM. Mechanism of the Smokeless Rich Diesel Combustion by Reducing Temperature. *SAE Transactions* 2001;110:648–62.
- [3] Yao M, Zheng Z, Liu H. Progress and recent trends in homogeneous charge compression ignition (HCCI) engines. *Progress in Energy and Combustion Science* 2009;35:398–437. <https://doi.org/10.1016/j.pecs.2009.05.001>.
- [4] Reitz RD. Directions in internal combustion engine research. *Combustion and Flame* 2013. <https://doi.org/10.1016/j.combustflame.2012.11.002>.
- [5] Ozaki J, Iida N. Effect of Degree of Unmixedness on HCCI Combustion Based on Experiment and Numerical Analysis. *SAE Transactions* 2006;115:1053–60.
- [6] Martinez-Frias J, Aceves SM, Flowers D, Smith JR, Dibble R. HCCI Engine Control by Thermal Management. *SAE Transactions* 2000;109:2646–55.
- [7] Chang K, Babajimopoulos A, Lavoie GA, Filipi ZS, Assanis DN. Analysis of Load and Speed Transitions in an HCCI Engine Using 1-D Cycle Simulation and Thermal Networks. *SAE Transactions* 2006;115:621–33.
- [8] Lu X, Han D, Huang Z. Fuel design and management for the control of advanced compression-ignition combustion modes. *Progress in Energy and Combustion Science* 2011;37:741–83. <https://doi.org/10.1016/j.pecs.2011.03.003>.
- [9] Pachiannan T, Zhong W, Rajkumar S, He Z, Leng X, Wang Q. A literature review of fuel effects on performance and emission characteristics of low-temperature combustion strategies. *Applied Energy* 2019;251:113380. <https://doi.org/10.1016/j.apenergy.2019.113380>.
- [10] Urushihara T, Hiraya K, Kakuhou A, Itoh T. Expansion of HCCI Operating Region by the Combination of Direct Fuel Injection, Negative Valve Overlap and Internal Fuel Reformulation. *SAE Transactions* 2003;112:1092–100.
- [11] Hunicz J, Kordos P. An experimental study of fuel injection strategies in CAI gasoline engine. *Experimental Thermal and Fluid Science* 2011;35:243–52. <https://doi.org/10.1016/j.expthermflusc.2010.09.007>.
- [12] Lawler B, Splitter D, Szybist J, Kaul B. Thermally Stratified Compression Ignition: A new advanced low temperature combustion mode with load flexibility. *Applied Energy* 2017;189:122–32. <https://doi.org/10.1016/j.apenergy.2016.11.034>.
- [13] Olesky LM, Lavoie GA, Assanis DN, Wooldridge MS, Martz JB. The effects of diluent composition on the rates of HCCI and spark assisted compression ignition combustion. *Applied Energy* 2014;124:186–98. <https://doi.org/10.1016/j.apenergy.2014.03.015>.
- [14] Lavy J, Dabadie J-C, Angelberger C, Duret P, Willand J, Juretzka A, et al. Innovative Ultra-low NOx Controlled Auto-Ignition Combustion Process for Gasoline Engines : the 4-SPACE Project. *SAE Transactions* 2000;109:1072–87.
- [15] Duan X, Lai M-C, Jansons M, Guo G, Liu J. A review of controlling strategies of the ignition timing and combustion phase in homogeneous charge compression ignition (HCCI) engine. *Fuel* 2021;285:119142. <https://doi.org/10.1016/j.fuel.2020.119142>.
- [16] Mueller CJ, Upatnieks A. Dilute clean diesel combustion achieves low emissions and high efficiency while avoiding control problems of HCCI. In: 11th Annual Diesel Engine Emissions Reduction (DEER) Conference, Chicago, Illinois; 2005.
- [17] Osborne RJ, Li G, Sapsford SM, Stokes J, Lake TH, Heikal MR. Evaluation of HCCI for Future Gasoline Powertrains. *SAE* 2003-01-0750 2003. <https://doi.org/10.4271/2003-01-0750>.
- [18] Fuerhapter A, Unger E, Piock WF, Fraidl GK. The new AVL CSI Engine - HCCI Operation on a Multi Cylinder Gasoline Engine. *SAE* 2004-01-0551 2004. <https://doi.org/10.4271/2004-01-0551>.
- [19] Mackay S. **New hope for internal combustion engines.** EIT | Engineering Institute of Technology, <https://www.eit.edu.au/new-hope-for-internal-combustion-engines/>; 2017 [accessed 16.03.2021].
- [20] Nüesch SP, Stefanopoulou AG, Jiang L, Storniak J. Fuel Economy of a Multimode Combustion Engine With Three-Way Catalytic Converter. *Journal of Dynamic Systems, Measurement, and Control* 2014;137. <https://doi.org/10.1115/1.4028885>.
- [21] Han J, Wang S, Somers B. Comparative Study on the Effects of Inlet Heating, Inlet Boosting, and Double-Injection Strategy on Partially Premixed Combustion. *SAE* 2019-01-1149 2019. <https://doi.org/10.4271/2019-01-1149>.
- [22] Kim D, Ekoto I, Colban WF, Miles PC. In-cylinder CO and UHC Imaging in a Light-Duty Diesel Engine during PPCI Low-Temperature Combustion. *SAE International Journal of Fuels and Lubricants* 2009;1:933–56.
- [23] Kimura S, Aoki O, Kitahara Y, Aiyoshizawa E. Ultra-Clean Combustion Technology Combining a Low-Temperature and Premixed Combustion Concept for Meeting Future Emission Standards. *SAE Transactions* 2001;110:239–46.
- [24] Martin GC, Mueller CJ, Milam DM, Radovanovic MS, Gehrke CR. Early Direct-Injection, Low-Temperature Combustion of Diesel Fuel in an Optical Engine Utilizing a 15-Hole, Dual-Row, Narrow-Included-Angle Nozzle. *SAE International Journal of Engines* 2009;1:1057–82.
- [25] Dec JE. Advanced compression-ignition engines—understanding the in-cylinder processes. *Proceedings of the Combustion Institute* 2009;32:2727–42. <https://doi.org/10.1016/j.proci.2008.08.008>.
- [26] Sellnau M, Sinnamon J, Hoyer K, Husted H. Gasoline Direct Injection Compression Ignition (GDICI) - Diesel-like Efficiency with Low CO₂ Emissions. *SAE International Journal of Engines* 2011;4:2010–22.
- [27] Kumar P, Zhang Y, Traver M, Watson J. Tailored Air-Handling-System Development for Gasoline Compression Ignition in a Heavy-Duty Diesel Engine. *Frontiers in Mechanical Engineering* 2021;7:6.
- [28] Inagaki K, Fuyuto T, Nishikawa K, Nakakita K, Sakata I. Dual-Fuel PCI Combustion Controlled by In-Cylinder Stratification of Ignitability. *SAE* 2006-01-0028 2006. <https://doi.org/10.4271/2006-01-0028>.
- [29] Kokjohn SL, Hanson RM, Splitter DA, Reitz RD. Experiments and Modeling of Dual-Fuel HCCI and PCCI Combustion Using In-Cylinder Fuel Blending. *SAE International Journal of Engines* 2010;2:24–39.
- [30] Kokjohn SL, Musculus MPB, Reitz RD. Evaluating temperature and fuel stratification for heat-release rate control in a reactivity-controlled compression-ignition engine using optical diagnostics and chemical kinetics modeling. *Combustion and Flame* 2015;162:2729–42. <https://doi.org/10.1016/j.combustflame.2015.04.009>.
- [31] Chuahy F, Kokjohn SL. Single fuel RCCI combustion using reformed fuel. *Internal Combustion and Gas Turbine Engines*. Washington DC, USA: Eastern States Section of the Combustion Institute; 2017. p. 23–4.
- [32] Paykani A, Kakaee A-H, Rahnama P, Reitz RD. Progress and recent trends in reactivity-controlled compression ignition engines. *International Journal of Engine Research* 2016;17:481–524. <https://doi.org/10.1177/1468087415593013>.
- [33] Zhao H. **HCCI AND CAI ENGINES FOR THE AUTOMOTIVE INDUSTRY.** Elsevier; 2007.
- [34] Saxena S, Bedoya ID. Fundamental phenomena affecting low temperature combustion and HCCI engines, high load limits and strategies for extending these limits. *Progress in Energy and Combustion Science* 2013;39:457–88. <https://doi.org/10.1016/j.pecs.2013.05.002>.
- [35] Finney CE, Kaul BC, Daw CS, Wagner RM, Edwards KD, Green JB. Invited Review: A review of deterministic effects in cyclic variability of internal combustion engines. *International Journal of Engine Research* 2015;16:366–78. <https://doi.org/10.1177/1468087415572033>.
- [36] Reitz RD, Duraisamy G. Review of high efficiency and clean reactivity controlled compression ignition (RCCI) combustion in internal combustion engines. *Progress in Energy and Combustion Science* 2015;46:12–71. <https://doi.org/10.1016/j.pecs.2014.05.003>.
- [37] Paykani A, Garcia A, Shahbakhti M, Rahnama P, Reitz RD. Reactivity controlled compression ignition engine: Pathways towards commercial viability. *Applied Energy* 2021;282:116174. <https://doi.org/10.1016/j.apenergy.2020.116174>.
- [38] Liu X, Kokjohn S, Wang H, Yao M. A comparative numerical investigation of reactivity controlled compression ignition combustion using Large Eddy Simulation and Reynolds-Averaged Navier-Stokes approaches. *Fuel* 2019;257:116023. <https://doi.org/10.1016/j.fuel.2019.116023>.
- [39] Nazemi M, Saigaonkar H, Shahbakhti M. Thermo-kinetic modelling of variable valve timing effects on HCCI engine combustion /HCCI Motorun Yanmasina Degışken Supap Zamanlamasının Etkilerinin Termo-Kinetik Modeli. *International Journal of Automotive Engineering and Technologies* 2015;4:54–62. <https://doi.org/10.18245/ijaet.51525>.
- [40] Tekgöl B, Kahila H, Karimkashi S, Kaario O, Ahmad Z, Lendormy É, et al. Large-eddy simulation of spray assisted dual-fuel ignition under reactivity-controlled dynamic conditions. *Fuel* 2021;293:120295. <https://doi.org/10.1016/j.fuel.2021.120295>.
- [41] Bhatgatala A, Chen JH, Lu T. Direct numerical simulations of HCCI/SACI with ethanol. *Combustion and Flame* 2014;161:1826–41. <https://doi.org/10.1016/j.combustflame.2013.12.027>.
- [42] Zhong S, Xu S, Bai X-S, Hadadpour A, Jangi M, Zhang F, et al. Combustion characteristics of n-heptane spray combustion in a low temperature reform gas/air environment. *Fuel* 2021;293:120377. <https://doi.org/10.1016/j.fuel.2021.120377>.
- [43] Reith M, Day M, Bansude S, Tianfeng L, Kweon C-B, Temme J, et al. Direct Numerical Simulation of Multi-Injection Ignition in Low-Temperature Compression Ignition Environments. *Bulletin of the American Physical Society*, 64. Seattle, WA: American Physical Society; 2019. Number.
- [44] Chen JH. DNS of Turbulent Combustion in Complex Flows. In: 11th Mediterranean Combustion Symposium, Tenerife, Spain; 2019.
- [45] Gadalla M, Kannan J, Tekgöl B, Karimkashi S, Kaario O, Vuorinen V. Large-eddy simulation of tri-fuel combustion: Diesel spray assisted ignition of methanol-hydrogen blends. *International Journal of Hydrogen Energy* 2021;46:21687–703. <https://doi.org/10.1016/j.ijhydene.2021.03.238>.
- [46] Zhong S, Zhang F, Du Q, Peng Z. Characteristics of reactivity controlled combustion with n-heptane low temperature reforming products. *Fuel* 2020;275:117980. <https://doi.org/10.1016/j.fuel.2020.117980>.
- [47] Fathi M, Jahanian O, Shahbakhti M. Modeling and controller design architecture for cycle-by-cycle combustion control of homogeneous charge compression ignition (HCCI) engines – A comprehensive review. *Energy Conversion and Management* 2017;139:1–19. <https://doi.org/10.1016/j.enconman.2017.02.038>.
- [48] Hall C, Kassa M. Advances in combustion control for natural gas-diesel dual fuel compression ignition engines in automotive applications: A review. *Renewable and Sustainable Energy Reviews* 2021;148:111291. <https://doi.org/10.1016/j.rser.2021.111291>.
- [49] Atkinson C. Fuel Efficiency Optimization using Rapid Transient Engine Calibration. *SAE* 2014-01-2359 2014. <https://doi.org/10.4271/2014-01-2359>.
- [50] Ghojel JI. Review of the development and applications of the Wiebe function: A tribute to the contribution of Ivan Wiebe to engine research. *International Journal of Engine Research* 2010;11:297–312. <https://doi.org/10.1243/14680874JER06510>.
- [51] **GT-Suite Engine Performance Application Manual.** Illinois, USA: Gamma Technologies LLC; 2019.

- [52] Verhelst S, Sheppard CGW. Multi-zone thermodynamic modelling of spark-ignition engine combustion – An overview. *Energy Conversion and Management* 2009;50:1326–35. <https://doi.org/10.1016/j.enconman.2009.01.002>.
- [53] Kumar S, Kumar Chauhan M, Varun. Numerical modeling of compression ignition engine: A review. *Renewable and Sustainable Energy Reviews* 2013;19:517–30. <https://doi.org/10.1016/j.rser.2012.11.043>.
- [54] Allen C. FIRE Lab. Marquette University FIRE Lab; 2017. <https://cslabs.wixsite.com/allen/research> [accessed 22.06.2021].
- [55] Wilson D, Allen C. Application of a multi-zone model for the prediction of species concentrations in rapid compression machine experiments. *Combustion and Flame* 2016;171:185–97. <https://doi.org/10.1016/j.combustflame.2016.05.018>.
- [56] Mikulski M, Balakrishnan PR, Doosje E, Bekdemir C. VARIABLE VALVE ACTUATION STRATEGIES FOR BETTER EFFICIENCY LOAD RANGE AND THERMAL MANAGEMENT IN AN RCCI ENGINE. SAE International; 2018. <https://doi.org/10.4271/2018-01-0254>.
- [57] Mikulski M, Ramesh S, Bekdemir C. Reactivity Controlled Compression Ignition for clean and efficient ship propulsion. *Energy* 2019;182:1173–92. <https://doi.org/10.1016/j.energy.2019.06.091>.
- [58] Eichmeier JU, Reitz RD, Rutland C. A Zero-Dimensional Phenomenological Model for RCCI Combustion Using Reaction Kinetics. *SAE Int J Engines* 2014;7:106–19. <https://doi.org/10.4271/2014-01-1074>.
- [59] Narayanaswamy K, Rutland CJ. Cycle Simulation Diesel HCCI Modeling Studies and Analysis. SAE 2004-01-2997 2004. <https://doi.org/10.4271/2004-01-2997>.
- [60] Ekberg K, Leek V, Eriksson L. Validation of an Open-Source Mean-Value Heavy-Duty Diesel Engine Model. In: Proceedings of The 59th Conference on Simulation and Modelling. 153. Oslo Metropolitan University, Norway: Linköping University Electronic Press, Linköpings universitet; 2018. p. 290–6. <https://doi.org/10.3384/ecp18153290>.
- [61] Wahlström J, Eriksson L. Modelling diesel engines with a variable-geometry turbocharger and exhaust gas recirculation by optimization of model parameters for capturing non-linear system dynamics. Proceedings of the Institution of Mechanical Engineers, Part D: Journal of Automobile Engineering 2011;225: 960–86. <https://doi.org/10.1177/0954407011398177>.
- [62] Indrajana A, Bekdemir C, Feru E, Willems F. Towards Model-Based Control of RCCI-CDF Mode-Switching in Dual Fuel Engines. SAE 2018-01-0263 2018. <https://doi.org/10.4271/2018-01-0263>.
- [63] Bidarvatan M, Gray-Box Shahbakhti M. Modeling for Performance Control of an HCCI Engine With Blended Fuels. *Journal of Engineering for Gas Turbines and Power* 2014;136. <https://doi.org/10.1115/1.4027278>.
- [64] Indrajana A, Bekdemir C, Luo X, Willems F. Robust Multivariable Feedback Control of Natural Gas-Diesel RCCI Combustion. IFAC-PapersOnLine 2016;49: 217–22. <https://doi.org/10.1016/j.ifacol.2016.08.033>.
- [65] Nazoktabar M, Jazayeri SA, Parsa M, Ganji DD, Arshatabar K. Controlling the optimal combustion phasing in an HCCI engine based on load demand and minimum emissions. *Energy* 2019;182:82–92. <https://doi.org/10.1016/j.energy.2019.06.012>.
- [66] Komninos NP, Rakopoulos CD. Heat transfer in hcci phenomenological simulation models: A review. *Applied Energy* 2016;181:179–209. <https://doi.org/10.1016/j.apenergy.2016.08.061>.
- [67] Tzanetakis T, Singh P, Chen J-T, Thomson MJ, Koch Charles R. Knock limit prediction via multi-zone modelling of a primary reference fuel HCCI engine. *International Journal of Vehicle Design* 2010;54:47–72. <https://doi.org/10.1504/IJVD.2010.03487>.
- [68] Dec JE, Hwang W, Sjöberg M. An Investigation of Thermal Stratification in HCCI Engines Using Chemiluminescence Imaging. *SAE Transactions* 2006;115:759–76.
- [69] Hultqvist A, Engdard U, Johansson B, Klingmann J. Reacting Boundary Layers in a Homogeneous Charge Compression Ignition (HCCI) Engine. SAE 2001-01-1032 2001. <https://doi.org/10.4271/2001-01-1032>.
- [70] Maghbouli A, Lucchini T, D'Errico G, Izadi Najafabadi M, Somers B. Numerical Investigation of PPCI Combustion at Low and High Charge Stratification Levels. SAE 2017-01-0739 2017. <https://doi.org/10.4271/2017-01-0739>.
- [71] Komninos NP, Hountalas DT, Kouremenos DA. Description of in-Cylinder Combustion Processes in HCCI Engines Using a Multi-Zone Model. SAE 2005-01-0171 2005. <https://doi.org/10.4271/2005-01-0171>.
- [72] Noda T, Foster DE. A Numerical Study to Control Combustion Duration of Hydrogen-Fueled HCCI by Using Multi-Zone Chemical Kinetics Simulation. *SAE Transactions* 2001;110:186–91.
- [73] Aceves SM, Flowers DL, Westbrook CK, Smith JR, Pitz W, Dibble R, et al. A Multi-Zone Model for Prediction of HCCI Combustion and Emissions. SAE 2001-01-0327 2000. <https://doi.org/10.4271/2000-01-0327>.
- [74] Orlandini I, Kulzer A, Weberbauer F, Rauscher M. Simulation of Self Ignition in HCCI and Partial HCCI Engines Using a Reduced Order Model. SAE 2005-01-0159 2005. <https://doi.org/10.4271/2005-01-0159>.
- [75] Aceves SM, Flowers DL, Martinez-Frias J, Smith JR, Westbrook CK, Pitz WJ, et al. A Sequential Fluid-Mechanic Chemical-Kinetic Model of Propane HCCI Combustion. SAE 2001-01-1027 2001. <https://doi.org/10.4271/2001-01-1027>.
- [76] Aceves SM, Martinez-Frias J, Flowers DL, Smith JR, Dibble RW, Wright JF, et al. A Decoupled Model of Detailed Fluid Mechanics Followed by Detailed Chemical Kinetics for Prediction of Iso-Octane HCCI Combustion. SAE Transactions 2001; 110:2135–46.
- [77] Aceves SM, Flowers DL, Espinosa-Loza F, Babajimopoulos A, Assanis DN. Analysis of Premixed Charge Compression Ignition Combustion With a Sequential Fluid Mechanics-Multizone Chemical Kinetics Model. SAE Transactions 2005;114: 252–62.
- [78] Hergart C-A, Barths H, Siewert RM. Modeling Approaches for Premixed Charge Compression Ignition Combustion. SAE 2005-01-0218 2005. <https://doi.org/10.4271/2005-01-0218>.
- [79] Babajimopoulos A, Assanis DN, Fiveland SB. An Approach for Modeling the Effects of Gas Exchange Processes on HCCI Combustion and Its Application in Evaluating Variable Valve Timing Control Strategies. SAE Transactions 2002;111: 1794–809.
- [80] Babajimopoulos A, Assanis DN, Flowers DL, Aceves SM, Hessel RP. A fully coupled computational fluid dynamics and multi-zone model with detailed chemical kinetics for the simulation of premixed charge compression ignition engines. *International Journal of Engine Research* 2005;6:497–512. <https://doi.org/10.1243/146808705X30503>.
- [81] Kodavasil J, McNenly MJ, Babajimopoulos A, Aceves SM, Assanis DN, Havstad MA, et al. An accelerated multi-zone model for engine cycle simulation of homogeneous charge compression ignition combustion. *International Journal of Engine Research* 2013;14:416–33. <https://doi.org/10.1177/1468087413482480>.
- [82] Flowers DL, Aceves SM, Martinez-Frias J, Dibble RW. Prediction of carbon monoxide and hydrocarbon emissions in iso-octane HCCI engine combustion using multizone simulations. Proceedings of the Combustion Institute 2002;29: 687–94. [https://doi.org/10.1016/S1540-7489\(02\)80088-8](https://doi.org/10.1016/S1540-7489(02)80088-8).
- [83] Flowers D, Aceves S, Martinez-Frias J, Hessel R, Dibble R. EFFECT OF MIXING ON HYDROCARBON AND CARBON MONOXIDE EMISSIONS PREDICTION FOR ISOCTANE HCCI ENGINE COMBUSTION USING A MULTI-ZONE DETAILED KINETICS SOLVER. SAE International; 2003. <https://doi.org/10.4271/2003-01-1821>.
- [84] Aceves SM, Flowers DL, Martinez-Frias J, Espinosa-Loza F, Christensen M, Johansson B, et al. ANALYSIS OF THE EFFECT OF GEOMETRY GENERATED TURBULENCE ON HCCI COMBUSTION BY MULTI-ZONE MODELING. SAE International; 2005. <https://doi.org/10.4271/2005-01-2134>.
- [85] Jia M, Xie M, Peng Z. A Comparative Study of Multi-zone Combustion Models for HCCI Engines. SAE 2008-01-0064 2008. <https://doi.org/10.4271/2008-01-0064>.
- [86] Mikulski M, Balakrishnan PR, Hunicz J. Natural gas-diesel reactivity controlled compression ignition with negative valve overlap and in-cylinder fuel reforming. *Applied Energy* 2019;254:113638. <https://doi.org/10.1016/j.apenergy.2019.113638>.
- [87] Neshat E, Saray RK. Development of a new multi zone model for prediction of HCCI (homogenous charge compression ignition) engine combustion, performance and emission characteristics. *Energy* 2014;73:325–39. <https://doi.org/10.1016/j.energy.2014.06.025>.
- [88] Komninos NP. Modeling HCCI combustion: Modification of a multi-zone model and comparison to experimental results at varying boost pressure. *Applied Energy* 2009;86:2141–51. <https://doi.org/10.1016/j.apenergy.2009.01.026>.
- [89] Kongsereparp P, Checkel MD. Novel Method of Setting Initial Conditions for Multi-Zone HCCI Combustion Modeling. SAE 2007-01-0674 2007. <https://doi.org/10.4271/2007-01-0674>.
- [90] Kozarac D, Sjeric M, Mahalec I. Introducing Initial Conditions with Non-uniform Mixtures and Fuel Injection into the Multi Zone HCCI Simulation Model. SAE 2010-01-1083 2010. <https://doi.org/10.4271/2010-01-1083>.
- [91] Fiveland SB, Assanis DN. Development and Validation of a Quasi-Dimensional Model for HCCI Engine Performance and Emissions Studies Under Turbocharged Conditions. SAE Transactions 2002;111:842–60.
- [92] Mikulski M, Bekdemir C, Willems F. Experimental validation of a combustion kinetics based multi-zone model for natural gas-diesel RCCI engines. In: 2016 Symposium for Combustion Control (SCC 2016), Aachen, Germany; 2016. p. 83–91.
- [93] Ogink R, Golovitchev V. Gasoline HCCI Modeling: An Engine Cycle Simulation Code with a Multi-Zone Combustion Model. SAE 2002-01-1745 2002. <https://doi.org/10.4271/2002-01-1745>.
- [94] Easley WL, Agarwal A, Lavoie GA. Modeling of HCCI Combustion and Emissions Using Detailed Chemistry. SAE 2001-01-1029 2001. <https://doi.org/10.4271/2001-01-1029>.
- [95] Lashkarpour SM, Khoshbakhti Saray R, Najafi M. Multi-zone model for reactivity controlled compression ignition engine based on CFD approach. *Energy* 2018; 156:213–28. <https://doi.org/10.1016/j.energy.2018.05.084>.
- [96] Bissoli M, Frassoldati A, Cuoci A, Ranzi E, Mehl M, Faravelli T. A new predictive multi-zone model for HCCI engine combustion. *Applied Energy* 2016;178: 826–43. <https://doi.org/10.1016/j.apenergy.2016.06.062>.
- [97] Kozarac D, Lulic Z, Sagi G. A six-zone simulation model for HCCI engines with a non-segregated solver of zone state. *Combustion Theory and Modelling* 2010;14: 425–51. <https://doi.org/10.1080/13647830.2010.489959>.
- [98] Angelos JP, Puignou M, Andrea MM, Cheng WK, Green WH, Singer MA. Detailed chemical kinetic simulations of homogeneous charge compression ignition engine transients. *International Journal of Engine Research* 2008;9:149–64. <https://doi.org/10.1243/14680874JER02207>.
- [99] Kongsereparp P, Kashani B, Checkel MD. A Stand-Alone Multi-Zone Model for Combustion in HCCI Engines. In: ASME 2005 Internal Combustion Engine Division Fall Technical Conference (ICEF2005); 2005. p. 265–74. <https://doi.org/10.1115/ICEF2005-1241>.
- [100] Egüz U, Leermakers CA, Somers LM, de Goey LP. Premixed charge compression ignition combustion modelling with a multi-zone approach including inter-zonal mixing. Proceedings of the Institution of Mechanical Engineers, Part D: Journal of Automobile Engineering 2013;227:1313–24. <https://doi.org/10.1177/0954407012474193>.
- [101] Mikulski M, Bekdemir C. Understanding the role of low reactivity fuel stratification in a dual fuel RCCI engine – A simulation study. *Applied Energy* 2017;191:689–708. <https://doi.org/10.1016/j.apenergy.2017.01.080>.
- [102] Voshtani S, Reyhanian M, Ehteram M, Hosseini V. Investigating various effects of reformer gas enrichment on a natural gas-fueled HCCI combustion engine.

- International Journal of Hydrogen Energy 2014;39:1979–809. <https://doi.org/10.1016/j.ijhydene.2014.09.130>.
- [103] Bissoli M, Cuoci A, Frassoldati A, Faravelli T, Ranzi E, Lucchini T, et al. Detailed Kinetic Analysis of HCCI Combustion Using a New Multi-Zone Model and CFD Simulations. *SAE International Journal of Engines* 2013;6:1594–609.
- [104] Komninos NP, Kosmadakis GM. Heat transfer in HCCI multi-zone modeling: Validation of a new wall heat flux correlation under motoring conditions. *Applied Energy* 2011;88:1635–48. <https://doi.org/10.1016/j.apenergy.2010.11.039>.
- [105] Kook S, Bae C, Miles PC, Choi D, Pickett LM. The Influence of Charge Dilution and Injection Timing on Low-Temperature Diesel Combustion and Emissions. *SAE Transactions* 2005;114:1575–95.
- [106] Perini F, Busch S, Reitz RD. A phenomenological rate of injection model for predicting fuel injection with application to mixture formation in light-duty diesel engines. *Proceedings of the Institution of Mechanical Engineers, Part D: Journal of Automobile Engineering* 2020;234:1826–39. <https://doi.org/10.1177/0954407019898062>.
- [107] Baratta M, Catania A, Ferrari A, Finesso R, Spessa E. Innovative multizone premixed-diffusion combustion model for performance and emission analysis in conventional and PCCI diesel engines. In: *Proceedings of the 7th International Conference on Modeling and Diagnostics for Advanced Engine Systems, COMODIA 2008* 2008. 7; 2008. p. 351–62. <https://doi.org/10.1299/jmsedm.2008.7.351>.
- [108] Kuleshov A, Kozlov AV, Mahkamov K. Self-Ignition Delay Prediction in PCCI Direct Injection Diesel Engines Using Multi-Zone Spray Combustion Model and Detailed Chemistry. *SAE* 2010-01-1960 2010. <https://doi.org/10.4271/2010-01-1960>.
- [109] Baratta M, Catania AE, Ferrari A, Finesso R, Spessa E. Premixed-Diffusive Multizone Model for Combustion Diagnostics in Conventional and PCCI Diesel Engines. *Journal of Engineering for Gas Turbines and Power* 2011;133. <https://doi.org/10.1115/1.4003048>.
- [110] Hiroyasu H, Kadota T, Arai M. Development and Use of a Spray Combustion Modeling to Predict Diesel Engine Efficiency and Pollutant Emissions : Part 1 Combustion Modeling. *Bulletin of JSME* 1983;26:569–75. <https://doi.org/10.1299/jsmc.1983.26.569>.
- [111] Dos Santos F, Le Moyné L. Spray Atomization Models in Engine Applications, from Correlations to Direct Numerical Simulations. *Oil & Gas Science and Technology - Revue d'IFP. Energies Nouvelles* 2011;66:801–22. <https://doi.org/10.2516/ogst/20111116>.
- [112] Felsch C, Hoffmann K, Vanegas A, Drews P, Barths H, Abel D, et al. Combustion model reduction for diesel engine control design. *International Journal of Engine Research* 2009;10:359–87. <https://doi.org/10.1243/14680874JER04509>.
- [113] Felsch C, Dahms R, Glodde B, Vogel S, Jerzembeck S, Peters N, et al. An Interactively Coupled CFD-Multi-Zone Approach to Model HCCI Combustion. *Flow, Turbulence and Combustion* 2009;82:621–41. <https://doi.org/10.1007/s10494-009-9202-6>.
- [114] Wei H, Chen C, Feng D, Gao D, Chen L. Combustion Simulations under IC Engine-Relevant Conditions Using Dynamic Adaptive Multi-Zone Method. *Combustion Science and Technology* 2017;189:2242–65. <https://doi.org/10.1080/00102202.2017.1369971>.
- [115] Kodavasal J, Keum S, Babajimopoulos A. An extended multi-zone combustion model for PCI simulation. *Combustion Theory and Modelling* 2011;15:893–910. <https://doi.org/10.1080/13647830.2011.578663>.
- [116] Shi Y, Hessel RP, Reitz RD. An adaptive multi-grid chemistry (AMC) model for efficient simulation of HCCI and DI engine combustion. *Combustion Theory and Modelling* 2009;13:83–104. <https://doi.org/10.1080/13647830802401101>.
- [117] Bhave A, Kraft M, Montorsi L, Mauss F. Sources of CO emissions in an HCCI engine: A numerical analysis. *Combustion and Flame* 2006. <https://doi.org/10.1016/j.combustflame.2005.10.015>.
- [118] Mosbach S, Su H, Kraft M, Bhave A, Mauss F, Wang Z, et al. Dual injection homogeneous charge compression ignition engine simulation using a stochastic reactor model. *International Journal of Engine Research* 2007;8:41–50. <https://doi.org/10.1243/14680874JER01806>.
- [119] Ahmedi A, Ahmed SS, Kalghatgi GT. Simulating combustion in a PCI (premixed compression ignition) engine using DI-SRM and 3 components surrogate model. *Combustion and Flame* 2015;162:3728–39. <https://doi.org/10.1016/j.combustflame.2015.07.011>.
- [120] Montorsi L, Mauss F, Bianchi GM, Bhave A, Kraft M. Analysis of the HCCI Combustion of a Turbocharged Truck Engine Using a Stochastic Reactor Model. In: *ASME 2002 Internal Combustion Engine Division Fall Technical Conference (ICEF2002)*; 2002. p. 97–108. <https://doi.org/10.1115/ICEF2002-488>.
- [121] Cao L, Su H, Mosbach S, Kraft M, Bhave A, Kook S, et al. Studying the influence of direct injection on pcci combustion and emissions at engine idle condition using two dimensional CFD and stochastic reactor model. *SAE Technical Papers* 2008. <https://doi.org/10.4271/2008-01-0021>.
- [122] Lundgren M, Tuner M, Johansson B, Bjerkborn S, Frojd K, Andersson A, et al. Gasoline PPC: A parametric study of late cycle mixing conditions using a predictive two-zone SRM modeling tool. *SAE Technical Papers* 2013;11. <https://doi.org/10.4271/2013-01-2621>.
- [123] Tunér M. *Stochastic Reactor Models for Engine Simulations*. Doctoral Thesis (monograph). Division of Combustion Physics, Department of Physics, Lund University; 2008.
- [124] Kraft M, Maigaard P, Mauss F, Christensen M, Johansson B. Investigation of combustion emissions in a homogeneous charge compression injection engine: Measurements and a new computational model. *Proceedings of the Combustion Institute* 2000;28:1195–201. [https://doi.org/10.1016/S0082-0784\(00\)80330-6](https://doi.org/10.1016/S0082-0784(00)80330-6).
- [125] Nazoktabar M, Jazayeri SA, Arshatabar K, Ganji DD. Developing a multi-zone model for a HCCI engine to obtain optimal conditions using genetic algorithm. *Energy Conversion and Management* 2018;157:49–58. <https://doi.org/10.1016/j.enconman.2017.12.001>.
- [126] Chang J, Güralp O, Filipi Z, Assanis D, Kuo T-W, Najt P, et al. New Heat Transfer Correlation for an HCCI Engine Derived from Measurements of Instantaneous Surface Heat Flux. *SAE Transactions* 2004;113:1576–93.
- [127] Annand WJD. Heat Transfer in the Cylinders of Reciprocating Internal Combustion Engines. *Proceedings of the Institution of Mechanical Engineers* 1963;177:973–96. https://doi.org/10.1243/PIME_PROC_1963_177_069_02.
- [128] Hohenberg GF. *Advanced Approaches for Heat Transfer Calculations*. *SAE Transactions* 1979;88:2788–806.
- [129] Woschni G. A Universally Applicable Equation for the Instantaneous Heat Transfer Coefficient in the Internal Combustion Engine. *SAE* 1967;670931. <https://doi.org/10.4271/670931>.
- [130] Fiveland SB, Assanis DN. A Four-Stroke Homogeneous Charge Compression Ignition Engine Simulation for Combustion and Performance Studies. *SAE Transactions* 2000;109:452–68.
- [131] Neshat E, Saray RK. Effect of different heat transfer models on HCCI engine simulation. *Energy Conversion and Management* 2014;88:1–14. <https://doi.org/10.1016/j.enconman.2014.07.075>.
- [132] Heywood JB. *Internal combustion engine fundamentals*. New York: McGraw-Hill; 1988.
- [133] Kongsereparp P, Checkel MD. Investigating the Effects of Reformed Fuel Blending in a Methane- or n-Heptane-HCCI Engine Using a Multi-Zone Model. *SAE* 2007-01-0205 2007. <https://doi.org/10.4271/2007-01-0205>.
- [134] Guo H, Li H, Neill WS. A Study on the Performance of Combustion in a HCCI Engine Using n-Heptane by a Multi-Zone Model. In: *ASME 2009 Internal Combustion Engine Division Fall Technical Conference (ICEF2009)*; 2009. p. 489–97. <https://doi.org/10.1115/ICEF2009-14117>.
- [135] Mehl M, Tardani A, Faravelli T, Ranzi E, D'Errico G, Lucchini T, et al. A Multizone approach to the detailed kinetic modeling of HCCI combustion. *SAE* 2007-24-0086 2007. <https://doi.org/10.4271/2007-24-0086>.
- [136] Bargende M. PhD Thesis. University of Darmstadt; 1991.
- [137] Xu H, Liu M, Gharahbaghi S, Richardson S, Wyszynski M, Megaritis T. Modelling of HCCI Engines: Comparison of Single-zone, Multi-zone and Test Data. *SAE* 2005-01-2123 2005. <https://doi.org/10.4271/2005-01-2123>.
- [138] Visakhmoorthy S, Tzanetakis T, Haggith D, Sobiesiak A, Wen JZ. Numerical study of a homogeneous charge compression ignition (HCCI) engine fueled with biogas. *Applied Energy* 2012;92:437–46. <https://doi.org/10.1016/j.apenergy.2011.11.014>.
- [139] Komninos NP, Hountalas DT. Improvement and validation of a multi-zone model for HCCI engine combustion concerning performance and emissions. *Energy Conversion and Management* 2008;49:2530–7. <https://doi.org/10.1016/j.enconman.2008.05.008>.
- [140] Nobakht AY, Khoshbakhli Saray R, Rahimi A. A parametric study on natural gas fueled HCCI combustion engine using a multi-zone combustion model. *Fuel* 2011; 90:1508–14. <https://doi.org/10.1016/j.fuel.2010.12.026>.
- [141] Eğüz Ü, Maes NCJ, Leermakers CAJ, Somers LMT, Goey LPHD. Predicting auto-ignition characteristics of RCCI combustion using a multi-zone model. *International Journal of Automotive Technology* 2013;14:693–9. <https://doi.org/10.1007/s12239-013-0075-2>.
- [142] Fathi M, Jahanian O, Ganji DD, Wang S, Somers B. Stand-alone single- and multi-zone modeling of direct injection homogeneous charge compression ignition (DI-HCCI) combustion engines. *Applied Thermal Engineering* 2017;125:1181–90. <https://doi.org/10.1016/j.applthermaleng.2017.07.123>.
- [143] Barroso G, Escher A, Boulouchos K. Experimental and Numerical Investigations on HCCI-Combustion. *SAE* 2005-24-038 2005. <https://doi.org/10.4271/2005-24-038>.
- [144] Han Z, Reitz RD. A temperature wall function formulation for variable-density turbulent flows with application to engine convective heat transfer modeling. *International Journal of Heat and Mass Transfer* 1997;40:613–25. [https://doi.org/10.1016/0017-9310\(96\)00117-2](https://doi.org/10.1016/0017-9310(96)00117-2).
- [145] Fiveland SB, Assanis DN. Development of a Two-Zone HCCI Combustion Model Accounting for Boundary Layer Effects. *SAE* 2001-01-1028 2001. <https://doi.org/10.4271/2001-01-1028>.
- [146] Puzinauskas P, Borgnakke C. Evaluation and Improvement of an Unsteady Heat Transfer Model for Spark Ignition Engines. *SAE Transactions* 1991;100:345–60.
- [147] Lyford-Pike EJ, Heywood JB. Thermal boundary layer thickness in the cylinder of a spark-ignition engine. *International Journal of Heat and Mass Transfer* 1984;27: 1873–8. [https://doi.org/10.1016/0017-9310\(84\)90169-8](https://doi.org/10.1016/0017-9310(84)90169-8).
- [148] Fonseca L, Novella Rosa R, Olmeda P, Valle RM. Internal Combustion Engine Heat Transfer and Wall Temperature Modeling: An Overview. *Archives of Computational Methods in Engineering* 2019;27:1661–79. <https://doi.org/10.1007/s11831-019-09361-9>.
- [149] Kongsereparp P, Environmental Checkel MD. Thermodynamic and Chemical Factor Effects on Heptane- and CNG-fueled HCCI Combustion with Various Mixture Compositions. *SAE* 2008-01-0038 2008. <https://doi.org/10.4271/2008-01-0038>.
- [150] Sjöberg M, Dec JE. An Investigation of the Relationship Between Measured Intake Temperature, BDC Temperature, and Combustion Phasing for Premixed and DI HCCI Engines. *SAE Transactions* 2004;113:1271–86.
- [151] Mikulski M, Wierzbicki S. Validation of a zero-dimensional and 2-phase combustion model for dual-fuel compression ignition engine simulation. *Thermal Science* 2017;21:387–99. <https://doi.org/10.2298/TSCI160127076M>.

- [152] Versteeg HK, Malalasekera W. An introduction to computational fluid dynamics the finite volume method. 2 ed. Harlow: Pearson/Prentice Hall; 2007.
- [153] Hida N, Ichikura T, Kase K, Enomoto Y. Self-ignition and combustion stability in a methanol fueled low heat rejection ceramic ATAC engine—analysis of cyclic variation at high wall temperatures and lean burn operation. *JSAE Review* 1997; 18:233–40. [https://doi.org/10.1016/S0389-4304\(97\)00012-X](https://doi.org/10.1016/S0389-4304(97)00012-X).
- [154] Law CK. *COMBUSTION PHYSICS*. Cambridge: Cambridge University Press; 2006. <https://doi.org/10.1017/CBO9780511754517>.
- [155] Yu R, Bai XS, Lehtiniemi H, Ahmed SS, Mauss F, Richter M, et al. EFFECT OF TURBULENCE AND INITIAL TEMPERATURE INHOMOGENEITY ON HOMOGENEOUS CHARGE COMPRESSION IGNITION COMBUSTION. SAE International; 2006. <https://doi.org/10.4271/2006-01-3318>.
- [156] Vasudev A. TURBULENCE BASED INTER-ZONAL MIXING IN A MULTI-ZONE MODEL FOR PREDICTIVE RCCI COMBUSTION SIMULATIONS. Master of Science Thesis. Eindhoven University of Technology; 2018.
- [157] Wong VW, Hoult DP. Rapid Distortion Theory Applied to Turbulent Combustion. *SAE Transactions* 1979;88:1243–62.
- [158] Yang J, Martin JK. Approximate solution—One-dimensional energy equation for transient, compressible, low mach number turbulent boundary layer flows. *Journal of Heat Transfer (Transactions of the ASME (American Society of Mechanical Engineers), SERIES C); (UNITED STATES)* 1989. <https://doi.org/10.1115/1.3250727>.
- [159] Westbrook CK, Dryer FL. Simplified Reaction Mechanisms for the Oxidation of Hydrocarbon Fuels in Flames. *Combustion Science and Technology* 1981;27: 31–43. <https://doi.org/10.1080/00102208108946970>.
- [160] Mikulski M, Wierzbicki S, Piętak A. Numerical Studies on Controlling Gaseous Fuel Combustion by Managing the Combustion Process of Diesel Pilot Dose in a Dual-Fuel Engine 2015:225–38.
- [161] Westbrook CK, Dryer FL. Chemical kinetics and modeling of combustion processes. *Symposium (International) on Combustion* 1981;18:749–67. [https://doi.org/10.1016/S0082-0784\(81\)80079-3](https://doi.org/10.1016/S0082-0784(81)80079-3).
- [162] Zheng J, Miller DL, Cernansky NP. A Global Reaction Model for the HCCI Combustion Process. SAE 2004-01-2950 2004. <https://doi.org/10.4271/2004-01-2950>.
- [163] Miller JA, Kee RJ, Westbrook CK. Chemical Kinetics and Combustion Modeling. *Annu Rev Phys Chem* 1990;41:345–87. <https://doi.org/10.1146/annurev.pc.41.100190.002021>.
- [164] Ogink R, Golovitchev V. Gasoline HCCI Modeling: Computer Program Combining Detailed Chemistry and Gas Exchange Processes. 2001. <https://doi.org/10.4271/2001-01-3614>. 2001-01-3614.
- [165] Pfahl U, Fieweger K, Adomeit G. Shock Tube Investigation of Ignition Delay Times of Multicomponent Fuel/Air-Mixtures under Engine Relevant Conditions. Final Report, Subprogramme FK. 4. IDEA-EFFECT 1996.
- [166] Chen Y-H, Chen JY. Development of Isooctane Skeletal Mechanisms for Fast and Accurate Predictions of SOC and Emissions of HCCI Engines based on LLNL Detailed Mechanism. In: 2005 Fall Meeting Western States Combustion Institute, Stanford, California; 2005.
- [167] Curran HJ, Gaffuri P, Pitz WJ, Westbrook CK, Leppard WR. Autoignition Chemistry of the Hexane Isomers: An Experimental and Kinetic Modeling Study. *SAE Transactions* 1995;104:1184–95.
- [168] Golovitchev VI. n.d. <http://www.tfd.chalmers.se/~valeri/MECH.html>.
- [169] Andrae JCG, Brinck T, Kalghatgi GT. HCCI experiments with toluene reference fuels modeled by a semidetailed chemical kinetic model. *Combustion and Flame* 2008;115:696–712. <https://doi.org/10.1016/j.combustflame.2008.05.010>.
- [170] Seiser R, Pitsch H, Seshadri K, Pitz WJ, Gurran HJ. Extinction and autoignition of n-heptane in counterflow configuration. *Proceedings of the Combustion Institute* 2000;28:2029–37. [https://doi.org/10.1016/S0082-0784\(00\)80610-4](https://doi.org/10.1016/S0082-0784(00)80610-4).
- [171] Peters N, Paczko G, Seiser R, Seshadri K. Temperature cross-over and non-thermal runaway at two-stage ignition of n-heptane. *Combustion and Flame* 2002;128: 38–59. [https://doi.org/10.1016/S0010-2180\(01\)00331-5](https://doi.org/10.1016/S0010-2180(01)00331-5).
- [172] Smith GP, Golden DM, Frenklach M, Moriarty NW, Eiteneer B, Goldenberg M, et al. GRI-MECH 3.0. http://www.me.berkeley.edu/gri_mech/.
- [173] Hergart C, Barths H, Peters N. Modeling the Combustion in a Small-Bore Diesel Engine Using a Method Based on Representative Interactive Flamelets. SAE 1999001-3550 1999. <https://doi.org/10.4271/1999-01-3550>.
- [174] Tanaka S, Ayala F, Keck JC. A reduced chemical kinetic model for HCCI combustion of primary reference fuels in a rapid compression machine. *Combustion and Flame* 2003;133:467–81. [https://doi.org/10.1016/S0010-2180\(03\)00057-9](https://doi.org/10.1016/S0010-2180(03)00057-9).
- [175] Faravelli T, Ranzi E, Frassoldati A, Cuoci A, Mehl M, Stagni A, et al. The CRECK modeling group. <http://creckmodeling.chem.polimi.it/>; [accessed 21.07.2021].
- [176] Curran HJ, Gaffuri P, Pitz WJ, Westbrook CK. A comprehensive modeling study of iso-octane oxidation. *Combustion and Flame* 2002;129:253–80. [https://doi.org/10.1016/S0010-2180\(01\)00373-X](https://doi.org/10.1016/S0010-2180(01)00373-X).
- [177] Ra Y, Reitz RD. A reduced chemical kinetic model for IC engine combustion simulations with primary reference fuels. *Combustion and Flame* 2008;155: 713–38. <https://doi.org/10.1016/j.combustflame.2008.05.002>.
- [178] Golovitchev VI, Atarashiya K, Tanaka K, Yamada S. Towards Universal EDC-based combustion model for compression ignited engine simulations. *SAE Transactions* 2003;112:1329–43.
- [179] Babajimopoulos A, Lavoie GA, Assanis DN. Modeling HCCI Combustion with High Levels of Residual Gas Fraction - A Comparison of Two VVA Strategies. SAE 2003-01-3220 2003. <https://doi.org/10.4271/2003-01-3220>.
- [180] Warnatz J. A Reaction Mechanism for the Description of Low and High Temperature Oxidation of Hydrocarbon-Air Mixtures at Lean and Rich Conditions. *Personal Communication* 1999.
- [181] Rahimi A, Fatehifar E, Saray RK. Development of an optimized chemical kinetic mechanism for homogeneous charge compression ignition combustion of a fuel blend of n-heptane and natural gas using a genetic algorithm. *Proceedings of the Institution of Mechanical Engineers, Part D: Journal of Automobile Engineering* 2010;224:1141–59. <https://doi.org/10.1243/09544070JAUTO1343>.
- [182] Kee R, Rupley F, Miller J, Coltrin M, Grcar J, Meeks E, et al. *CHEMKIN Collection*. San Diego, California: Reaction Design; 2000.
- [183] Bekdemir C, Baert R, Willems FPT, Somers LMT. Towards Control-Oriented Modeling of Natural Gas-Diesel RCCI Combustion. SAE 2015-01-1745 2015. <https://doi.org/10.4271/2015-01-1745>.
- [184] Yadav J, Eise F, Preussker M, Cai L, vom Lehn F, Bekdemir C. RCCI-Combustion System in HD Applications Achieving Lowest Fuel Consumption and Emissions. FVV (The Research Association for Combustion Engines eV) 2020.
- [185] Hernández JJ, Ballesteros R, Sanz-Argent J. Reduction of kinetic mechanisms for fuel oxidation through genetic algorithms. *Mathematical and Computer Modelling* 2010;52:1185–93. <https://doi.org/10.1016/j.mcm.2010.02.035>.
- [186] McNeely MJ, Havstad MA, Aceves SM, Pitz WJ. Integration Strategies for Efficient Multizone Chemical Kinetics Models. SAE Int J Fuels Lubr 2010;3:241–55. <https://doi.org/10.4271/2010-01-0576>.
- [187] Kozalka G, Hunicz J. Comparative study of energy losses related to the ring pack operation in homogeneous charge compression ignition and spark ignition combustion. *Energy* 2021;235:121388. <https://doi.org/10.1016/j.energy.2021.121388>.
- [188] Roberts CE, Matthews RD. Development and Application of an Improved Ring Pack Model for Hydrocarbon Emissions Studies. SAE Transactions 1996;105: 1480–502.
- [189] Namazian M, Heywood JB. Flow in the Piston-Cylinder-Ring Crevices of a Spark-Ignition Engine: Effect on Hydrocarbon Emissions, Efficiency and Power. SAE Transactions 1982;91:261–88.
- [190] Zheng J, Caton JA. Second law analysis of a low temperature combustion diesel engine: Effect of injection timing and exhaust gas recirculation. *Energy* 2012;38: 78–84. <https://doi.org/10.1016/j.energy.2011.12.034>.
- [191] Ferguson CR. *INTERNAL COMBUSTION ENGINES, APPLIED THERMOSCIENCES*. New York: Wiley; 1986.
- [192] Goodwin DG, Moffat HK, Speth RL. Cantera: An Object-Oriented Software Toolkit For Chemical Kinetics, Thermodynamics, And Transport Processes. Version 2.3.0. Zenodo; 2017. <https://doi.org/10.5281/zenodo.170284>.
- [193] Radhakrishnan K, Hindmarsh A. DESCRIPTION AND USE OF LSODE, THE LIVERMORE SOLVER FOR ORDINARY DIFFERENTIAL EQUATIONS. Livermore, CA: Lawrence Livermore National Lab.(LLNL); 1993. <https://doi.org/10.2172/15013302>.
- [194] Brown PN, Byrne GD, Hindmarsh AC. VODE: a variable-coefficient ODE solver. *SIAM J Sci Statist Comput* 1989;10:1038–51.
- [195] Cohen SD, Hindmarsh AC, Dubois PF, CVODE A. Stiff/Nonstiff ODE Solver in C. *Computers in Physics* 1996;10:138.
- [196] Wu H, Ma PC, Ihme M. Efficient time stepping for reactive turbulent simulations with stiff chemistry. In: 2018 AIAA Aerospace Sciences Meeting. American Institute of Aeronautics and Astronautics; 2018. <https://doi.org/10.2514/6.2018-1672>.
- [197] Fedkiw RP, Merriman B, Osher S. High Accuracy Numerical Methods for Thermally Perfect Gas Flows with Chemistry. *Journal of Computational Physics* 1997;132:175–90. <https://doi.org/10.1006/jcph.1996.5622>.
- [198] Sandu A, Verwer JG, Van Loon M, Carmichael GR, Potra FA, Dabdub D, et al. Benchmarking stiff ode solvers for atmospheric chemistry problems-I. implicit vs explicit. *Atmospheric Environment* 1997;31:3151–66. [https://doi.org/10.1016/S1352-2310\(97\)00059-9](https://doi.org/10.1016/S1352-2310(97)00059-9).
- [199] Petzold LR. DESCRIPTION OF DASSL: A DIFFERENTIAL/ALGEBRAIC SYSTEM SOLVER. Livermore, CA: Lawrence Livermore National Lab. (LLNL); 1982. <https://www.osti.gov/biblio/5882821>.
- [200] Barton PI, Allgor RJ, Feehery WF. ABACUSS Project Report. Massachusetts Institute of Technology; 1997.
- [201] Söderlind G, Wang L. Evaluating numerical ODE/DAE methods, algorithms and software. *Journal of Computational and Applied Mathematics* 2006;185:244–60. <https://doi.org/10.1016/j.cam.2005.03.009>.
- [202] Manca D, Buzzi-Ferraris G, Pleşu V, PŞ Agachi. The solution of DAE systems by a numerically robust and efficient solver. *Computer Aided Chemical Engineering*, 24. Elsevier; 2007. p. 93–8. [https://doi.org/10.1016/S1570-7946\(07\)80039-3](https://doi.org/10.1016/S1570-7946(07)80039-3).
- [203] Ferraris GB, Manca D. BzzOde: a new C++ class for the solution of stiff and non-stiff ordinary differential equation systems. *Computers & Chemical Engineering* 1998;22:1595–621. [https://doi.org/10.1016/S0098-1354\(98\)00233-6](https://doi.org/10.1016/S0098-1354(98)00233-6).
- [204] Knoll DA, Keyes DE. Jacobian-free Newton–Krylov methods: a survey of approaches and applications. *Journal of Computational Physics* 2004;193: 357–97. <https://doi.org/10.1016/j.jcp.2003.08.010>.
- [205] Ravi N, Liao H-H, Jungkuz AF, Widd A, Gerdes JC. Model predictive control of HCCI using variable valve actuation and fuel injection. *Control Engineering Practice* 2012;20:421–30. <https://doi.org/10.1016/j.conengprac.2011.12.002>.
- [206] Vaidhiyanathan A. NUMERICAL ESTIMATION OF FUEL DISTRIBUTION IN A MULTI-ZONE COMBUSTION MODEL. Master of Science Thesis. Eindhoven University of Technology; 2016.
- [207] Musculus MPB, Kattke K. Entrainment Waves in Diesel Jets. SAE International Journal of Engines 2009;2:1170–93.
- [208] Somers LMT, Evlampiev AV, Goev de LPH. Modelling Auto-Ignition of Automotive Fuels using Detailed Mechanisms. In: *Proceedings of the 3rd European Combustion Meeting ECM 2007*, Chania, Greece; 2007. p. 22. –14.
- [209] Aceves SM, Flowers DL, Espinosa-Loza F, Martinez-Frias J, Dibble RW, Christensen M, et al. Piston-Liner Crevice Geometry Effect on HCCI Combustion by Multi-Zone Analysis. SAE Transactions 2002;111:2691–8.

- [210] Amano T, Morimoto S, Kawabata Y. Modeling of the Effect of Air/Fuel Ratio and Temperature Distribution on HCCI Engines. SAE 2001-01-1024 2001. <https://doi.org/10.4271/2001-01-1024>.
- [211] Sher E. *HANDBOOK OF AIR POLLUTION FROM INTERNAL COMBUSTION ENGINES: POLLUTANT FORMATION AND CONTROL*. editor. Academic Press; 1998.
- [212] Hensel S. Modellierung der Verbrennung und des Wandwärmeeübergangs in Ottomotoren mit homogen kompressionsgezündeter Verbrennung. *Hochschulschrift. Karlsruher Institut für Technologie (KIT) 2009*.
- [213] Garcia-Guendulain JM, Ramirez-Barron A, Riesco-Avila JM, Whitesides R, Aceves SM. Computationally efficient evaluation of optimum homogeneous charge compression ignition operating range with accelerated multizone engine cycle simulation. *International Journal of Engine Research* 2020; 1468087420929488. <https://doi.org/10.1177/1468087420929488>.
- [214] Yang J, Pierce P, Martin JK, Foster DE. Heat Transfer Predictions and Experiments in a Motored Engine. *SAE Transactions* 1988;97:1608–22.
- [215] Zhang Y, Boehman AL. Oxidation of 1-butanol and a mixture of n-heptane/1-butanol in a motored engine. *Combustion and Flame* 2010;157:1816–24. <https://doi.org/10.1016/j.combustflame.2010.04.017>.
- [216] Dec JE, Hwang W. Characterizing the Development of Thermal Stratification in an HCCI Engine Using Planar-Imaging Thermometry. *SAE Int J Engines* 2009;2: 421–38. <https://doi.org/10.4271/2009-01-0650>.
- [217] Assanis DN, Heywood JB. Development and Use of a Computer Simulation of the Turbocompounded Diesel System for Engine Performance and Component Heat Transfer Studies. *SAE Transactions* 1986;95:451–76.
- [218] Aceves SM, Flowers DL, Espinosa-Loza F, Martinez-Frias J, Dec JE, Sjöberg M, et al. Spatial Analysis of Emissions Sources for HCCI Combustion at Low Loads Using a Multi-Zone Model. *SAE Transactions* 2004;113:1014–24.
- [219] Neshat E, Saray RK, Hosseini V. Effect of reformer gas blending on homogeneous charge compression ignition combustion of primary reference fuels using multi zone model and semi detailed chemical-kinetic mechanism. *Applied Energy* 2016; 179:463–78. <https://doi.org/10.1016/j.apenergy.2016.06.150>.
- [220] Lawton B. Effect of Compression and Expansion on Instantaneous Heat Transfer in Reciprocating Internal Combustion Engines. *Proceedings of the Institution of Mechanical Engineers, Part A: Power and Process Engineering* 1987;201:175–86. https://doi.org/10.1243/PIME_PROC_1987_201_022_02.
- [221] Dec JE, Yang Y. Boosted HCCI for High Power without Engine Knock and with Ultra-Low NOx Emissions - using Conventional Gasoline. *SAE Int J Engines* 2010; 3:750–67. <https://doi.org/10.4271/2010-01-1086>.
- [222] Mehl M, Faravelli T, Ranzi E, Miller D, Cernansky N. Experimental and kinetic modeling study of the effect of fuel composition in HCCI engines. *Proceedings of the Combustion Institute* 2009;32:2843–50. <https://doi.org/10.1016/j.proci.2008.08.001>.
- [223] Dempsey AB. PhD Thesis. University of Wisconsin-Madison; 2013.
- [224] Guo H, Neill WS. The effect of hydrogen addition on combustion and emission characteristics of an n-heptane fuelled HCCI engine. *International Journal of Hydrogen Energy* 2013;38:11429–37. <https://doi.org/10.1016/j.ijhydene.2013.06.084>.
- [225] Reyhanian M, Hosseini V. Various effects of reformer gas enrichment on natural-gas, iso-octane and normal-heptane HCCI combustion using artificial inert species method. *Energy Conversion and Management* 2018;159:7–19. <https://doi.org/10.1016/j.enconman.2017.12.074>.
- [226] Neshat E, Saray RK, Parsa S. Numerical analysis of the effects of reformer gas on supercharged n-heptane HCCI combustion. *Fuel* 2017;200:488–98. <https://doi.org/10.1016/j.fuel.2017.04.005>.
- [227] Ahari MF, Neshat E. Advanced analysis of various effects of water on natural gas HCCI combustion, emissions and chemical procedure using artificial inert species. *Energy* 2019;171:842–52. <https://doi.org/10.1016/j.energy.2019.01.059>.
- [228] Saxena S, Shah N, Bedoya I, Phadke A. Understanding optimal engine operating strategies for gasoline-fueled HCCI engines using crank-angle resolved exergy analysis. *Applied Energy* 2014;114:155–63. <https://doi.org/10.1016/j.apenergy.2013.09.056>.
- [229] Neshat E, Asghari M. Investigation on the effect of reformer gas on availability terms and waste heat recovery from exhaust gases of an HCCI engine considering radiation heat transfer. *Journal of the Brazilian Society of Mechanical Sciences and Engineering* 2019;42:55. <https://doi.org/10.1007/s40430-019-2139-3>.
- [230] Yelvington PE, Green WH. Prediction of the Knock Limit and Viable Operating Range for a Homogeneous-Charge Compression-Ignition (HCCI) Engine. SAE 2003-01-1092 2003. <https://doi.org/10.4271/2003-01-1092>.
- [231] Sjöberg M, Dec JE. Effects of Engine Speed, Fueling Rate, and Combustion Phasing on the Thermal Stratification Required to Limit HCCI Knocking Intensity. *SAE Transactions* 2005;114:1472–86.
- [232] Yoshizawa K, Teraji A, Miyakubo H, Yamaguchi K, Urushihara T. Study of high load operation limit expansion for gasoline compression ignition engines. *Journal of Engineering for Gas Turbines and Power* 2006;128:377–87. <https://doi.org/10.1115/1.1805548>.
- [233] Nelles O. *NONLINEAR SYSTEM IDENTIFICATION: FROM CLASSICAL APPROACHES TO NEURAL NETWORKS, FUZZY MODELS, AND GAUSSIAN PROCESSES*. Springer Nature; 2020.
- [234] Eng JA. Characterization of Pressure Waves in HCCI Combustion. SAE 2002-01-2859 2002. <https://doi.org/10.4271/2002-01-2859>.
- [235] Jia M, Dempsey AB, Wang H, Li Y, Reitz RD. Numerical simulation of cyclic variability in reactivity-controlled compression ignition combustion with a focus on the initial temperature at intake valve closing. *International Journal of Engine Research* 2015;16:441–60. <https://doi.org/10.1177/1468087414552088>.
- [236] Willems F. Is Cylinder Pressure-Based Control Required to Meet Future HD Legislation? IFAC-PapersOnLine 2018;51:111–8. <https://doi.org/10.1016/j.ifacol.2018.10.021>.
- [237] Li J, Yang W, Zhou D. Review on the management of RCCI engines. *Renewable and Sustainable Energy Reviews* 2017;69:65–79. <https://doi.org/10.1016/j.rser.2016.11.159>.
- [238] Pandey S, Diwan P, Sahoo PK, Thipse SS. A review of combustion control strategies in diesel HCCI engines. *Biofuels* 2018;9:61–74. <https://doi.org/10.1080/17597269.2016.1257315>.
- [239] Chowta PR, Murthy K, Mahesha GT. Emission control studies in homogeneous charge compression ignition, premixed charge compression ignition and common rail direct injection engines – a review. *Biofuels* 2021;12:363–8. <https://doi.org/10.1080/17597269.2019.1657660>.
- [240] Pinheiro A, Vuilleumier D, Kozarac D, Saxena S. Simulating a Complete Performance Map of an Ethanol-Fueled Boosted HCCI Engine, 2015, p. 2015-01-0821. <https://doi.org/10.4271/2015-01-0821>.
- [241] Kozarac D, Sjerić M, Ilincić Ing P. Numerical Study of Influencing Factors and the Possibility to Use Vibe Parameters in Crank-Angle Resolved HCCI Control Models 2011. <https://doi.org/10.4271/2011-01-0906>.
- [242] Taritas I, Kozarac D, Sjerić M. Numerical Study of Boosting Configurations and Valve Strategies for High Load HCCI Engine in Wide Range of Engine Speed, 2014, p. 2014-01-1267. <https://doi.org/10.4271/2014-01-1267>.
- [243] Bengtsson J, Strandh P, Johansson R, Tunestål P, Johansson B. Closed-loop combustion control of homogeneous charge compression ignition(HCCI) engine dynamics. *Int J Adapt Control Signal Process* 2004;18:167–79. <https://doi.org/10.1002/acs.788>.
- [244] Bengtsson J, Strandh P, Johansson R, Tunestål P, Johansson B. Hybrid modelling of homogeneous charge compression ignition (HCCI) engine dynamics—a survey. *Journal of Control* 2007;80:1814–47. <https://doi.org/10.1080/00207170701484869>.
- [245] Del Re L, Allgöwer F, Glielmo L, Guardiola C, Kolmanovskiy I. *AUTOMOTIVE MODEL PREDICTIVE CONTROL: MODELS, METHODS AND APPLICATIONS*. 1st ed. London: Springer; 2010.
- [246] Widd A, Tunesta P. Physical Modeling and Control of Homogeneous Charge Compression Ignition (HCCI) engines. In: 2008 47th IEEE Conference on Decision and Control, Cancun, Mexico; 2008. p. 5615–20.
- [247] Neshat E, Saray RK. An optimized chemical kinetic mechanism for HCCI combustion of PRFs using multi-zone model and genetic algorithm. *Energy Conversion and Management* 2015;92:172–83. <https://doi.org/10.1016/j.enconman.2014.11.057>.
- [248] Pelucchi M, Bissoli M, Rizzo C, Zhang Y, Somers K, Frassoldati A, et al. A Kinetic Modelling Study of Alcohols Operating Regimes in a HCCI Engine. SAE International Journal of Engines 2017;2354–70. <https://doi.org/10.4271/2017-24-0077>.
- [249] Luo X, Plomer M, Lu T, Som S, Longman DE, Sarathy SM, et al. A reduced mechanism for biodiesel surrogates for compression ignition engine applications. *Fuel* 2012;99:143–53. <https://doi.org/10.1016/j.fuel.2012.04.028>.
- [250] An H, Yang WM, Maghbouli A, Li J, Chua KJ. A skeletal mechanism for biodiesel blend surrogates combustion. *Energy Conversion and Management* 2014;81:51–9. <https://doi.org/10.1016/j.enconman.2014.02.012>.
- [251] Bedoya ID, Saxena S, Cadavid FJ, Dibble RW. Exploring Strategies for Reducing High Intake Temperature Requirements and Allowing Optimal Operational Conditions in a Biogas Fueled HCCI Engine for Power Generation. *Journal of Engineering for Gas Turbines and Power* 2012;134. <https://doi.org/10.1115/1.4006075>.
- [252] Felsch C, Sloane T, Han J, Barths H, Lippert A. Numerical Investigation of Recombression and Fuel Reforming in a SIDI-HCCI Engine. SAE 2007-01-1878 2007. <https://doi.org/10.4271/2007-01-1878>.
- [253] Bougrine S, Richard S, Michel J-B, Veynante D. Simulation of CO and NO emissions in a SI engine using a 0D coherent flame model coupled with a tabulated chemistry approach. *Applied Energy* 2014;113:1199–215. <https://doi.org/10.1016/j.apenergy.2013.08.038>.
- [254] Matriciano A, Franken T, Gonzales Mestre LC, Borg A, Mauss F. Development of a Computationally Efficient Tabulated Chemistry Solver for Internal Combustion Engine Optimization Using Stochastic Reactor Models. *Applied Sciences* 2020;10. <https://doi.org/10.3390/app10248979>.
- [255] Niemeyer KE, Sung C-J. Accelerating moderately stiff chemical kinetics in reactive-flow simulations using GPUs. *Journal of Computational Physics* 2014; 256:854–71. <https://doi.org/10.1016/j.jcp.2013.09.025>.
- [256] Komninos NP. Assessing the effect of mass transfer on the formation of HC and CO emissions in HCCI engines, using a multi-zone model. *Energy Conversion and Management* 2009;50:1192–201. <https://doi.org/10.1016/j.enconman.2009.01.026>.
- [257] Kozarac D, Vuilleumier D, Saxena S, Dibble RW. Analysis of benefits of using internal exhaust gas recirculation in biogas-fueled HCCI engines. *Energy Conversion and Management* 2014;87:1186–94. <https://doi.org/10.1016/j.enconman.2014.04.085>.
- [258] Neshat E, Saray RK. Mathematical modeling and validation of mass transfer phenomenon in homogeneous charge compression ignition engines based on a thermodynamic multi zone model. *Mathematical and Computer Modelling of Dynamic Systems* 2019;25:167–94. <https://doi.org/10.1080/13873954.2019.1596957>.
- [259] Clean Propulsion Technology. 2021. <https://cleanpropulsion.org/> [accessed 12.08.2021].



Aneesh Vasudev (MSc) is a PhD scholar and project researcher at the renewable energy research group at the University of Vaasa. He graduated from the Eindhoven University of Technology, with a combined internship and thesis focusing on multizone modelling for heavy-duty RCCI engines, performed at TNO Automotive. Afterwards, he joined the research group of Prof. Mikulski working for major marine engine OEMs. His research work lies in reciprocating combustion engines and uses computational modelling as the principal technique. His current focus is on reactivity controlled compression ignition (RCCI) and the development of associated control-oriented modelling tools. In the fall of 2020, he started his PhD studies pursuing the same subject. As such, he has accumulated over four years of experience within the domain of multizone modelling. For his contribution to industry-applicable combustion-modelling research, he has been recently awarded a scholarship from the Finnish Cultural Foundation.



Dr Maciej Mikulski is an Associate Professor in combustion engine technology at the University of Vaasa Finland and a Principle Scientist in the VEBIC internal combustion engine laboratory (Finland). He has 15 years of professional experience in combustion engine research in industry and academia. He has worked in several relevant engine/fuel development projects with the world's leading automotive, marine and off-road OEMs and co-established the first full-load capable, ultra-efficient RCCI natural gas engine. For his research on low-temperature combustion, he was recently honored with the Finnish Ostrobothnia Chamber of Commerce award. He is an author of over 85 research papers in the field and a member of several international expert groups and combustion research associations. He is currently (2020-2023), amongst others, a leader in a major (over 15M€ in total founding) Finish industry-academia consortium - the CLEAN PROPULSION TECHNOLOGY committed to advanced combustion and powertrain development.



Praveen Ramanujam Balakrishnan (MSc) received his degree in Automotive Technology from the Eindhoven University of Technology, The Netherlands, specializing in the field of vehicle powertrains. He continued as a Research Scientist at TNO for 3 years (Powertrains Department) working on improving the functionality of TNO's in house multi-zone Reactivity Controlled Compression Ignition (RCCI) simulation model. Currently, he is employed at Convergent Science GmbH, Linz, Austria, as a Research Engineer, working on development and support for the CFD simulation package 'CONVERGE', focusing on IC engine applications for the automotive industry. He has authored five research articles on the simulation-based development of internal combustion engines. Two of his publications are in the area of variable valve actuation for a multi-zone low-temperature combustion model – directly relevant to this review. His research interests also include model-based development of EuroVI-rated alternative-fuel propulsion for the heavy-duty sector, as well as optimizing the energy management of hybrid trucks.



Xiaoguo Storm (MSc) is a senior researcher and a PhD Scholar at the University of Vaasa Finland. Her research work is centred on internal combustion engine control system development. Her interests strongly focus on cylinder pressure-based control and model predictive control, range from conventional diesel and dual-fuel engines to advanced low-temperature types of combustion. She has experience from several European engine development initiatives (Hercules 2, FLEXe, INTENS). She works in close collaboration with Wärtsilä R&D in control functionality development for marine and powerplant engines. She was amongst others responsible for the commissioning of the rapid control prototyping system for the state of the art VEBIC- Wärtsilä 4L20 medium-speed engine. Currently, she is (2021-2023) working in the CLEAN PROPULSION TECHNOLOGY project in Prof. Mikulski's team, with the duty of control system development for the cutting-edge ultra-heavy duty, reactivity controlled compression ignition (RCCI) marine engine.



Jacek Hunicz (PhD, DSc.) is an associate professor and head of Powertrains Laboratory at the Lublin University of Technology, Poland. His track record includes experimental engine research and renewable low-carbon fuels. In the area of combustion research, his studies are centred on the control strategies for low-temperature combustion in HCCI engines, including the NVO fuel reforming. With over 23 years of professional expertise in combustion engines and powertrain development, prof. Hunicz is a grant holder of several relevant nationwide projects funded by the Ministry of Science and Higher Education and the National Science Centre. He is a member of several international research groups. He is also an innovation consultant for domestic off-road vehicle and bus manufacturer Ursus and a technical advisor to the Polish military industry in the field of powertrain testing. Since 2018, he has been a board member of the Polish Scientific Society for Combustion Engines.